A FLOWING AFTERGLOW SOURCE OF $NF(b^1\Sigma^+)$: QUENCHING RATE CONSTANT MEASUREMENTS

305

by

DAIMAY LIN

B.S., National Taiwan University, 1980

A MASTER'S THESIS

submitted in partial fulfillment of the

requirements for the degree

MASTER OF SCIENCE

Department of Chemistry

KANSAS STATE UNIVERSITY

Manhattan, Kansas

1984

Approved by:

D. W. Setser

Major Professor

-D
266
.T4
1984
L56
c. 2

A11202 960508

TABLE OF CONTENTS

LIST OF FIGURES

LIST OF TABLES

CHAPTER 1. INTRODUCTION

Excitation energy transfer and electronic quenching reactions of metastable electronic states have been of interest because of application in gas lasers as well as being model examples of the general phenomena. An example is the $O_2(^1\Delta_g)$-I chemical laser where $O_2(a\,^1\Delta_g)$ (0.98 ev) was used to pump the $I(^2P_{3/2}-^2P_{1/2})$ transition in a CW I atom laser.[1],[2],[3] Taking O_2 as an example, other molecules isoelectronic with O_2 may also be candidates as energy sources for gas lasers, since they have similar electronic states and electronic transition properties to O_2.

Molecules such as NX, PX (X = H, F, Cl, Br, I) and S_2, SO, SeO etc. are isoelectronic with O_2 according to MO theory. Some metastable singlet states of these molecules are known, including those for NF, NCl, NBr, PF, SO, SeO, etc.[4] NF is one of the molecules receiving more attention mainly because the NF(b) energy is in the visible range and chemically pumped sources appear feasible. Techniques to scale-up the concentration of NF(a) and NF(b) states are being studied[5],[6]. However, in spite of the current interest in possible laser application, the physical and chemical properties of many states of NF are still largely unknown. Therefore, studies of NF including the reactivity, the lifetime, the potential curves, and the energy transfer properties are being done to assess the NF singlet states as candidates for electronic transition lasers.

The properties of NF electronic states can be predicted utilizing the anticipated similarity between NF and O_2. The relative energy diagram for homonuclear diatomic molecules is shown in fig.

1.1.a[7],[8]; the ground state electronic configuration of O_2 is given by the diagram as $KK(2\sigma_g)^2(2\sigma_u)^2(3\sigma_g)^2(1\Pi_u)^4(1\Pi_g)^2$, which leads to three low lying electronic states, namely $X^3\Sigma_g^-$, $a^1\Delta_g$, and $b^1\Sigma_g^+$ in the order of increasing energy. The ground state configuration of NF, $KK(2\sigma)^2(2\sigma^*)^2(3\sigma)^2(1\Pi)^4(1\Pi^*)^2$, is the same as O_2 except the g-u symmetry, which is a characteristic of homonuclear diatomic molecules, is absent. Theoretical calculations[16][19] for NF electronic states were reported and spectroscopic data [20][21] for the states $X^3\Sigma^-$, $a^1\Delta$ and $b^1\Sigma^+$ are known. Fig. 1.2 shows the potential curves of the three low lying energy states of NF and O_2. The potentials for NF are quite similar to O_2, but, the energy separations between states are larger for NF. The absence of g-u symmetry in NF radical makes the b-X (528 nm) and a-X (874 nm) transitions of NF less forbidden than those of O_2, and the NF(b) and NF(a) states are shorter lived than the corresponding states of O_2. The excited states of NF are considered not only as candidates for energy storage but also laser candidates themselves.[22] The lifetime of NF(a) was measured to be ~ 5.6 sec by Malins and Setser[12]; the reported values for the lifetime of NF(b) show some disagreement, and lifetimes of 160[23], 15[24], and 22[13] msec have been reported, but a value near 20 msec must be about right.

While the MO theory predicts an analogy of NF to O_2, a different view is given by valance bond theory which is more related to the idea of molecules being held together by localized bonds. According to valance bond method, NF is formed by pairing one p electron of F atom with one p electron of N atom and leaves two unpaired p electrons remaining localized on the N atom. Thus, the function of F atom is mainly to bind one of N atom's unpaired electrons. Support of the VB

Fig. 1.1.a The energy diagram for homonuclear diatomic molecules

The figure shows only the relative position of the orbitals. The ground state configuration of O_2 molecule is also shown in the diagram.

Fig. 1.1.b The relative energy for the three low lying states of NF and O_2

Note the difference between two excited singlet states is only the change in angular momentum. These states are derived from same electronic configuration. The T_e values are from ref. (4), (9) and the lifetimes are from ref. (10), (11), (12), and (13).

Fig. 1-1.a

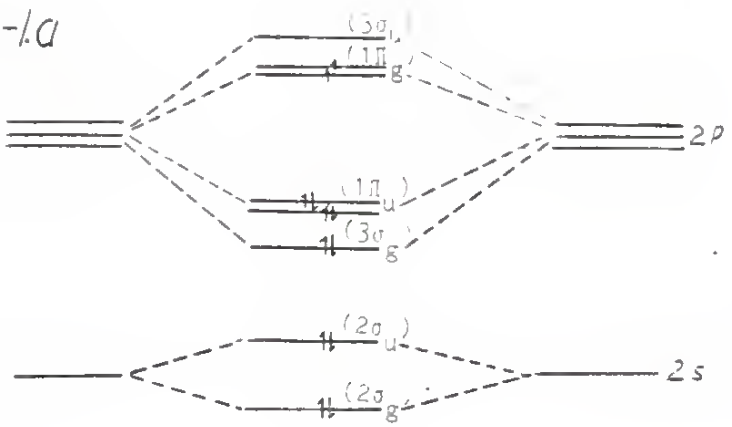

Fig 1-1. b

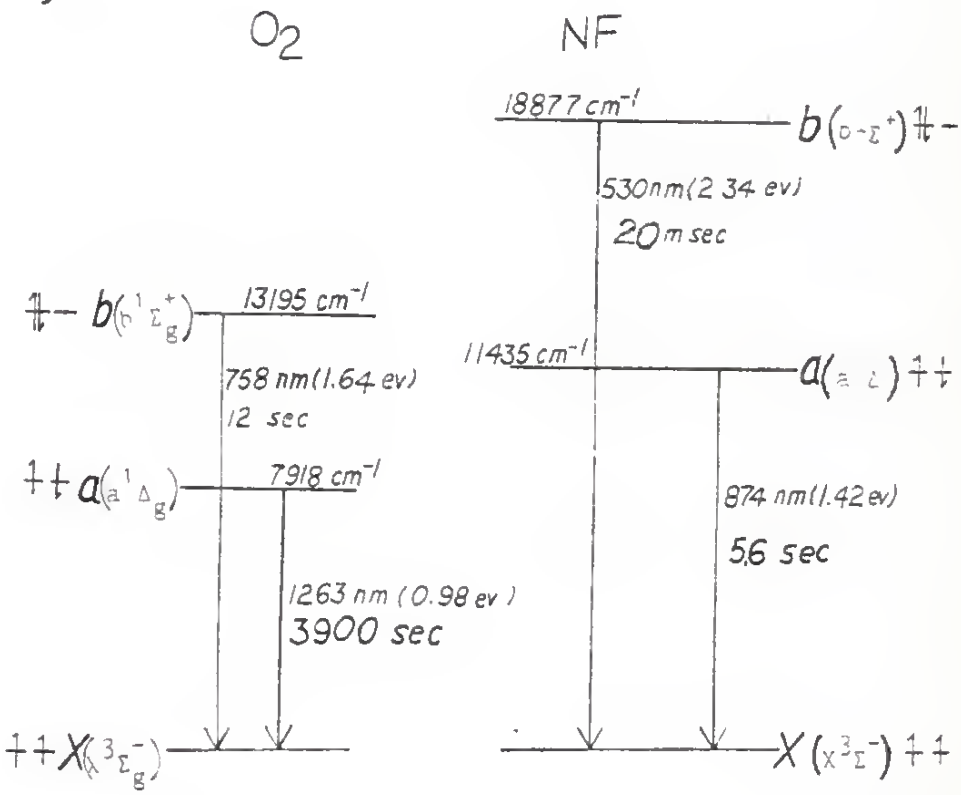

Fig. 1.2 Potential curves for the 3 lowest states of NF and O_2

The curves are obtained from ref. 14 and ref. 15. The spectroscopic constants for the three states of NF are:[20][21] (cm^{-1})

	T_e	ω_e	$\omega_e X_e$	γ_e(Å)	b_e	α_e	D_e
b($v \leq 1$)	18877.05	1197.49	8.64	1.3001	1.2377	0.01448	5.28×10^{-6}
a($v=0$)	11435.16	--	--	1.3082	1.2225	--	4.5×10^{-6}
X($v \leq 2$)	0	1141.37	8.79	1.3173	1.2056	0.01492	5.39×10^{-6}

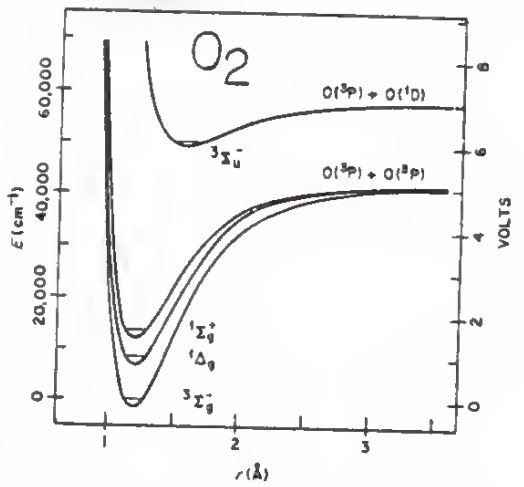
O2
O(3P) + O(1D)
O(3P) + O(3P)
3Σu-
1Σg+
1Δg
3Σg-
E (cm-1)
60,000
40,000
20,000
0
VOLTS
r (Å)

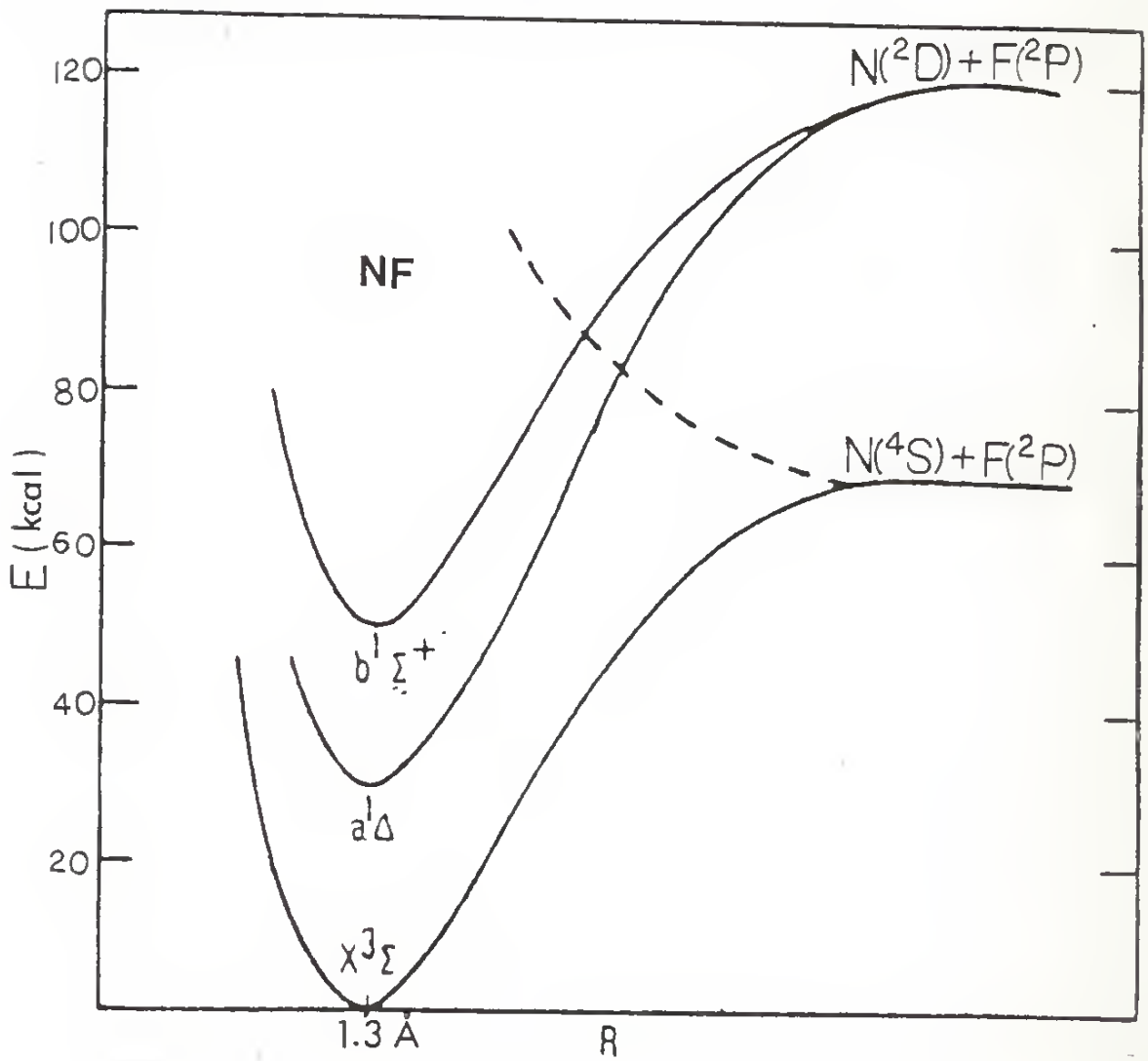
NF
N(2D)+F(2P)
N(4S)+F(2P)
b1Σ+
a1Δ
X3Σ
E (kcal)
120
100
80
60
40
20
1.3 Å
R

prediction was given by Herbelin,[14] who investigated the reactions of NF with other NF radicals using the conservation of electronic angular momentum with the assumption that F atom is only an inert inspectator in molecule when reacting with other species. With two unpaired electrons localizing on N atom, the reactivity of NF may resemble an O atom. In fact, insertion and abstraction reactions, the typical reactions of $O(^1D)$, $O(^3P)$ and CH_2, were observed for NH(a) + C_2H_6[25]. The chemical properties of NF may be more or less similar to NH or O atoms.

Since different theoretical approaches lead to different suggestions about the properties of NF radicals; experimental studies are necessary for better understanding of the molecule. For such work a clean kinetic source of NF(b) is needed. Reaction of NF_2 + H gives NF(a) (rxn. 1.2) with more than 90%[2] yield and this reaction is a good NF(a) source although the rate constant is slow for flwoing afterglow work. Several techniques have been reported to generate NF(b) state. One is the energy pooling between HF(v ≥ 2) and NF(a). However, this reaction has not yet been isolated and proven. This is not a favored NF(b) source for kinetic studies since the coupling of the relatively

$$H + NF_2 \rightarrow HF(v) + NF(a) \qquad \text{(rxn 1.2)}$$

$$HF(v \geq 2) + NF(a) \rightarrow NF(b) + HF(v - 2) \qquad \text{(rxn 1.3)}$$

slow NF(b) generation with its removal by quenching reagents introduce kinetic problems.

In the present work, the reactions between pure N_2F_4 or NF_2 with Ar*, Xe* and He* in a fast flow system were investigated as NF(b) source. It was found that Ar* + NF_2 is the most preferred NF(b) source.

The emissions from N_2F_4/NF_2 with Ar*, Xe* and He* were observed by scanning the monochromator from 2000Å to 6500Å, and the results are discussed as the characteristics of NF(b) soruce. The $\Delta v = 1, 0, -1$ sequences of NF(b-X) emission were observed up to $v' = 9$. The measured wavelengths of the NF(b-X) vibrational bands were used to examine the reliability of the Morse potential curves and the relative intensities of the emission bands were applied to calculate the relative population of NF(b) at different v levels. Measurements on the radiative lifetime, wall quenching, and quenching rate constants of ~ 25 molecules with NF(b) at room temperature were carried out. The k_Q values of NF(b) and $O_2(b)$ was compared and a close similarity in terms of reactivity and quenching pattern is found.

References

1. W. E. McDermott, N. R. Pchelkin, D. J. Benard and R. R. Bousek, Appl. Phys. Lett., 32, 469 (1978).

2. R. G. Derwent and B. A. Thnish, Faraday Discussion, Chem. Sco., 53, 162, 1972.

3. D. J. Benard, W. E. McDermott, N. R. Pchelkin and R. R. Bousek, Appl. Phys. Lett., 40, 34 (1978.

4. B. Rosen, Selected Constant, Spectroscopic Data Related to Diatomic Molecules, p. 273-275, Pergamon Press, 1970.

5. J. M. Herbelin, D. J. Spencer, and M. A. Kwok, J. Appl. Phys., 48, 3050, 1977.

6. J. M. Herbelin Electronic Transition Lasers 2, p. 104, 3rd, 1976, Ed. by L. E. Wilson, S. N. Suchard, and J. T. Steinfield, MIT Press, Cambridge, Mass.

7. J. E. Huheey, Inorganic Chemistry, p. 106, Harper and Row Publishers, 1972.

8. I. N. Levine, Quantum Chem., p. 320, 2nd ed.

9. G. Herzberg, Spectra of Diatomic Molecules, p. 560, Van Nostrand Reinhold Company, 1950.

10. D. E. Burch and D. A. Gryvnak, Appl. Opt., 8, 1493, 1969.

11. R. M. Badger, A. D. Wright, and R. F. Whitlock, J. Chem. Phys., 43, 3341, 1967.

12. R. J. Malins, and D. W. Setser, J. Chem. Phys., 85,1342, 1981.

13. P. H. Tennyson, A. Fontijn, M. A. A. Clyne, Chem. Phys., 62, 171, 1981.

14. J. M. Herbelin, Chem. Phys. Lett., 42, 367, 1976.

15. H. H. Wasserman, R. W. Murray, Singlet Oxygen, p. 2, Academic Press, 1979.

16. D. J. Ellis and K. E. Banyard, J. Phys. B.: Atom Molec. Phys., 7, 2021, 1974

17. D. J. Ellis, K. E. Banyard, A. D. Tait and M. Dixon, J. Phys. B.: Atom Molec. Phys., 6, L233, 1973.

18. R. C. Sahni, Trans Faraday Soc., 63, 801, 1969.

19. A. Andersen and Y. Ohrn, J. Molec. Spectros. 45, 358, 1973.

20. A. E. Douglas and W. E. Jonse, Can. J. Phys., 44, 2251, 1966.

21. W. E. Jonse, Can. J. Phys., 45, 21, 1967.

22. M. A. A. Clyne, J. Chem. Soc. Faraday II, 76, 711, 1980.

23. M. A. A. Clyne and I. F. White, Chem. Phys. Lett., 6, 465, 1965.

24. M. A. Koww, J. M. Herbelin and N. Cohen, Electron Transition Lasers, p. 8, 2nd Ed., Ed. by J. I. Steinfield, the MIT Press, 1975.

25. O. Kajmoto and T. Fueno, Chem. Phys., 80, 484, 1981.

26. A. T. Pritt, Jr., W. Patel and D. J. Benard, Chem. Phys. Lett., 97, 471, 1983.

27. W. E. Jones, Can. J. Phys., 45, 21, 1967.

CHAPTER 2. EXPERIMENTAL METHODS

Flowing Afterglow Source for NF(b) Radicals

As shown in fig. 2.1, the flow reactor was basically a Pyrex tube of 4.1 cm inside diameter and 60 cm length. NF(b) radicals were generated by the dissociative excitation transfer reactions from $Ar(^3P_{2,0})$ metastable atoms (11.7 eV) to N_2F_4 or NF_2 radicals. The Ar metastable atoms were produced by flowing Ar gas through a hollow cathode discharge[1]; typical concentrations of Ar metastable atoms are 10^{10} atoms/cm^3 for the method[2]. The Ar gas (Airco, 99.8%) was purified by passing through 3 molecular seive traps before entering discharge section. Two traps at low pressure were cooled to 77 K by liq. N_2. The high pressure trap was at 300 K. The flow of Ar was metered by a Fisher-Porter tri-flat flowmeter (Cat. No. 448-215) and monitored by a needle valve. Fig. 2.2 shows the calibration curve for this flowmeter. Two 1000 ℓ/min pumps were used in parallel to obtain satisfactory bulk gas flow speeds. For the typical Ar flow rate, 0.1 mole/min, the pressure in flow tube was ~ 1.5 torr and the pumping speed was about 15-17 m/sec. The pressure drop along the flow tube was negligible as determined by direct measurement.

The electrodes for the hollow cathode discharge were made of two pieces of 1.5 cm wide and 0.002 in. thick Tantalum foil (Fansteel Metals), which were cleaned with acetone before being inserted into a glass tube. The glass/metal connection was by epoxy. The discharge was

Fig. 2.1 Flow Reactor

The dark area around the N_2F_4 line and the Ar*, NF_2 mixing zone represents the heated zone; the heating was produced by heating tapes. The diameters of flow tube and N_2F_4 line, were 4.1 cm and 0.7 cm, respectively.

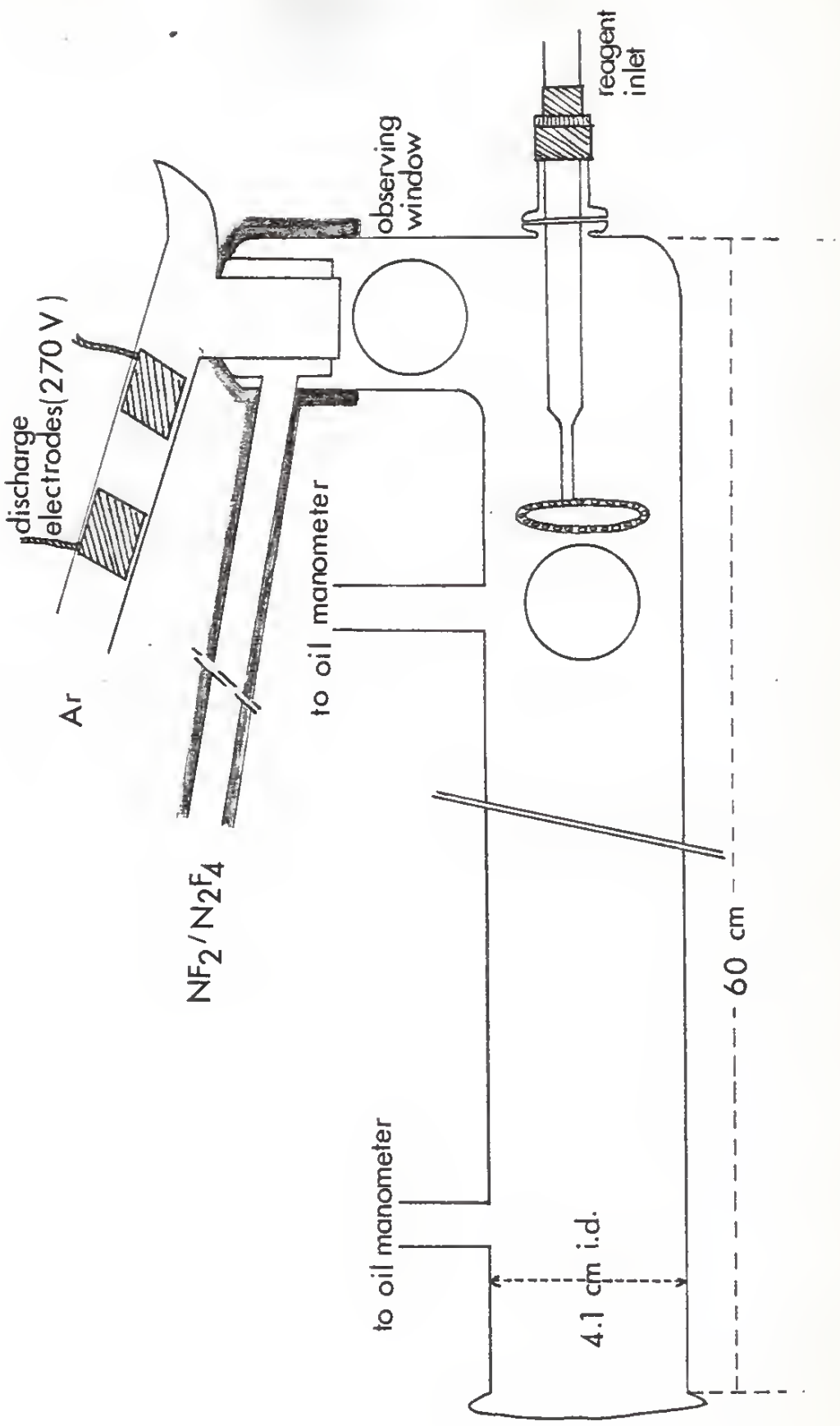
reagent inlet
observing window
discharge electrodes(270 V)
Ar
NF_2/N_2F_4
to oil manometer
to oil manometer
4.1 cm i.d.
60 cm

Fig. 2.2 Calibration curve of tri-flat flowmeter for Ar flow.

The flow meter was calibrated for Ar by a wet test meter under atmospheric pressure. The back pressure of Ar was ~1.3 atm (20 psi) and the wet test meter was under atmospheric pressure.

Comparing with the previous calibration curve done by T. D. Dreiling in 1980, good agreement was found for Ar flow in the range of 0.09 - 0.135 mole/min (~1% deviation), but larger deviation (6%) for flows in the ragne of 0.03-0.09 mole/min was observed. The meter scale under 8 was not previously calibrated by T. D. Dreiling.

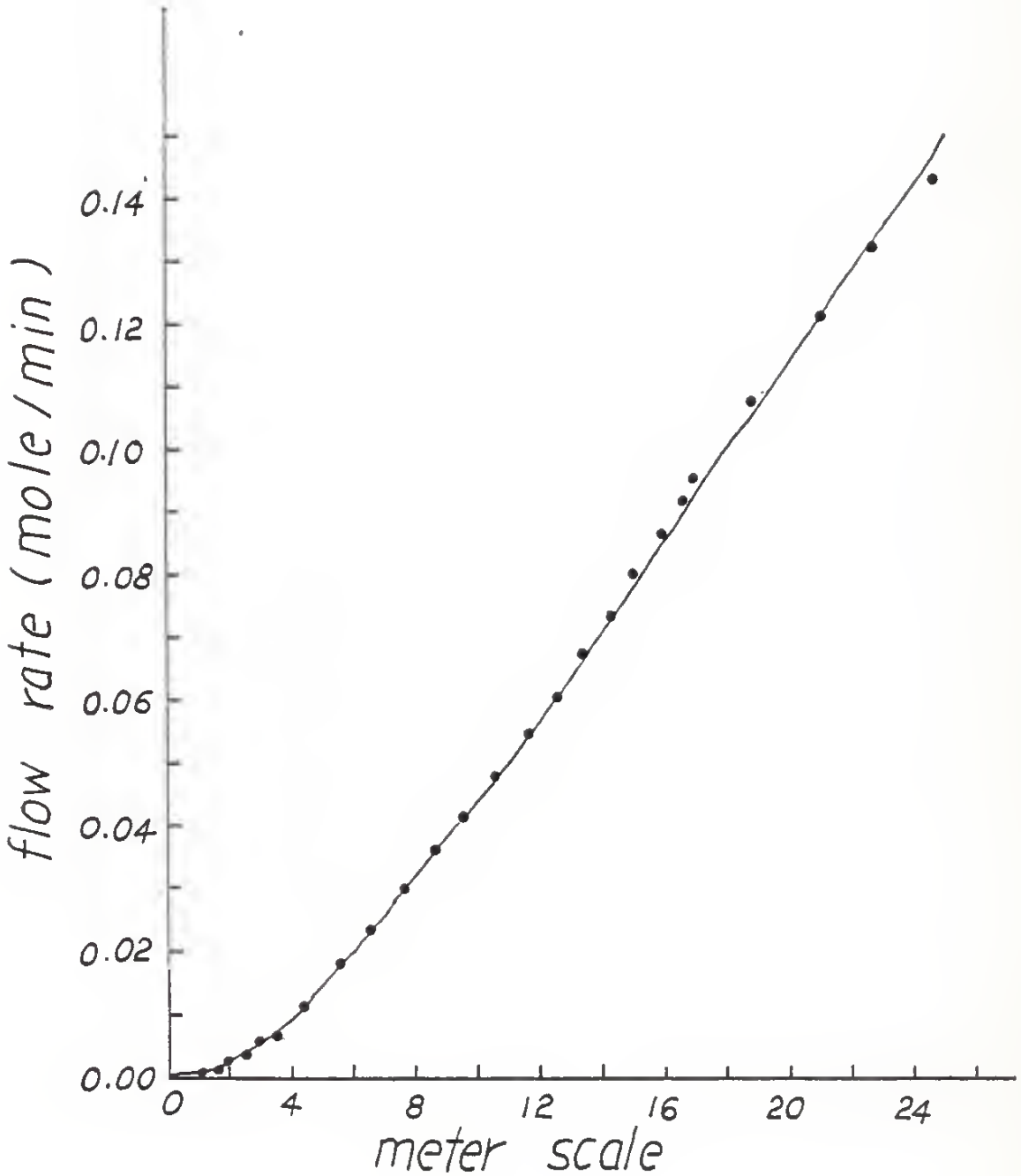
flow rate (mole/min)
0.14
0.12
0.10
0.08
0.06
0.04
0.02
0.00
0
4
8
12
16
20
24
meter scale

operated at ~ 270 V with a resistor of 40 K to give a stable $Ar(^3P_{0,2})$ concentration. The electrodes were 3 cm apart.

The N_2F_4 flow was regulated by a fine needle valve and measured by a calibrated capillary flowmeter; the calibration curve for Ar gas is shown in fig. 2.3. This flow is not critical and only modest effort was used to get this calibration. In Ar* + NF_2 experiments, a 60 cm section of the N_2F_4 line before the Ar*/NF_2 mixing zone heated to 500 K to generate NF_2 radicals by the thermodissociation of N_2F_4. The degree of N_2F_4 dissociation was monitored by the observation of the ArF(C-A)[3] emission band at ~ 260 nm, which is a characteristic emission of N_2F_4 + Ar* reaction. 500 K was found adequate for 100% dissociation. The NF_2 flow was optimized by monitoring the emission intensity of NF(b,0-x,0) transition at 530 nm. Optimum flow rate was ~ 3×10^{-5} mole N_2F_4/min, corresponding to 4×10^{13} molec/cm^3 NF_2 concentration; higher flows did not give more NF(b) because all the Ar* atoms were quenched. This concentration is of the same order of magnitude as that (7×10^{13} molec/cm) used by J. P. Singh[4] for a NF(b) flow reactor of slightly different design in W122 of Kansas State University.

The interactions of $Xe(^3P_2)$ and $He(2^3S)$ with N_2F_4 and NF_2 were also studied as potential NF(b) sources. The Xe metastable atoms were produced by adding a small amount of Xe into Ar stream prior to the discharge. The energy transfer reaction from Ar metastable atoms as well as direct excitation lead to $Xe(^3P_2)$ atoms[5]. The rate constants for $Ar(^3P_{0,2})$ quenching were reported by D. W. Setser[6],[7] and M. A. A. Clyne et al.[7] to be 18×10^{-11} $cm^3molec^{-1}sec^{-1}$ for $Ar(^3P_2)$ and 3×10^{-11} $cm^3molec^{-1}sec^{-1}$ for $Ar(^3P_0)$. Complete quenching of Ar metastable atoms with Xe was checked by adding N_2 downstream of the discharge.

Fig. 2.3 Calibration Curve for the Capillary Flowmeter Used to Measure the N_2F_4 Flow Rate.

The flowmeter was calibrated for Ar. The measurement of N_2F_4 flow by this calibration curve was checked by measuring the pressure drop of N_2F_4 in reservoir after being pumped for a time interval, Δt. The flow rate and $\bar{P}\Delta P$ values were calculated by the equations in Appendix B. The resulting N_2F_4 flow showed ~ 10% deviation from the value given by the Ar calibration curve. The data for this rough check on the next page:

Time (min)	$P_{N_2F_4}$ (cm Hg)	P_{Ave}	ΔP (mm Hg)	ΔP_{ave}	$\bar{P}\Delta P$ (mc Hg)^2	F_{Ar} (10^{-5}mole/min)	F_{exp} (10^{-5}mole/min)
0	7.7		21.6				
		7.2		20.7	12.76	5.88	5.94
90	6.7		19.8				

where F_{Ar} is the value obtained from the calibration curve at $\bar{P}\Delta P$ = 12.76 cm Hg^2 and F_{exp} is the N_2F_4 flow rate obtained experimentally.

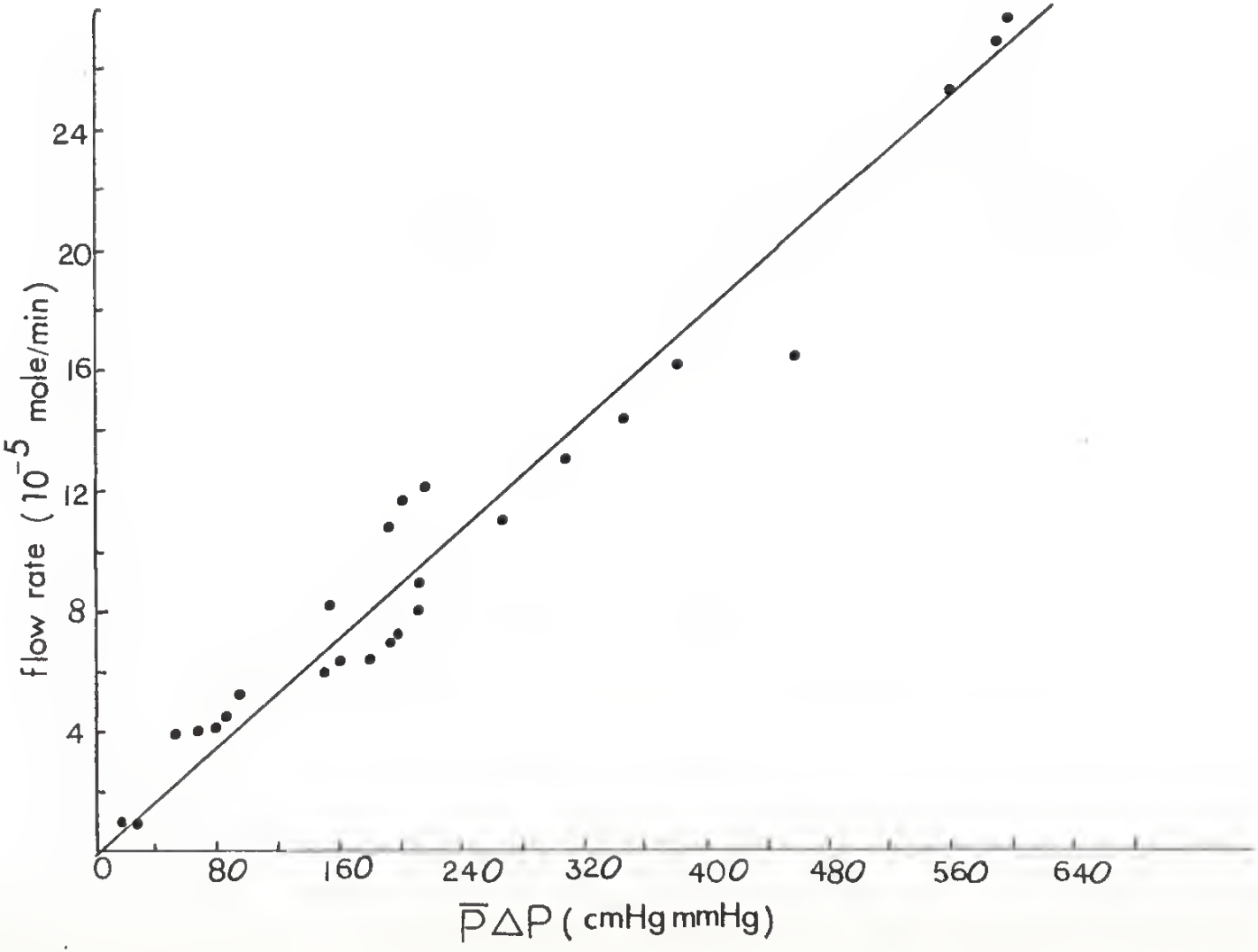
flow rate (10^{-5} mole/min)
24
20
16
12
8
4
0
80
160
240
320
400
480
560
640
$\overline{P}\Delta P$ (cmHg mmHg)

Since residual Ar metastable atoms will give $N_2(C-B)$ from the reaction of Ar* and N_2[7],[8], the disappearance of the $N_2(C,\dot{0}-B,0)$ emission at 3371 Å can be used to find the optimum Xe flow rate. The Xe gas was taken directly from a tank and the flow was regulated by a needle valve. He metastable atoms were prepared by passing He through hollow cathode discharge.

The emissions of N_2F_4 and NF_2 with Ar*, Xe* and He* from 2000 Å to 6000 Å were investigated with a monochromator described in the section "Spectroscopic Studies".

The flows of reagents used for study of NF(b) quenching were measured wtih a carefully calibrated flowmeter (Fig. 2.4). The gas handling of reagents and N_2F_4 and the calibration of the reagent flowmeter are discussed in the following sections: "Kinetic Studies", "Handling of N_2F_4" and "Calibration of Capillary Flowmeter".

Spectroscopic Studies

To study the emissions from reactions of Ar*, Xe* and He* atoms with NF_2/N_2F_4, a 0.3 m Czerny-Turner type monochromator (McPherson, Model 218) was used. This monochromator also was used to characterize the NF(b-X) emission. A 1200 grooves/mm grating blazed at 300 nm as the dispersing element, gave a reciprocal linear dispersion of 26.5 Å/mm. For 10 μm slits the resolution is then 0.6 Å. The dispersed light was detected by a RCA 31034 photomultipler tube and the signals from PMT were measured by a SSR1105 photon counter after transmitted through a discriminator. The analog output from the photon counter was fed into a

Fig. 2.4 Calibration curve of the capillary flowmeter used for measuring the flows of quenching reagents

The pressure ranged from 700-90 torr of Ar and ΔP was 2.5 to 15 torr during the calibration. The flow rates given by the calibration curve need to be corrected by the viscosity coefficient for pure gas flows. The uncertainty caused by this correction is ~ 10% as shown in Appendix B.

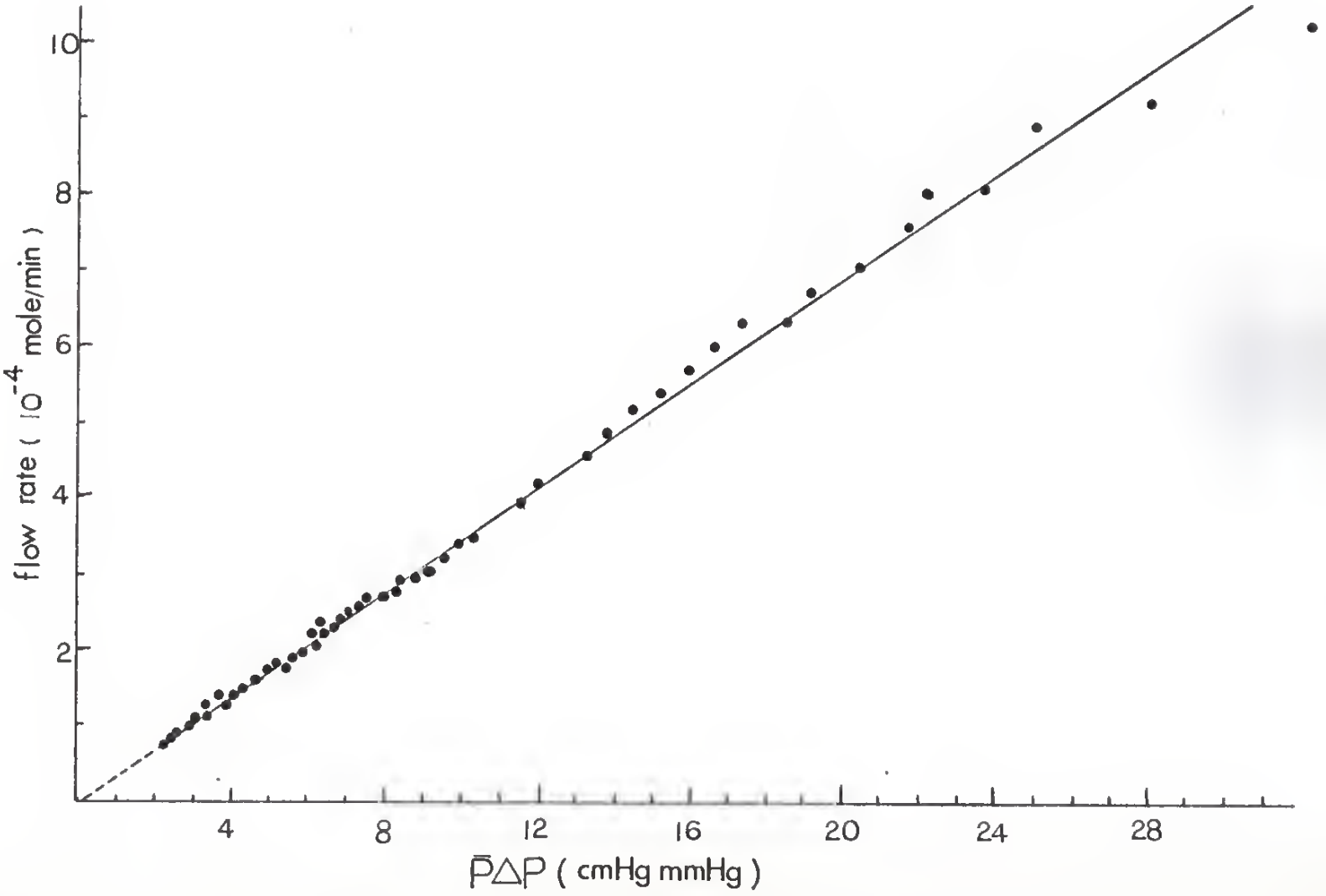
flow rate (10^{-4} mole/min)
10
8
6
4
2
4
8
12
16
20
24
28
$\bar{P}\Delta P$ (cmHg mmHg)

strip chart recorder to generate spectra. The spectral response of the detecting string (monochromator, grating, and PMT) was calibrated from 2000 Å to 8500 Å using a D_2 lamp (Optronic Lab. Inc., Model UV-40) and a quartz-I_2 lamp (Optronic Lab. Inc., Model 2451C) as standards. Three polynomials were fitted by a computer program[9] to describe the response curve (Fig. 2.5) of the detecting system in three different wavelength ranges.

The $\Delta v = 1, 0, -1$ sequences of the NF(b-X) emission were studied by slowly scanning (12.5 Å/min and 50 Å/min) with 200 μm wide slits. A back mirror was placed behind the observing window to increase the signal intensities. The band pass was calculated based on eq. 2.1[10] to be 5.3 Å for 200 μm slits, which was sufficient to give the band maximum positions of the vibrational transitions.

band pass = slit width x reciprocal linear dispersion (eq 2.1)

Kinetic Studies -- Measurements of Quenching Rate Constants

The NF(b) quenching rate constants were measured by recording the NF(b-X) emission along the flow tube for several constant quencher concentrations or by the fixed point method, in which Δt was held constant and [Q] was varied. The data were analyzed by pseudo first order kinetics. Details of how data were obtained and reduced to rate constant are discussed in "Model of Calculating Rate Constants". Here the apparatus design is summarized.

Fig. 2.5 Response curve of the monochromator detection system

The detecting string included 0.3 m McPherson monochromator, grating, and RCA 31034 PMT. The polynomials fitted for the curves are:

(a) 200-310 nm

$$R(\lambda) = 9.15958 - 0.111407\lambda + 0.431874 \times 10^{-3}\lambda^2 - 0.515566 \times 10^{-6}\lambda^3$$

(b) 310-500 nm

$$R(\lambda) = -0.133232 \times 10^{-2} + 0.992624 \times 10^{-1}\lambda - 0.224860 \times 10^{-3}\lambda^2 + 0.165320 \times 10^{-6}\lambda^3$$

(c) 500-850 nm

$$R(\lambda) = 0.880674 + 0.317821 \times 10^{-2}\lambda - 0.101136 \times 10^{-4}\lambda^2 + 0.629814 \times 10^{-8}\lambda^3$$

The polynomials (a) and (b) were saved in program IL1N1 for spectrum correction from 200-500 nm and (b) and (c) were recorded in program IL1N2 for the spectral range 310-850 nm.

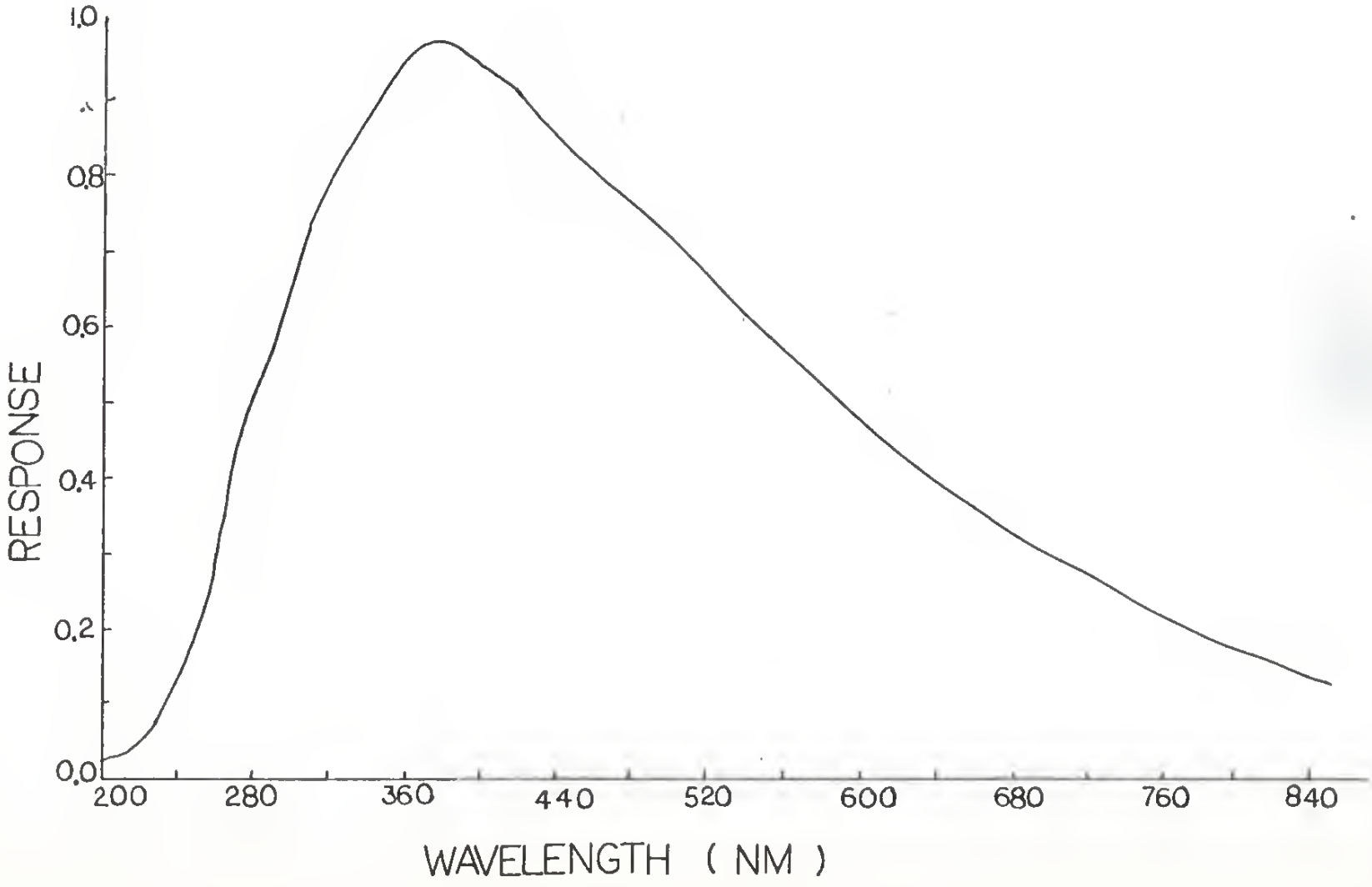
1.0
0.8
0.6
0.4
0.2
0.0
RESPONSE
200
280
360
440
520
600
680
760
840
WAVELENGTH (NM)

A Hammamatsu R212 photomultiplier tube, seated in a homemade movable aluminum housing was used as a movable detector[11]. An interference filter (Ealing, 35-3607) of 10 nm band pass centered at 530 nm was set in front of PMT to eliminate undesired emission and scattered light. The uncertainty in the distance from reagent inlet to the observing point was reduced by putting a 4 mm slit in front of the filter. The signal from the PMT tube is a dc current and was measured by an electrometer (Keithley Instruments, Model 610B) and recorded by a strip chart recorder.

Most of the quenching rate constants were measured with the fixed point method. The variation of the NF(b-X) emission intensity with quenching reagent concentration was monitored while the detector was at the same position. The concentrations of reagent varied from 10^{12}molec/cm^3 to 10^{14}molec/cm^3. Usually the detector was placed at 35.5 cm downstream of the reagent inlet, corresponding to about 21 msec for a typical pumping speed of 15-17 m/sec. To determine the uncertainty of the plug flow assumption, the rate constants for CH_3Cl were measured by fixed point method with the detector at 10.5, 19, 23,7, 27.1 and 35.5 cm downstream of the reagent inlet. The resulting rate constants are within 10% of each other.

The fixed point method is not ideal for every situation. Moving detector technique was appplied to measure the quenching of NF(b) by the wall of flow tube, the radiative lifetime of NF(b), and the quenching by NF_2. This method was also used to double check abnormal kinetics of H_2 and the Br_2 which had an especially large rate constant.

Because of the required high concentrations, pure reagents were used for most of the experiments, except for Cl_2 and Br_2. Correction of

the apparent flow rate by the viscosity coefficients for Ar vs that of the reagents was therefore necessary. Cl_2 and Br_2 were done at low concentration in Ar, 1.64% and 1.51% respectively, and the direct calibration for Ar is satisfactory for these cases.

To purify HCl, HBr, CF_3NO, Cl_2, CF_3Br, CH_3Cl and CH_3Br, fractional vaporization[12] was used. In this method the middle one-third of the liquid sample was vaporized and stored while the first and the third fractions were discarded. N_2F_4 was purified by pumping out the most volatile portion and storing the rest of the liquified sample. H_2, D_2, CO_2, NO, O_2, CO, and CH_4 were loaded directly from Matheson tank without undergoing further purification. The reagents were stored in Pyrex bulbs and metered to the flow reactor.

Handling of N_2F_4

N_2F_4 is a very reactive chemical of unknown toxicity;[13] and great care must be taken when handling it. Since N_2F_4 is a strong oxidizer[13], fuel such as H_2 may react with N_2F_4 vigorously if both are of high concentration. Generally, large amounts of inert diluent were used as recommended[14] to carry N_2F_4 through the pump structures and oil; however, in some instances about 100 torr of N_2F_4 was pumped out without any dilution, when preparing the N_2F_4 sample. Frequent change of pump oil was performed (about every two weeks) if N_2F_4 was being used intensively. Kwok[14] reported passing the unused N_2F_4 through a 200°C charcoal trap to give CF_4 as a method of removing N_2F_4. This setup was not empoloyed in our flow system shown in fig. 2.1 since we are only

working with very low N_2F_4 concentration (10^{13} molec/cm^3) in the flow tube comparing to that of argon carrier gas (10^{16} molec/cm^3). The reactivity of N_2F_4 with the reagents is not a general problem when measuring the quenching rate of NF(b) because both are of relatively low concentration compared to argon and the thermal explosive reaction never develops.

The maximum N_2F_4 storage period without severe decompsotion in glass reservoirs seemed to be about 7 to 10 days. Decomposition of N_2F_4 were observed both in glass containers and stainless steel tanks, after stored in tank for more than one year. The decomposed product, a light pink liquid when condensed by liq. N_2 is more volatile than N_2F_4. The separation of N_2F_4 and its decomposed product is thus possible.

The most likely impurity in the tank N_2F_4 is N_2, and N_2F_4 was purified by pumping away the uncondensable impurity and the most volatile portion of the frozen sample from the tank N_2F_4. The dark blue liquid N_2F_4 was then vaporized into the reservoir. It would be a good idea to passivate the reservoir either by N_2F_4 or F_2 before N_2F_4 is stored, especially for those reservoirs previously storing hydrocarbons. In our laboratory, decomposition of N_2F_4 also gave a brown gas and light brown polymers by unknown reactions after being stored in glass reservoir for more than one month.

N_2F_4 is known to be in equilibrium with NF_2 at room temperatures; however, the concentration of NF_2 is low. The thermodynamic properties of N_2F_4 are discussed in Chapter 3.

Calibration of Capillary Flowmeter

Capillary flowmeters (fig. 2.6) were used to measure the flow rate of quenching reagents and N_2F_4. For gas flowing through a capillary tube with constants flow rate, Poiseulla's formula can be expressed as eq. 2.2[15],[16]. For the same capillary tube, a and L are constants

$$F = \frac{a^4(\bar{P}\Delta P)}{8\ \eta\ RTL} \qquad \text{(eq. 2.2)}$$

where F: mole/sec, gas flow rate

a: cm, radius of capillar tube

R: $erg^{-1}sec^{-1}mol^{-1}$, gas constant

T: K, temperature

P_2: $dyne/m^2$, pressure in reservoir

P_1: $dyne/m^2$, pressure at the other end of capillary tube

$\bar{P}$: $dyne/me^2$, average pressure $\frac{P_1 + P_2}{2}$

ΔP: $dyne/m^2$, pressure difference between two ends of capillary tube, P_2-P_1

L = cm length of capillary tube

η = $gcm^{-1}sec^{-1}$ viscosity coefficient of gas

and eq. 2.2 is reduced to eq. 2.3. As shown in eq. 2.3, F is a linear

$$F = (\frac{a^4}{8\eta RTL})\bar{P}\Delta P$$

$$F = k\bar{P}\Delta P \qquad \text{(eq. 2.3)}$$

Fig. 2.6 Capillary Flowmeter

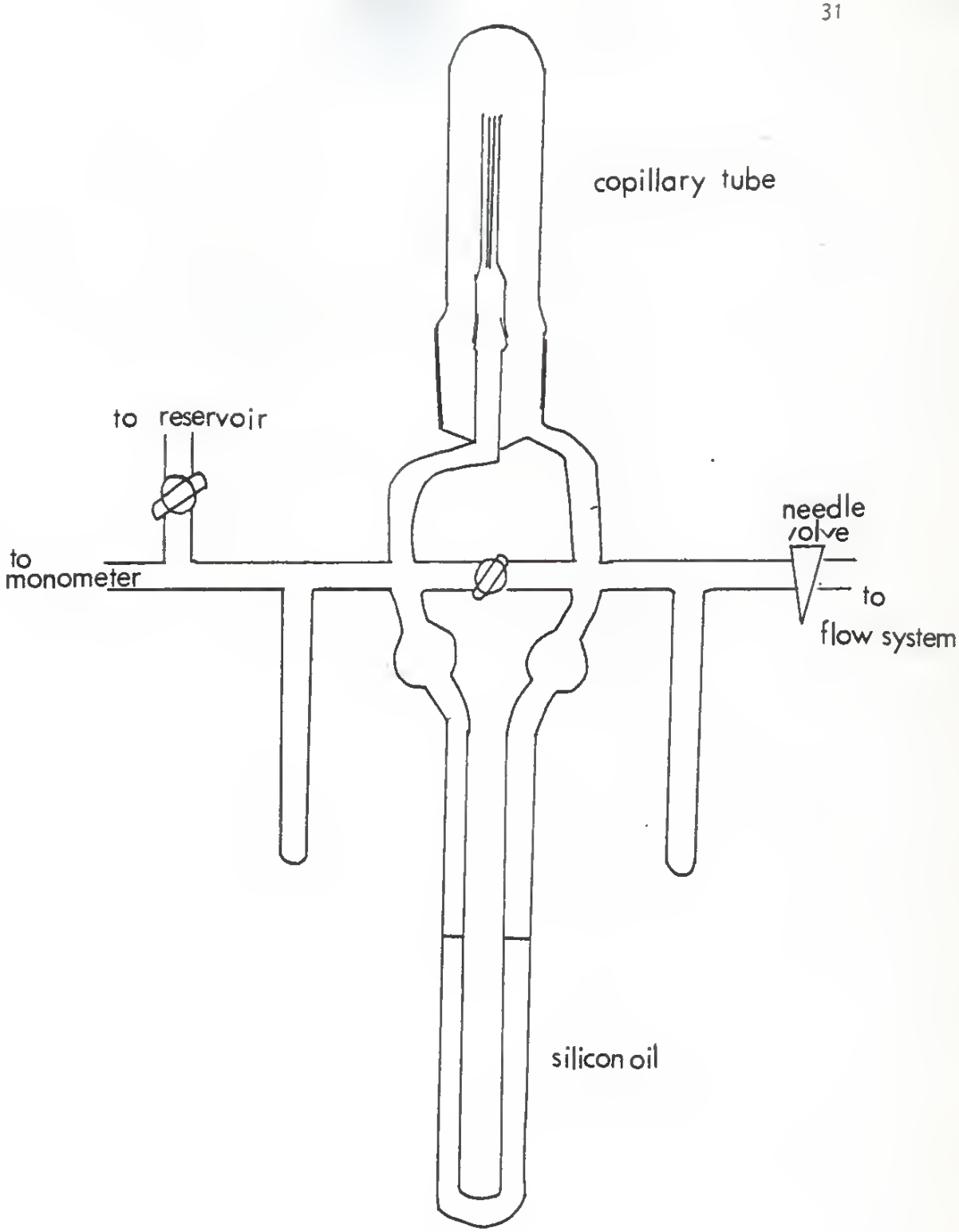
copillary tube
to reservoir
needle valve
to monometer
to flow system
silicon oil

function of $\bar{P}\Delta P$. Thus, the flow rate can be determined by measuring the $\bar{P}\Delta P$ value provided a calibrated working curve of F vs $\bar{P}\Delta P$ plot is given.

The construction of capillary flowmeter is shown in fig. 2.6. The capillary tube was attached to a standard ground joint and interchangable for various flow rate ranges. The stopcock of the flowmeter was closed during the measurements so that the reagent was pumped through the capillary tube. Flow rate was regulated by a needle valve after the flowmeter. The pressure difference, ΔP, between both ends of capillary tube was measured by a U-tube oil monometer. The silicon oil used was Dow Corning 704 diffusion pump oil (D=1.07 at 25°C). The pressure at the reagent reservoir side, P_2, was measured by a mercury U-tube monometer while the pressure at the other end, P_1, was calculated by $P_1 = P_2 - \Delta P$. The average pressure, $\bar{P}$, was therefore calculated by $\bar{P} = \frac{2P_2 - \Delta P}{2}$ and eq. 2.3 becomes:

$$F = k\left(\frac{2P_2 - \Delta P}{2}\right)\Delta P \qquad \text{(eq. 2.4)}$$

The flow rate of a gas pumped through the flowmeter from a calibrated volume can be calculated by eq. 2.5 assuming the ideal gas law is obeyed.

$$F = \frac{\Delta n}{\Delta T} \qquad \text{(eq. 2.5)}$$

$$= \frac{v\Delta P_2}{RT\Delta t}$$

where R is the gas constant, v is the volume of gas reservoir, ΔP_2 is the pressure drop in the reservoir and Δt is the time interval for ΔP_2.

With eq. 2.3 and 2.5, the calibration of a capillary flowmeter can be done by calcuating the flow rate using eq. 2.5 and plotting F vs. $\bar{P}\Delta P$ if Δt's are measured for a constant ΔP. However, ΔP depends very much on the back pressure (P_2) for a given needle valve setting. It's difficult to keep constant ΔP for a time interval Δt when a pressure drop, ΔP_2, was measured. Therefore a modification on eq. 2.5 is necessary (eq. 2.6). Fig. 2.7 is a plot of $\frac{1}{p}$ vs. t of the flowmeter for quencher flow rate measurement; it shows that $\frac{1}{P}$ and t are of good linearity within small t range although the whole curve is not a perfect

$$F = \frac{v}{RT}\frac{\Delta P}{\Delta t}$$

$$= \frac{v}{RT}\frac{dP}{dt}$$

$$= -\frac{V}{RT}P^2\frac{d(\frac{1}{P_2})}{dt} \qquad \text{(eq. 2.6)}$$

straight line. The back pressure (P_2) can be predicted by the $1/P_2$ vs. t plot for a given t when ΔP was read. The flow rate was calculated by eq. 3.6 with $d(\frac{1}{P_2})/dT$ being the slope of the plot at point $(t, \frac{1}{P_2})$. $\bar{P}\Delta P$ was calculated by eq. 2.7. The final calibration curves,plotted by F

$$\bar{P}\Delta P = (\frac{2P_2-\Delta P}{2})\Delta P \qquad \text{(eq. 2.7)}$$

vs. $\bar{P}\Delta P$, for the flowmeter measuring the flow rate of N_2F_4 and quenching reagents are shown in fig. 2.4 and fig. 2.3 respectively.

Fig. 2.7 Plot of $\frac{1}{P}$ vs. t for capillary flowmeter measuring the reagent flow rate

The volume of the reservoir was measured by gas expansion technique using ideal gas law assumption.

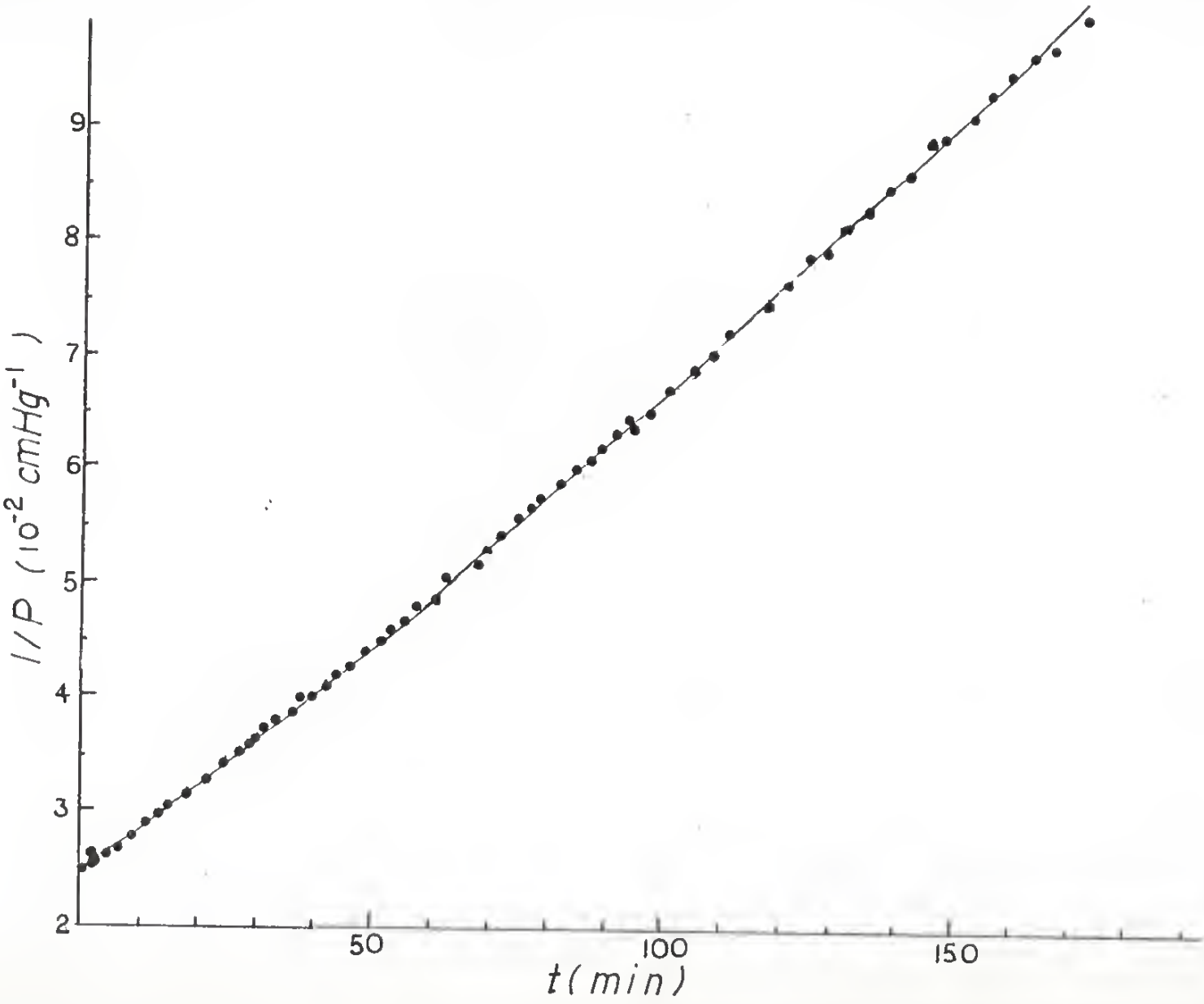
1/P (10^-2 cmHg^-1)
9
8
7
6
5
4
3
2
50
100
150
t(min)

The calibrations were done using Ar. For dilute mixture (< 15%) of reagent in the argon, the flow rate of a given $\bar{P}\Delta P$ value can be read directly from the calibration curves. But for concentrated mixtures or pure reagents, the gas viscosity must be used to connect the Ar calibration to that for the gas in question by eq. 2.8 derived from eq.

$$F_{reagent} = F_{argon} \times \frac{\eta_{argon}}{\eta_{reagent}} \qquad \text{(eq. 2.8)}$$

2.3. The viscosity coefficients of the quenching reagents used in this work are listed in Appendix A; correction of reagent flow rates by eq. 2.8 has an uncertainty of ~ 10% (Appendix B).

References:

1. J. H. Kolts and D. W. Setser, Reactive Intermediates in the Gas Phase, Chapter 3, Academic Press, Inc., New York, 1979.
2. D. W. Setser, D. H. Stedman and J. A. Coxon, J. Chem. Phys., 53, 1004, 1970.
3. J. H. Kolts and D. W. Setser, J. Phys. Chem., 82, 1766, 1978.
4. J. P. Singh and D. W. Setser, unpublished work, Chem. Dept., Kansas State Univ.
5. D. H. Stedman and D. W. Setser, J. Chem. Phys., 52, 3957, 1970.
6. L. G. Piper, J. E. Velazco and D. W. Setser, J. Chem. Phys., 59, 3323, 1973.
7. L. G. Piper, D. W. Setser and M. A. A. Clyne, J. Chem. Phys., 63, 5018, 1975.
8. E. S. Fishburn, J. Chem. Phys., 47, 58, 1967.
9. P. Bevington, Data Reduction and Error Analysis for Scientific Application, McGraw-Hill Book Co., 1969.
10. H. H. Willard, L. L. Merritt, J. A. Dean, and F. A. Settle, Instrumental Methods of Analysis, p. 39, 6th Ed., Litton Educational Publishing, Inc., 1981.
11. J. A. Meyer, Ph.D. Thesis, p. 23, Chem. Dept., Kansas State Univ., Manhattan, KS, 1969.
12. H. Melville, and B. G. Gowenlock, Experimental Methods in Gas Reaction, p. 170 MacMillan & Co., Ltd., 1964.
13. N_2F_4 gas Analysis Report, Hercules Inc., 1975.
14. Private communication, M. Kwok, The Aerospace Corporation, 1978.
15. H. Melville and B. G. Gowenlock, Experimental Methods in Gas Reactions, p. 109, MacMillan & Co., Ltd., 1964.

16. J. A. Meyer, Ph.D. Thesis, p. 8, Chem. Dept., Kansas State University, Manhattan, KS, 1969.

CHAPTER 3. EXPERIMENTAL CHARACTERIZATION OF THE NB(b) SOURCE

Introduction

The existence of the $N_2F_4 \rightleftharpoons 2NF_2$ thermoequilibrium[1] makes it necessary to evaluate the N_2F_4 and NF_2 concentrations at the experimental conditions used for generating the NF(b) radicals. Furthermore, the quenching behavior of Ar* and NF(b) by NF_2 and N_2F_4 are expected to be different, since NF_2 is a radical but N_2F_4 is a neutral closed-shell molecule[2]. Even if N_2F_4 is dissociated in the heated zone, the recombination of NF_2 to N_2F_4 along the flow tube must be considered, since the reactor section of the flowing afterglow operated at room temperature. Fortunately, the thermochemistry and kinetics of the N_2F_4/NF_2 + Ar system are known and we can evaluate the expected characteristics which are confirmed by experiment. The Ar* + NF_2 reaction is the preferred NF(b) source and the complete thermal dissociation of N_2F_4 can be achieved. Hence NF_2 is the source species for our experiments.

This chapter reviews the thermodynamic and kinetic properties of $N_2F_4 \rightleftharpoons 2NF_2$; this is followed by a description of the reactions which were investigated as NF(b) sources and a complete characterization of the best source, NF_2 + Ar($^3P_{0,2}$). The NF(b-X) spectra are discussed and the vibrational distribution of NF(b) is characterized. The model for quenching kinetics is presented in the last section and the quenching data are given in Chapter 4.

Thermodynamic and Kinetic Properties of $N_2F_4 \rightleftharpoons 2NF_2$ in a Flowing Afterglow System

N_2F_4 is in equilibrium with NF_2 via the reaction:

$$N_2F_4(g) \overset{K_p}{\rightleftharpoons} 2NF_2(g) \quad \Delta H^\circ_{298} = 20.9 \pm 0.4 \text{ kcal mol}^{-1} \text{ (3)} \qquad \text{(Rxn. 3.1)}$$

Evans and Tschuikow-Roux determined the heat of formation of N_2F_4 and NF_2 to be -5.3 ± 1.4 and 7.8 ± 1.0 kcal mol^{-1}, respectively[3]. The $D(NF_2\text{-}NF_2)$ and D(N-F) in N_2F_4 were then calculated to be 20.9 and 70.5 kcal mol^{-1}, respectively. The temperature dependence of K_p in rxn. 3.1 has been studied and Evans and Tschuikow-Roux showed that K_p followed a Van't Hoff plot (fig. 3.1)[3]. The linear extrapolation of fig. 3.1 predicts K_p values of $10^{-6.013}$ atm at 300 K and $10^{0.108}$ atm at 500K. The extent of dissociation for a system containing N_2F_4 is related to K_p and the initial pressure of N_2F_4, P_0, by eq. 3.2 or by eq. 3.2' based on rxn. 3.1

$$\alpha_{eq} = \frac{-K_p + (K_p^2 + 16K_pP_0)^{1/2}}{8P_0} \qquad \text{eq. 3.2}$$

$$\alpha_{eq} = \left(\frac{K_p}{P_t + K_p}\right)^{1/2} \qquad \text{eq. 3.2'}$$

where α_{eq} is the percentage of dissociation at equilibrium and P_t is the total pressure of N_2F_4 and NF_2. Since K_p is a function of temperature, α depends on both temperature and $P_0(P_t)$. For instance, α_{eq} is 0.15%

Fig. 3.1 Van't Hoff Plot for $N_2F_4 \overset{K_p}{\rightleftharpoons} 2\ NF_2$ Reaction

The units for K_p and T are atm and K, respectively. Data were taken from ref. 3, the K_p values at 300 K and 500 K were obtained by extrapolation.

$$K_p = 9.71 \times 10^{-7} \text{ atm at } 300 \text{ K}$$

$$K_p = 1.28 \text{ atm at } 500 \text{ K}$$

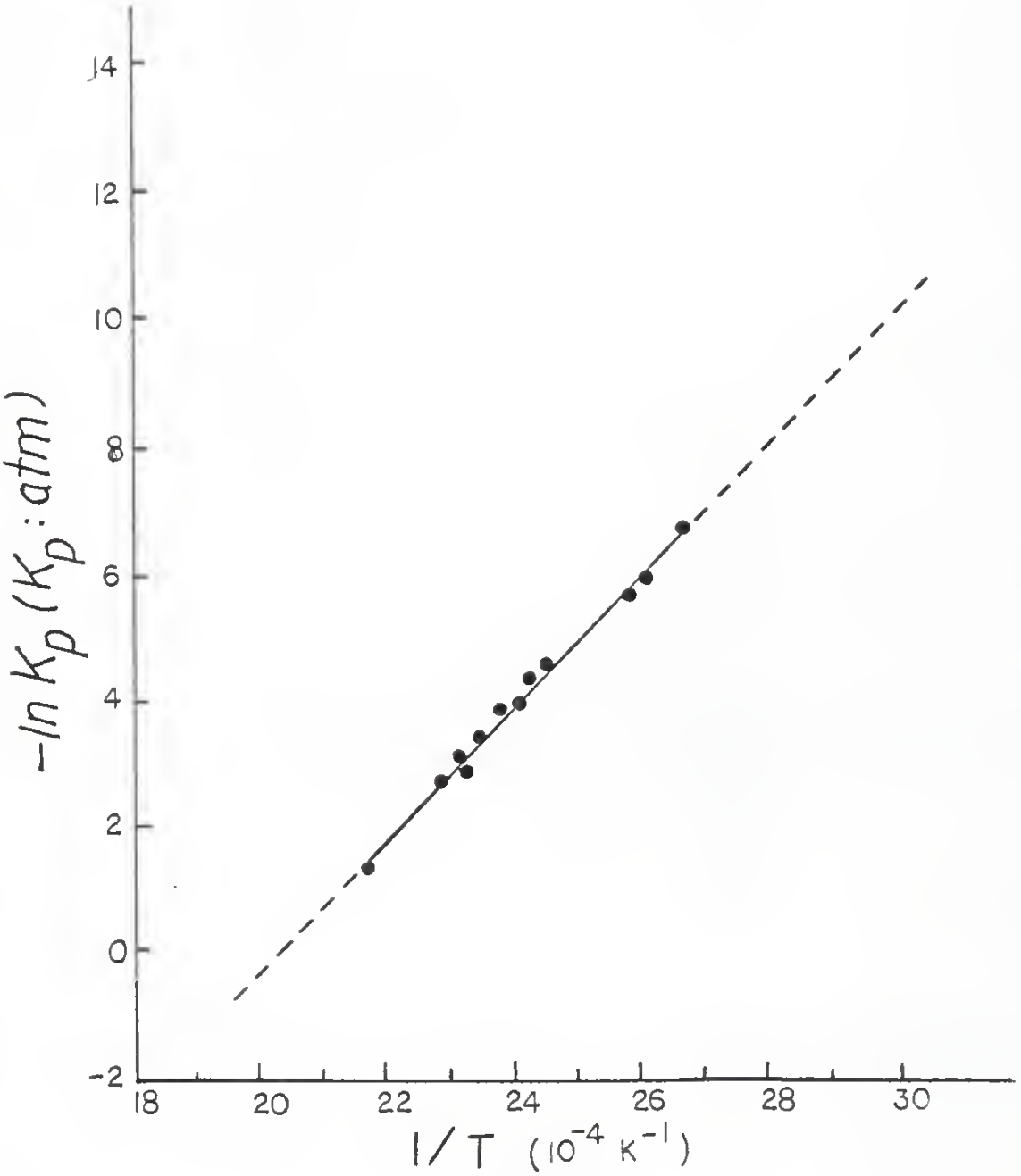
14
12
10
8
6
4
2
0
-2
18
20
22
24
26
28
30
$-\ln K_p\ (K_p : atm)$
$1/T\ (10^{-4}\ K^{-1})$

for P_o = 100 torr and 1.10% for P_o = 1.5 torr at 300 K, while α_{eq} equals 76.2% and 99.4% for P_o = 100 and 1.5 torr at 500 K. For a total pressure of 1.5 torr at equilibrium about 2.22% and 99.92% of the original N_2F_4 are dissociated at 300 K and 500 K, respectively. Clearly, at room temperature N_2F_4 is the dominant species in the N_2F_4 reservoir and at reagent inlet, since P_o is typically 100 and 1.5 torr at these two positions. After entering the flow tube with 1.5 torr Ar, the pressure of N_2F_4 changes from 1.5 torr to ~ 10^{-3} torr and α_{eq} would be ~ 35% (by eq. 3.2) for such a low N_2F_4 pressure even at 300 K. Thus, the rate of dissociation of N_2F_4 becomes the dominant consideration for evaluating the concentration at mixing zone.

The kinetics of N_2F_4 dissociation in Ar has been determined to be second order for pressure lower than 2 atm[4],[5] and is represented by:

$$Ar + N_2F_4 \underset{k_{recomb}}{\overset{k^\circ_{bi,Ar}}{\rightleftharpoons}} 2NF_2 + Ar \qquad \text{(rxn. 3.3)}$$

$$k^\circ_{bi,Ar}(M^{-1}sec^{-1}) = 10^{13.56}e^{-(15300 \pm 600)/RT} \qquad \text{(rxn. 3.4)}$$

In the flow tube, Ar is of large excess and pseudo first order kinetics for rxn. 3.3 is approached. The differential and integrated rate laws for rxn. 3.3 are shown as following under the assumption of pseudo first

$$\frac{-d[N_2F_4]}{dt} = k^\circ_{bi,Ar}[Ar]\,[N_2F_4] = k_d\,[N_2F_4] \qquad \text{(eq. 3.5)}$$

$$\text{where } k_d = k^\circ_{bi,Ar}[Ar] \qquad \text{(eq. 3.6)}$$

$$\ln \frac{[N_2F_4]_t}{[N_2F_4]_o} = -k_d \Delta t \qquad \text{(eq. 3.7)}$$

order kinetics. The half time for the forward reaction of rxn. 3.3 can be calculated by eq. 3.8:

$$\Delta t_{1/2} = \frac{\ln 2}{k_d} \qquad \text{(eq. 3.8)}$$

For 1.5 torr Ar, k_d is 0.024 sec^{-1} and $\Delta t_{1/2}$ will be 28.9 sec. Compared with the resident time, ~ 20 msec, of N_2F_4 in the flow tube and perhaps 0.2 msec from the reagent inlet to the Ar* mixing zone, there can be almost no dissociation of N_2F_4. We can conclude that at 300 K and for our system, N_2F_4 will be the major species in the mixing zone, and the reaction under observation would be $N_2F_4 + Ar^*$.

Next consider the situation where N_2F_4 is thermally dissociated at 500 K and then added to the reactor which is at 300 K. Will N_2F_4 be totally dissociated in the heated zone and will there be recombination in the flow reactor? The dissociation rate constant of N_2F_4 was reported to be 1.8 times of that by Ar[5]. The second order kinetics in the furnace are as following:

$$N_2F_4 + N_2F_4 \underset{k_{recomb}}{\overset{k^\circ_{bi,N_2F_4}}{\rightleftharpoons}} 2NF_2 + N_2F_4 \qquad \text{(rxn. 3.9)}$$

$$k^\circ_{bi,N_2F_4} = 1.8\ k^\circ_{bi,Ar} \qquad \text{(rxn. 3.10)}$$

$$\frac{1}{[N_2F_4]_t} - \frac{1}{[N_2F_4]_o} = k^\circ_{bi,\ N_2F_4}\ \Delta t \qquad \text{(rxn. 3.11)}$$

$$\Delta t_{1/2} = \frac{1}{[N_2F_4]_0 \, k^{\circ}_{bi,\ N_2F_4}} \qquad \text{(eq. 3.11)}$$

In the present apparatus, the heated zone started after the needle valve and the pressure should be of the same order of magnitude as in flow tube; therefore, P_o = 2 torr. The $k^{\circ}_{bi,\ N_2F_4}$ value is given by eq. 3.4 and 3.10 as 2.46 x 10^{-14} $cm^3 molec^{-1} sec^{-1}$ at 500 K and the half time, $\Delta t_{1/2}$, is 0.63 msec (eq. 3.11). The flow rate of N_2F_4 was optimized at ~ 3 x 10^{-5} mole/min which corresponds to a flow speed of 7.79 cm^3/sec for 2 torr N_2F_4 at 500 K, provided that the ideal gas law is obeyed. For the 7 mm i.d. and 60 cm long heated zone, the resident time of N_2F_4 is 3.0 sec which is longer than $\Delta t_{1/2}$ and complete dissociation of N_2F_4 was obtained; this agrees with the experimental results. The NF_2 radicals then enetered the reactor at room temperature with partial pressure of NF_2 ~ 10^{-3} torr in the flow tube. The recombination of NF_2 in Ar is a third order reaction[6]. The recombination rate of NF_2 is characterized by eq. 3.12, with large excess of Ar. The rate constant, k_{recomb}, is (1.26 ± 0.15) x 10^{-32} $cm^6 molec^{-2} sec^{-1}$ at 298 K. For the

$$\frac{-d[NF_2]}{dt} = k_{recomb} [Ar][NF_2]^2$$

$$= k'_{recomb} [NF_2]^2$$

$$\frac{1}{[NF_2]_t} - \frac{1}{[NF_2]_0} = k'_{recomb} \Delta t$$

$$\Delta t_{1/2} = \frac{1}{k'_{recomb}} \frac{1}{[NF_2]_0} \qquad \text{(eq. 3.12)}$$

flow system with 1.5 torr Ar and 10^{-3} torr NF_2, the half time of NF_2 is 164 sec, which is much longer than the 20 msec resident time of NF_2 in flow tube. Hence, Ar*, Ar and NF_2 are the only reagents entering the reactor and flow tube, and NF(b) and other products are generated by the NF_2 + Ar* reaction.

Experiments were done to prove the above conclusions of N_2F_4 + Ar* at 300 K and NF_2 + Ar* at 500 K which were derived mainly by "working on scratch paper". The N_2F_4 + Ar* reaction gives ArF(C-A)[7], ArF(B-X)[7] and NF(b-X) emissions (fig. 3.2). Increasing the temperature had opposite effects on the NF(b-X) and ArF(C-A) emission intensities (fig. 3.3, 3.4); the $\frac{NF(b-X)}{ArF(C-A)}$ ratio increased with increasing temperature (Tab. 3.1) and ArF(C-A) eventually disappeared when the temperature was 500 K. Therefore, we can conclude that more than 99% of N_2F_4 was dissociated at 500 K. The disappearance of the ArF(C-A) emission hereafter will be used as an indicator of total dissociation of N_2F_4. We conclude that NF_2 is the only precursor of NF(b) radicals in the 500 K experiments.

The dissociation of N_2F_4 at the mixing zone was also investigated with the ArF(C-A) and NF(b-X) emission. Same total pressures but different concentrations of N_2F_4/Ar mixtures were used at room temperature. These mixtures were prepared in such a way that the α_{eq} values in the reservoir were more or less equal, but fairly large change in α_{eq} would occur at the reagent inlet and mixing zone if the

Fig. 3.2 Spectrum of N_2F_4 + $Ar(^3P_{2,0})$ at Room Temperature

The spectrum was obtained by a 0.3 McPherson monochromator; the data were stored in Dec-tape of digital computer PDP-8 and the response function was applied prior to plotting. The ArF(C-A) band is observed at ~ 260 nm and NF(b-X) is at 530 nm. The bands at ~ 327 nm are N_2(C-B) emission from impurity N_2 in the N_2F_4 sample.

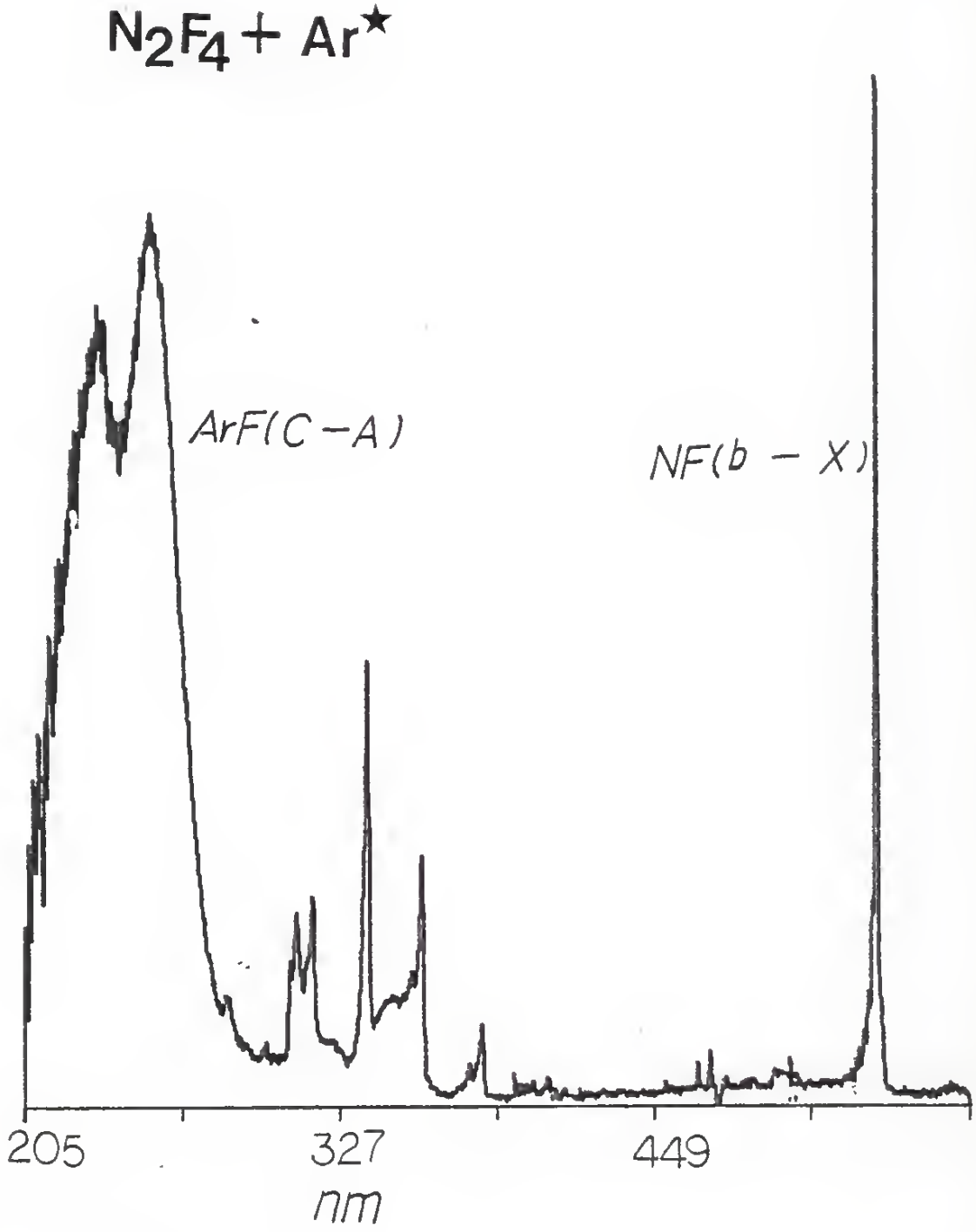
$N_2F_4 + Ar^*$
ArF(C−A)
NF(b − X)
205
327
449
nm

Fig. 3.3 Temperature Dependence of ArF(C-A) Emission

The intensity decreases with increasing temperature in the N_2F_4 flow line and finally disappears when the temperature is above 500K. The detecting system is the same as fig. 3.2. Spectra were stored on Dec-tape and corrected for λ response.

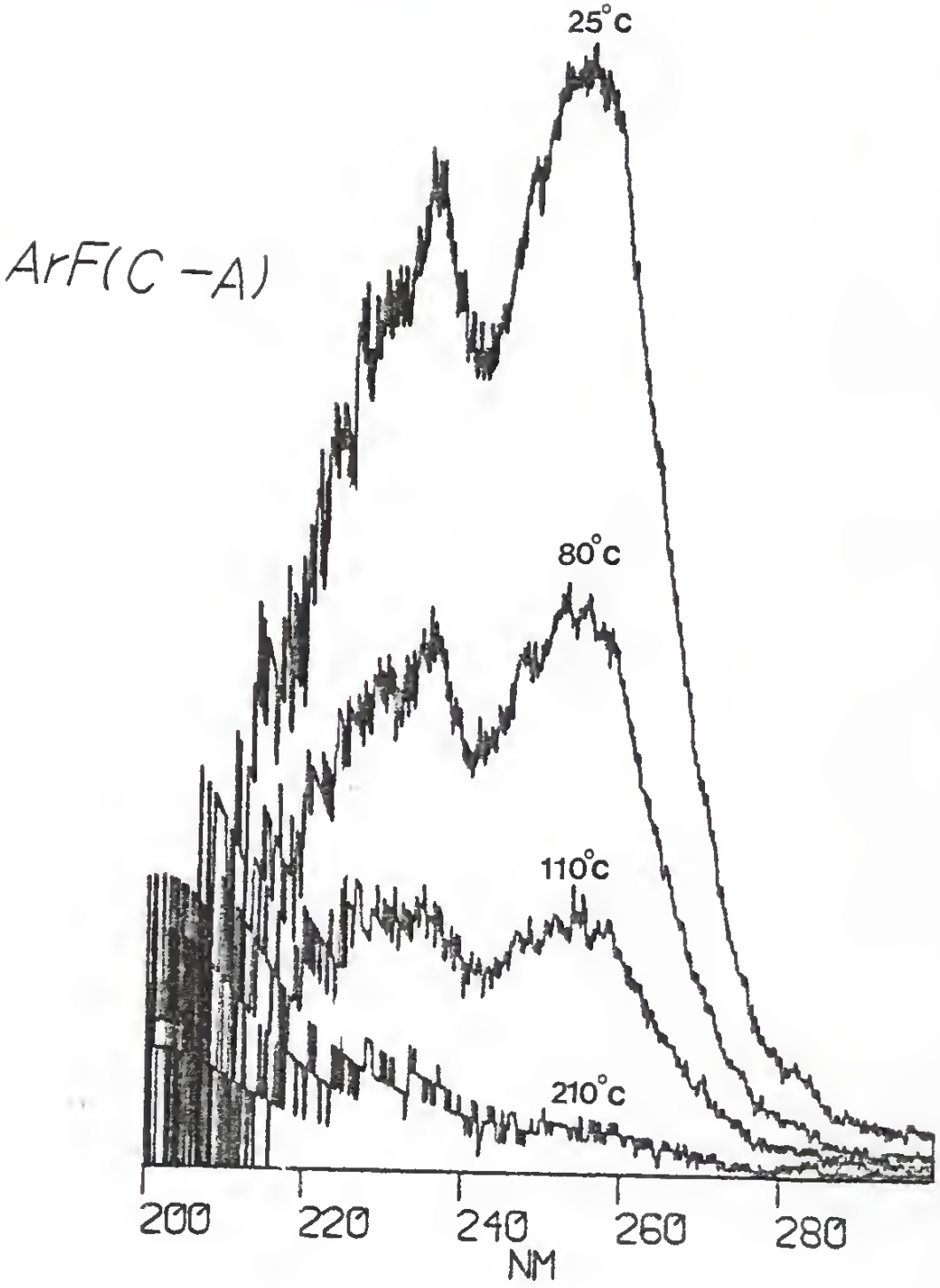
ArF(C-A)
25°C
80°C
110°C
210°C
200
220
240
260
280
NM

Fig. 3.4 Temperature Dependence of NF(b-X) Emission for NF_2/N_2F_4 + Ar* Reaction.

The intensity of NF(b-X) emission increases as the temperature increases.

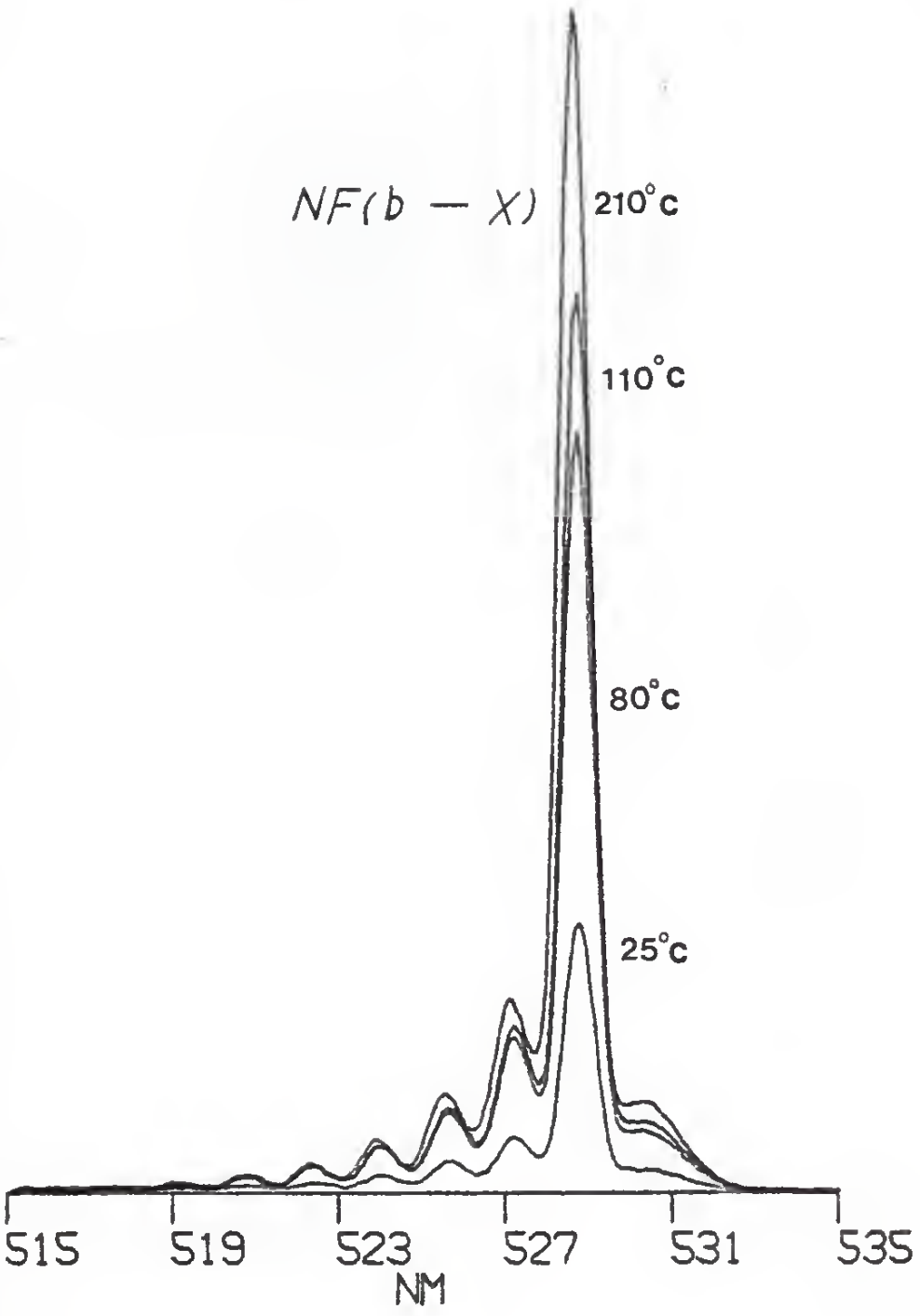
NF(b — X)
210°c
110°c
80°c
25°c
515
519
523
527
531
535
NM

equilibrium was established for the low P_o. Thus, I_{NF}/I_{ArF} would be different for these mixtures if equilibrium resulted. The results (Tab. 3.2) show rather constant I_{NF}/I_{ArF} ratios for the mixtures. This implies that the new equilibrium was not achieved and that the NF_2/N_2F_4 concentrations are controlled by kinetics rather than thermodynamics. As a conclusion, both theoretical and experimental approaches show that N_2F_4/NF_2 concentrations are more thermodynamically controlled in the N_2F_4 flow line and kinetically controlled in the flow tube.

$R^* + N_2F_4$ Reactions (R^* = Ar*, Xe* and He*)

The reactions of $Ar(^3P_0$, 11.73 eV), $Ar(^3P_2$, 11.55 eV), $Xe(^3P_2$, 8.32 eV), and $He(2^3S$, 19.81 eV) with N_2F_4 and NF_2 were investigated as potential sources for NF(b) radicals. In addition to NF(b), RF* were also observed except for NF_2 + Ar*. The He* + N_2F_4 and He* + NF_2 reactions were studied only by taking exploratory spectra; the results are summarized in the next paragraph. The N_2F_4/NF_2 + Ar* and N_2F_4/NF_2 + Xe* reactions were studied in more detail.

The spectrum from He* + NF_2 displayed NF(b-X) and $F(^4S-^4P)$[8] atomic emission. The NF(b) radicals were generated from dissociative energy transfer from He* to NF_2 and the excited F atoms were from the predissociation of excited HeF* molecules. In contrast to Ar* and Xe*, He* + NF_2 generated less NF(b) than He* + N_2F_4. The NF(b-X) intensity from He* + N_2F_4 was comparable to that from Xe* + NF_2. The N_2F_4 + He* reaction was a rich source of emission and the spectrum was more complicated than that from NF_2 + He*. The F atomic emissions ($^4S-^4P$)

Table 3.1 Temperature effects on NF(b-X) and ArF(C-A) emissions

T(°K)	K(atm)	α(%)	I_{ArF}	I(NF)	I_{NF}/I_{ArF}
480	0.58	> 99	16	1435	89.7
380	2.24×10^{-3}	50	28	1090	38.9
350	2.44×10^{-4}	19	56	918	16.4
320	1.5×10^{-5}	5	88	517	5.9
300	1.85×10^{-6}	2	100	330	3.3

Table 3.2 Kinetic control of N_2F_4 $2NF_2$ at the N_2F_4/Ar* mixing zone

N_2F_4/Ar	p(back pressure)	α(reservoir)	p(reagent inlet)	α(reagent inlet)	$\frac{I_{NF}}{I_{ArF}}$
pure	5 cm Hg	0.2%	0.7	1.62%	3.3
3.8%	5 cmHg	0.97%	0.7	8.22%	2.7
0.81%	5 cm Hg	2.13%	0.7	17.75%	3.3

were more intense and overlapped with N_2 first positive $(B-A)^{(9)}$ emission, which contributed to a red flame at the N_2F_4/He* mixing zone. A series of vibrational bands between 2000Å-3000Å were identified to be NO γ bands $(A^2\Sigma^+-X^2\Pi)^{(10),(11)}$ which arise from $N_2(A)$ + an NO impurity. Some vibrational structures around 3000Å-3750Å showing similar characteristics as NF(b-X) emission might be interesting because Herbelin suggested a NF(A-X) emission at 3344Å[12]; the NF(A) state is unreported. However, the emission is very weak and the spectrum was not adequate for analysis.

It was known that Ar* + N_2F_4 gives ArF(B,C)[7]. Both ArF(C-A) and NF(b-X) were observed (fig. 3.2) in the present work; the observation of ArF(B-X) emission at 193 nm was limited by the extremely low spectral response of monochromator and atmospheric absorption. The intensity of ArF(C-A) emission decreased with increasing temperature (fig. 3.3), i.e. increasing NF_2 concentration, whereas an opposite effect of temperature on NF(b-X) (fig. 3.4) emission was observed. For the reaction of Ar* + NF_2, NF(b-X) was the only major emission in spectral range from 2000Å to 6000Å. The NF(b-X) emission from NF_2 + Ar* was four times as intense as from N_2F_4 + Ar*. The NF(b) concentration generated by this technique was estimated to be ~ 10^9 molec/cm^3 by eq. 3.13 using $N_2(A-X)$ from N_2 + Ar* as reference.

$$\frac{I_{NF(b)}}{I_{N_2(A)}} = \frac{\tau_{NF(b)}^{-1}[NF(b)]}{\tau_{N_2(A)}^{-1}[N_2(A)]} \qquad \text{(eq. 3.13)}$$

Since enough amount of N_2 was known to be able to convert Ar* totally to $N_2(A)$ and the lifetime of NF(b) and $N_2(A)$ (1.36 sec) were reported, [NF(b)] could be calculated. The absence of $N_2(B-A)$ emission shows that the N atom concentration must be low and the recombination

would be slow for very low [N]. Although no excited F atomc emission was observed, ground state F atom must be present from the stoichiometry. The observation of NF(a) radicals was limited by the spectral response of monochromator at the wavelength of NF(a-X) emission (874 nm), and by the lifetime (5.6 sec), but NF(a) would be another possible product. As NF(b) decays along the flow tube, NF(x) or NF(a) would be obtained down stream. However, the main complication in kinetic study is expected to be from F or the excess NF_2.

The Xe* + NF_2 and Xe* + N_2F_4 reactions both generated NF(b) radicals and XeF(B,C) excited states (fig. 3.5). The NF(b) concentration generated by Xe* + NF_2 was comparable to that from N_2F_4 + Ar* but only very weak NF(b-X) emission was observed from reaction of N_2F_4 + Xe*. On the contrary, the XeF(B-X) emission from N_2F_4 + Xe* was ~ 6 times as intense as from NF_2 + Xe*. The formation constant of XeF* from reaction N_2F_4 + Xe* was measured[13] to be 15×10^{-11} $cm^3 molec^{-1} sec^{-1}$, while a much smaller value, 1.3×10^{-11} $cm^3 molec^{-1} sec^{-1}$, was reported for NF_2 + Xe*.[13] Although no measurement of the formation rate constant for ArF* from NF_2 + Ar* was reported, it is expected to be $\leq 0.6 \times 10^{-11}$ $cm^3 molec^{-1} sec^{-1}$ based on the formation rate constant for N_2F_4 + Ar* is 5.7×10^{-11} $cm^3 molec^{-1} sec^{-1}$ [7] and the analogy between Ar* and Xe*[14] was studied. The predicted rate constant explains the disappearance of ArF*(C-A) emission for NF_2 + Ar* reaction.

One thing to note in fig. 3.5 is the different band shapes of XeF(B-X) emission from these reactions. Different vibrational populations are expected for XeF* generated using different parent molecules. The diffused bands of XeF(C-A) transition spreads over a

Fig. 3.5 Spectra for NF_2 + Xe* and N_2F_4 + Xe*

Spectra are stored and plotted in the same way as previous plots. The Xe(B-X) peaks for each spectrum are normalized to the same height. For real relative scale, XeF(B-X) emission from N_2F_4 + Xe* is six times as intense as that from NF_2 + Xe*.

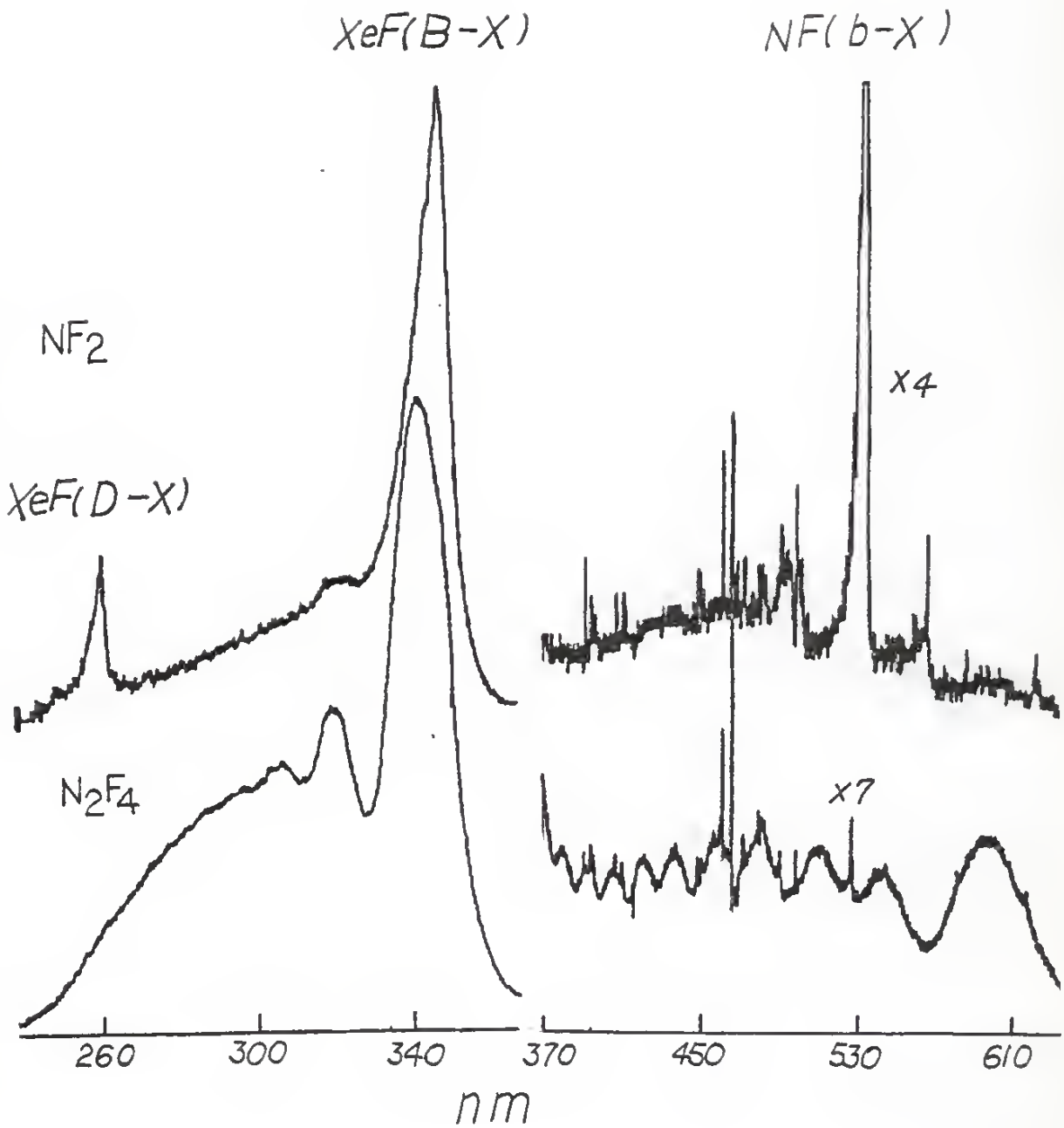
XeF(B-X)
NF(b-X)
NF2
XeF(D-X)
N2F4
x4
x7
260
300
340
370
450
530
610
nm

broad spectral range and overlaps with NF(b-x) vibrational bands. As seen in fig. 3.5, the spectral interference of XeF(C-A) with NF(b-X) was still observable even for NF_2 + Xe* reaction. Spectroscopic study at mixing zone using Xe* + NF_2 as NF(b) source is therefore less ideal than Ar* + NF_2.

Vibrational Bands of NF(b,v'-X,v") Transitions

Twenty five bands of NF(b-X) were observed and assigned to be Δv = 1, 0, -1 sequences from the NF_2 + Ar* source. The wavelengths and relative intensities of each band are summarized in Tab. 3.3. The vibrational bands are quite well separated (fig. 3.6, 3.7) at our resolution, but accurate wavelength assignments of these bands were limited by the resolving power of the monochromator which was of 5.3Å band pass. The wavelength positions were measured at the maximum intensity of the peaks and corrected from air to vacuum. There are some deviations between the wavelengths obtained in this work and the band heads of 0-0, 1-1, 2-2, 0-1, 1-2 transition reported by Douglas and Jones. However, the band origins given by eq. 3.14[16] are almost identical to the results in this work.

$$\nu_{origin}(cm^{-1}) = T_e + G(v') - G(v") \qquad \text{(eq. 3.14)}$$

$$\text{where } G(v) = \omega_e(v + \tfrac{1}{2}) - \omega_e x_e(v + \tfrac{1}{2})^2 \qquad \text{(eq. 3.15)}$$

The vibrational constants to be used in eq. 3.15 were reported as[15]:

Table 3.3 NF(b-X), $\Delta v = 1, 0, -1$ sequences

Spectrum was obtained with a 0.3 McPherson monochromator with spectral calibration curve shown in fig. 2.5. NF_2 + Ar* and N_2F_4 + Ar* reactions were used as NF(b) source.

Table 3.3

v'-v"	$\lambda_{cal.}$(Å)	$\lambda_{measured}$(Å)	I_{rel} (NF_2 + Ar*)	I_{rel} (N_2F_4 + Ar*)
		$\Delta v = 1$		
1-0	4978.74	4979.39	1.36	
2-1	4968.96	4969.39	1.35	
3-2	4959.04	4959.39	1.34	
4-3	4948.99	4949.36	1.15	
5-4	4938.82	4938.36	1.06	
6-5	4928.51	4928.36	0.89	
7-6	4918.08	4917.36	0.80	
8-7	4907.52	4908.36	0.52	
9.8	4896.84	~4887		
		$\Delta v = 0$		
0-0	5289.55	5289.41	100.00	100
1-1	5273.70	5273.41	16.60	22.1
2-2	5257.75	5258.47	9.47	11.8
3-3	5241.71	5241.44	4.66	8.4
4-4	5225.57	5225.44	3.36	5.2
5-5	5209.34	5209.40	1.97	3.4
6-6	5193.02	5192.40	1.27	2.6
7-7	5176.62	5176.40	1.07	1.9
8-8	5160.13	~5155		
9-9	5143.56	~5132		

Table 3.3, continued

v'=v"	$\lambda_{calc.}$(A)	$\lambda_{measured}$(A)	I_{rel} (NF_2 + Ar*)	I_{rel} (N_2F_4 + Ar*)
		$\Delta v = -1$		
0-1	5623.72	5623.55	3.76	2.1
1-2	5600.17	5599.55	1.68	2.0
2-3	5576.59	5575.55	1.33	1.3
3-4	5552.99	5551.55	1.21	1.2
4-5	5529.38	5529.52	1.10	
5-6	5505.76	5505.52	0.97	
6-7	5482.12	5481.52	0.76	
7-8	5458.48	~5456	0.61	
8-9	5434.84	~5424		
0-10	5411.19	~5406		

Fig. 3.6, 3.7 $\Delta v = 1, 0, -1$ Sequences of NF(b-X) Emission

The slit widths were 200 μm. The scanning speeds were 50Å/min for fig. 3.6 and 12.5Å/min for fig. 3.7.

Fig. 3.6

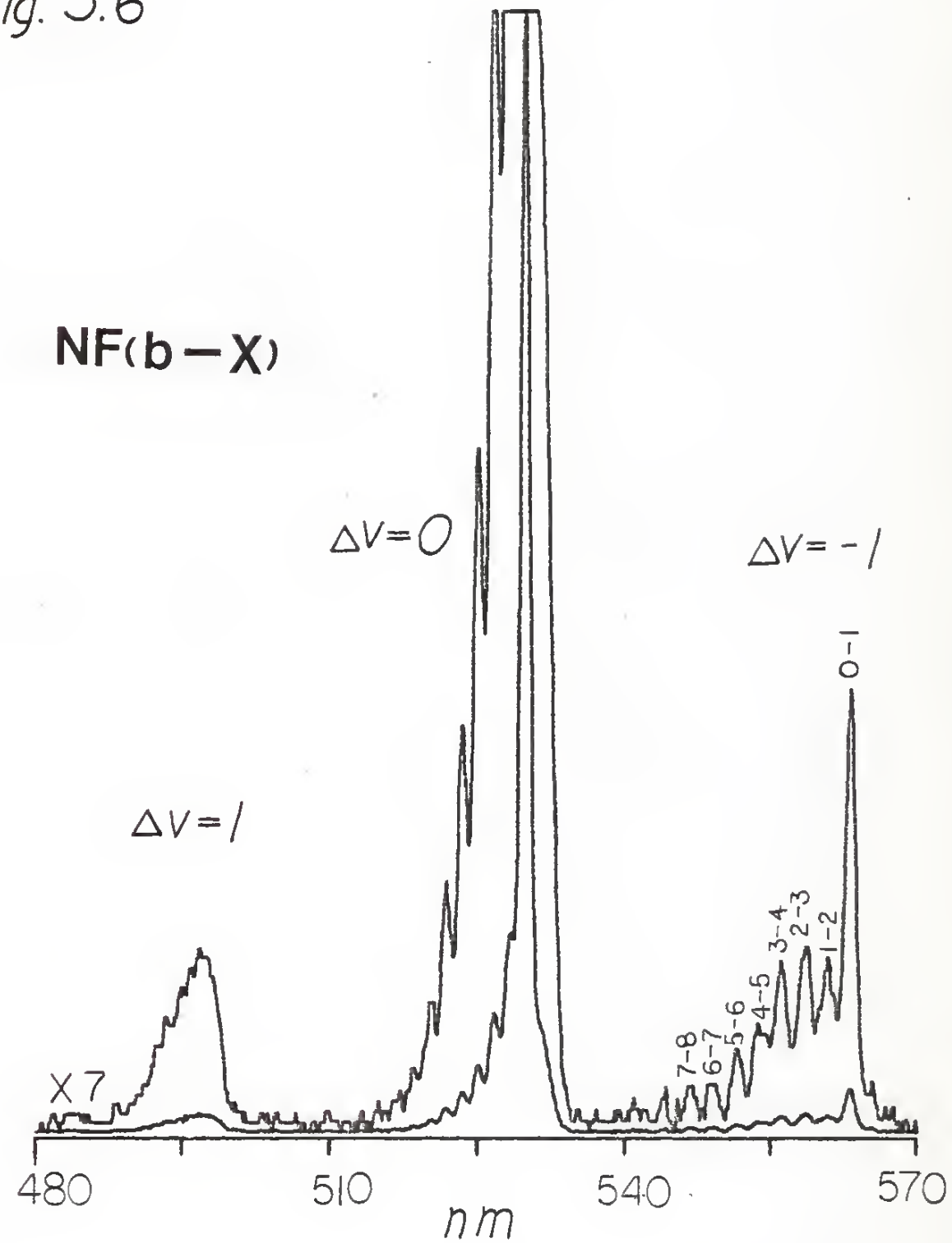

Fig. 3.7

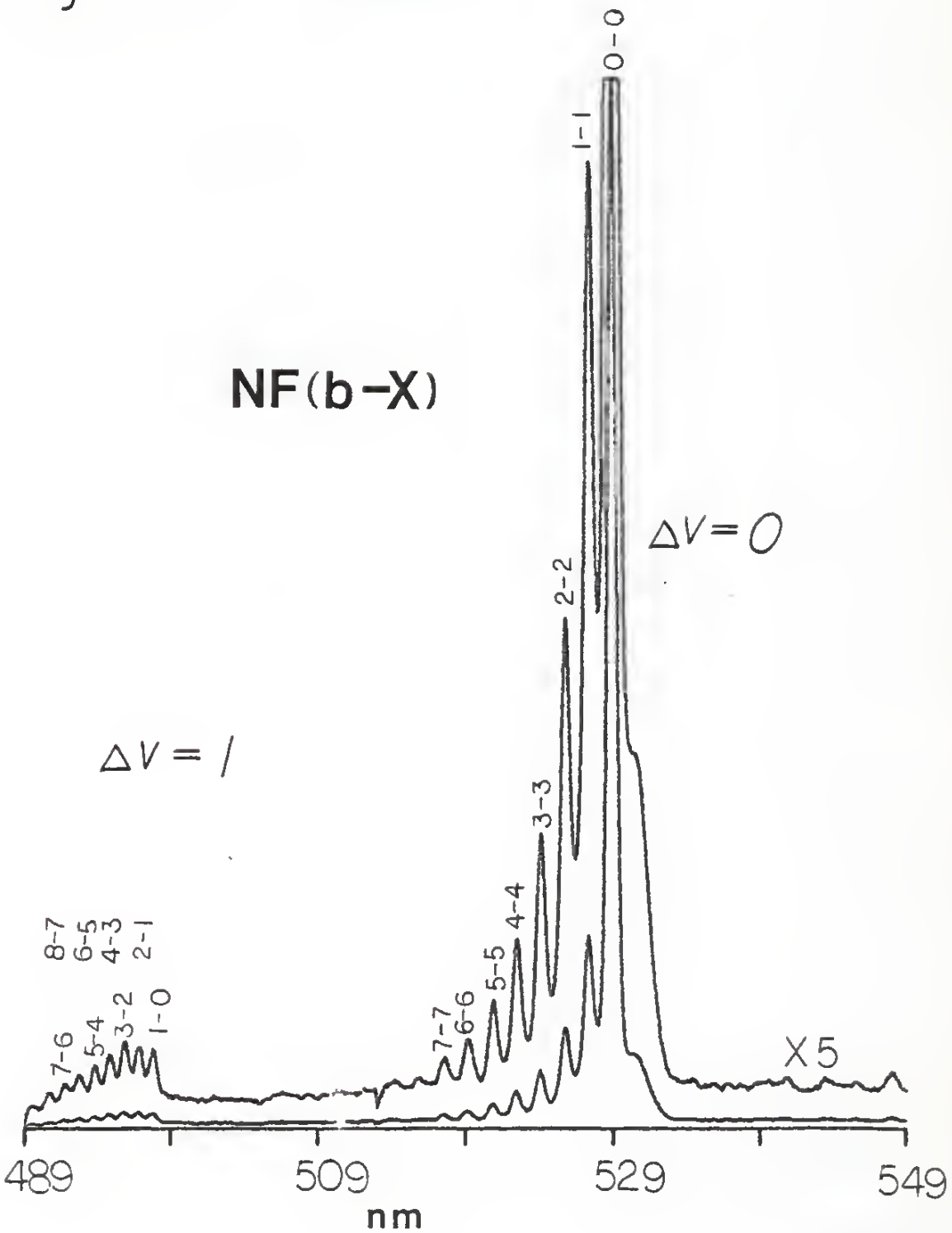
NF(b–X)
ΔV=0
ΔV=1
0-0
1-1
2-2
3-3
4-4
5-5
6-6
7-7
8-7
6-5
4-3
2-1
7-6
5-4
3-2
1-0
X5
489
509
529
549
nm

$\omega_e' = 1197.49\ cm^{-1}$

$\omega_e'x_e' = 8.64\ cm^{-1}$

$\omega_e'' = 1141.37\ cm^{-1}$

$\omega_e''x_e'' = 8.99\ cm^{-1}$

The agreement of the measured and calculated band positions shows that the previously determined vibrational constants based on v" and v" ≤ 2 are adequate for characterizing v levels up to v' = 9 and v" = 9. Nevertheless, better constants probably could be obtained by using a higher resolution monochromator and the NF_2 + Ar* as NF(b) source, since 25 bands should be able to give more information than 5 bands from v' = 0, 1 and 2. If rotational analysis was also done, more accurate potential curves are then possible by RKR technique; this would lead to better calculations on Franck-Condon factors relative to the method applying Morse potential curves[17,18].

The relative intensities were obtained by taking the peak heights from the uncorrected spectrum and applying the spectral response factor from fig. 2.5 at the wavelength of each band (Tab. 3.3). The most intense emission, 0-0 transition, was arbitrarily assigned to be 100. The Δv=0 sequence is most intense among the three sequences. The Franck-Condon factors of some (b,v'-X,v") bands were reported[17,18] by using Morse curve approximation. Though the spectrum showed populations of high NF(b) vibrational levels up to v'=9, none of the Δv=2, Δv=3 sequences was observed. This is explained by the small values of the Franck-Condon factors; M. A. A. Clyne calculated these values as 1.3 x 9^{-3} for 2-0, 7.82 x 1^{-2} for 3-1, and 5.1 x 10^{-5} for 3-0 transitions[18]. Fig. 3.8 also lists the Franck-Condon factors and the

Fig. 3.8

Plots of $\ln P_{v'}$ vs. $E_{v'}$ for NF(b) Generated from NF_2 + Ar*

The values of $q_{v'v''}$ for NF(b-X, v'-v"), $P_{v'}$, and $E_{v'}$, are as following. The values for FC factors are from ref. 16.

v'	v'-v"	$q_{v'v''}$	$\Delta E_{v'}$ (cm^{-1})	$P_{v'}$ (%) (NF_2 + Ar*)	ln $P_{v'}$	$P_{v'}$ (%) N_2F_4 + Ar*)	ln $P_{v'}$
0	0-0	0.9584	0	100	0	100	0
	0-1	0.0402		108		57	
1	1-0	0.0411	1180.2	25	-1.43		-1.33
	1-1	0.8772		17		24	
	1-2	0.0773		23		29	
2	2-1	0.0812	2343.1	13	-2.09		-2.00
	2-2	0.7985		11		14	
	2-3	0.1111		13		13	
3	3-2	0.1198	3488.8	9	-2.59		-2.21
	3-3	0.7198		6		11	

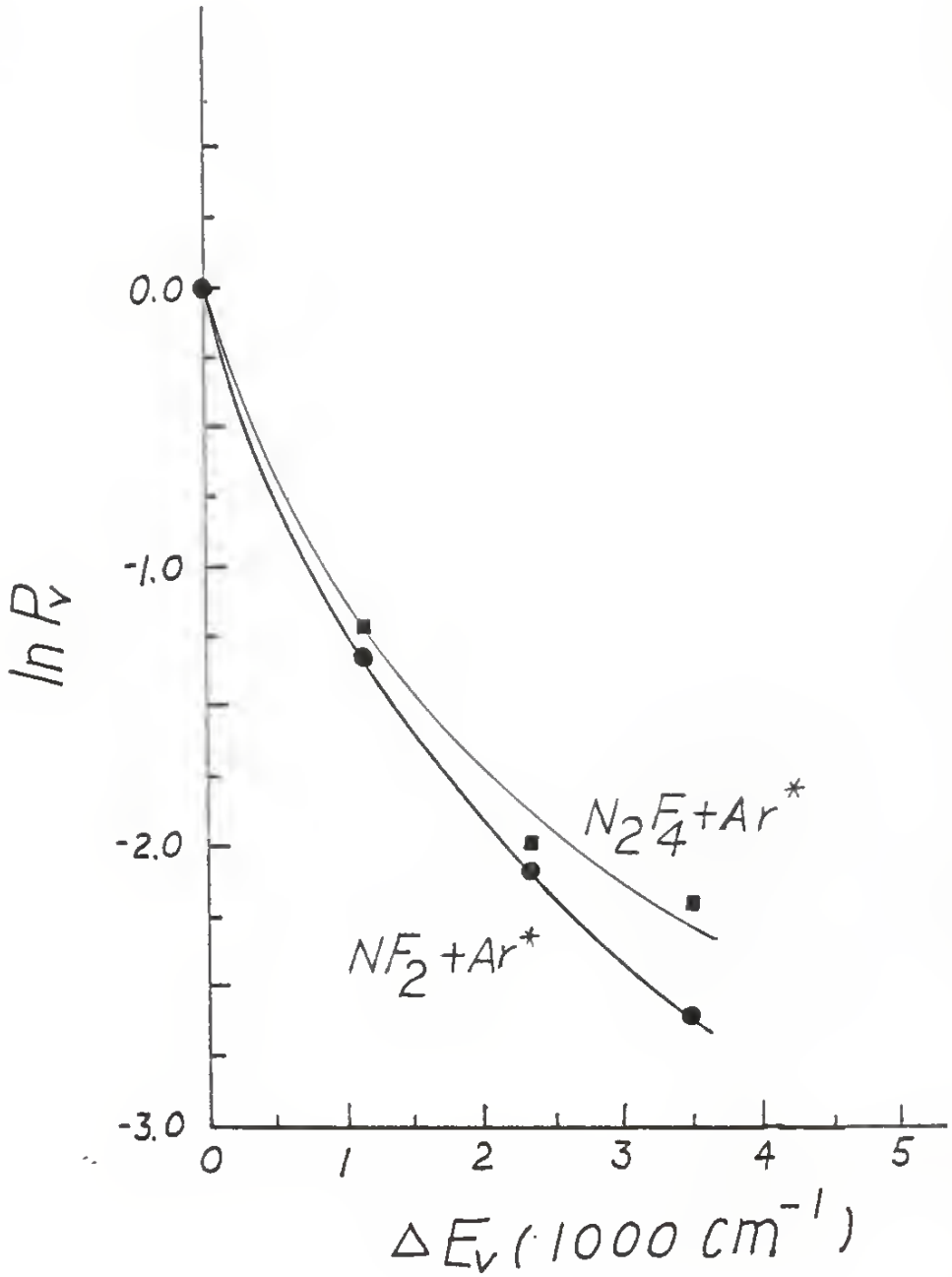
0.0
-1.0
-2.0
-3.0
ln P_v
0
1
2
3
4
5
ΔE_v (1000 cm^{-1})
N_2F_4+Ar*
NF_2+Ar*

relative populations of v'=0, 1, 2, and 3 levels. The relative population of two vibration levels is given by eq. 3.17 for constant R_e $(\bar{r})$[19,11].

$$I_{v'v''} = C'N_{v'}\bar{R}_e^2(\bar{r}_{v'v''})q_{v'v''}\nu^3_{v'v''} \quad \text{(eq. 3.16)}$$

where $I_{v'v''}$ = the intensity of v'-v" emission (photon/sec)

C' = a constant

$N_{v'}$ = population of v' level

$\bar{R}_e$ $(\bar{r}_{v'v''})$ = transition moment of r-centroid $\bar{r}_{v'v''}$

$q_{v'v''}$ = Franck-Condon factor

$\nu_{v'v''}$ = frequency of v'-v" transition

$$P_{v'} = \frac{N_{v_1'}}{N_{v_0'}} = \frac{I_{v_1'v''}\, q_{v_0'\, v''}\, \nu^3_{v_0'v''}}{I_{v_0'v''}\, q_{v_1'v''}\, \nu^3_{v_1'v''}} \quad \text{(eq. 3.17)}$$

The relative population $P_{v'}$ of the vibrational levels were determined by using the 0-0 band as reference, provided FC factors were available. Fig. 3.8 is a plot of $\ln P_{v'}$ vs. ΔE for v = 0-3. For Boltzmann distribution, the plot should be linear according to the equations[20]:

$$P_v = \frac{e^{-\Delta E_v/kT}}{Q} \quad \text{(eq. 3.18)}$$

$$\ln P_v = -\Delta E_v/kT - \ln Q \quad \text{(eq. 3.19)}$$

The nonlinear relationship between $\ln P_v$, and ΔE_v, suggests non-Boltzman distribution of NF(b) for v' = 0-3. As a cross check, the population of v'=0 was calculated, using 0-1 bands, to be 108%; which is within the experimental error and Franck-Condon factors uncertainty. The distribution from Ar* + N_2F_4 spectrum is very simlar to that from NF_2 + Ar* except v' = 3 (Fig. 3.8). But the experiment was done less carefully larger uncertainty must be concerned.

Model for Calculating the Quenching Rate Constants

The model for the kinetics of NF(b) in the flow tube and the methods for the determination of the rate constants are discussed in this section. The decay of NF(b) in a flow system using Ar* + NF_2 as source can be caused by natural radiative decay, wall quenching, quenching by Ar, NF_2, impurities and added reagents. The recombination/interaction of NF(b) with itself can be ignored at the low 10^9 $molec^{-1}sec^{-1}$ cm^3 level. The kinetics for NF(b) decay are therefore set up in terms of a differential rate law considering those factors (eq. 3.20).

$$\frac{-d[NF(b)]}{dt} = \{\tau^{-1} + \frac{k_w}{[Ar]} + k_{Ar}[Ar] + k_{NF_2}[NF_2] + k_Q[Q]\}[NF(b)] \qquad \text{(eq. 3.20)}$$

where τ^{-1}: natural radiative decay rate constant

k_w: wall quenching rate constant

k_{Ar}: quenching rate constant by Ar

k_{NF_2}: quenching rate constant by NF_2

k_Q: quenching rate constant by added reagent Q

For the particular flow reactor used in this work, the concentrations of Ar, NF_2, and Q are all much higher than that of NF(b) radical. Hence, the kinetics become pseudo first order and eq. 3.20 is reduced to eq. 3.21 if $[NF_2]$, [Ar] and [Q] are constant.

$$\frac{-d[NF(b)]}{dt} = k_{total}[NF(b)] \qquad \text{(eq. 3.21)}$$

and

$$k_{total} = \tau^{-1} + \frac{k_w}{[Ar]} + k_{Ar}[Ar] + k_{NF_2}[NF_2] + k_Q[Q] \qquad \text{(eq. 3.22)}$$

Eq. 3.21 is then rewritten as eq. 3.23 after modified by variable separation and integration.

$$\ln \frac{[NF(b)]_t}{[NF(b)]_o} = -k_{total}\Delta t \qquad \text{(eq. 3.23)}$$

where $[NF(b)]_o$ and $[NF(b)]_t$ are the concentrations of NF(b) at time zero and t, respectively,and Δt is the time interval of quenching. A good aspect of eq. 3.23 is that absolute concentration of NF(b) is not required since only the ratio of concentrations appears in the equation. The emission intensity is proportional to the concentration of the excited species, and eq. 3.23 is in fact equivalent to eq. 3.24 with I being the NF(b-X) emission intensity.

$$\ln \frac{I_t}{I_o} = -k_{total}\Delta t \qquad \text{(eq. 3.24)}$$

A plot of lnI versus t should be linear with a slope of -k, and the total quenching rate constant can be evaluated from this plot.

An advantage of the moveable detector is the possibility of monitoring the emission intensities by moving the PMT along the flow tube. The time intervals, Δt, is related to the distance from reagent inlet to the detecting point, Δx, by eq. 3.25 with plug flow assumption. And k_{total} is

$$\Delta t = \frac{\Delta x}{\text{pumping speed}} \qquad \text{(eq. 3.25)}$$

determined by the slope of log I vs. Δt. For the current 4.1 cm i.d. flow tube, the typical Ar flow rate is ~0.1 mole/min which causes a pressure of 1.6 torr in the tube at room temperature; the pumping speed is ~ 1600 cm given by eq. 3.26.

$$V = \frac{\frac{F_{Ar}}{60} \cdot \frac{RT}{P}}{\pi r^2} \qquad \text{(eq. 3.26)}$$

where
- v: the pumping speed
- F_{Ar}: the Ar flow rate given by fig. 2.2, mole/min
- P: the pressure in the flow tube
- T: the temperature, K
- r: the radius of flow tube, 2.05 cm

k_{total} is a function of [Ar], [NF_2] and [Q] as shown in eq. 3.9. If the concentrations of Ar and NF_2 are held constant, a plot of k_{total}, evaluated by the method mentioned above for several [Q], versus [Q] leads to a slope of k_Q. The k_{NF_2} value can be determined by the same technique but [NF_2] must be varied. The [Ar] appears in two terms of

the equation, namely $\frac{k_w}{[Ar]}$ and $k_{Ar}[Ar]$; this could make the determination of k_w a bit difficult. To simplify the relation between k_{total} and [Ar], an approximation is necessary. Since Clyne, et al. reported a very small k_{Ar} value, $<10^{-17}$ $cm^3 molec^{-1} sec^{-1}$, it seems to be reasonable to assume the quenching by Ar to be negligible compared to that of $\frac{k_w}{[Ar]}$ for the experimental pressure range (0.2 torr ~ 5 torr). Fortunately, as will be seen later in the next chapter dealing with quenching rate constants, this is the case. Therefore, a plot of k_{total} versus $\frac{1}{[Ar]}$ should be linear with slope of k_w provided that concentration of NF_2 held constant and no quenching reagent is added. The wall quenching rate is determined by the slope and the intercept of this plot gives the radiative lifetime of NF(b) if $k_{NF_2}[NF_2]$ and $k_{Ar}[Ar]$ are much smaller than τ^{-1}.

A second method employed in the present apparatus was the fixed point method. The method is based on eq. 3.23.

$$\ln \frac{I_t}{I_o} = -k\Delta t$$

$$= -\{\tau^{-1} + \frac{k_w}{[Ar]} + k_{NF_2}[NF_2]\Delta t + k_Q\}\Delta t$$

$$= k'\Delta t + k_Q[Q]\Delta t$$

$$\text{where } k' = \tau^{-1} + \frac{k_w}{[Ar]} + k_{NF_2}[NF_2]$$

The value of k' is constant for constant [Ar] and [NF_2]. k_Q is then evaluated by the plot of log I vs [Q] which has a slope of $k_Q\Delta t$. If Δt is specified, k_Q is obtained. The experiments for this method were done by setting the detector at one position and monitoring I vs. added [Q].

References:

1. J. A. N. A. F. Thermochem. Tables, 1965-7.
2. J. M. Herbelin, J. Chem. Phys., 42, 367, 1976.
3. P. J. Evans and E. Tschuikow-Roux, J. Phys. Chem., 82, 182, 1978.
4. E. Tschuikow-Roux, K. O. MacFadden, K. H. Jung and O. A. Armstrong, J. Phys. Chem., 77, 734, 1973.
5. A. P. Modica and O. F. Hornig, J. Chem. Phys. 49, 629, 1968.
6. M. A. A. Clyne and J. Connor, J. Chem. Soc., Faraday Trans., 2, 1220, 1972.
7. J. H. Kolts and O. W. Setser, Phys. Chem., 82, 1766, 1978.
8. Atomic Transition Probabilities, vol. 1, p. 113, NSROS-NBS4, 1966.
9. R. W. B. Pearse and A. G. Gaydon, The Identification of Molecular Spectra, p. 209, 1965.
10. R. W. B. Pearse and A. G. Gaydon, the Identification of Molecular Spectrum, 1965.
11. G. R. Möhlmann, H. A. Van Sprang, E. Bloemen and F. J. Deheer, Chem. Phys., 32, 239, 1978.
12. J. M. Herbelin and N. Cohen, 20, 605, 1973.
13. O. Lin, O. W. Setser and Y. C. Yu, to be published.
14. O. W. Setser, T. O. Oreiling, H. C. Brashears, and J. H. Kolts, Chem Soc., Faraday Oiscussion, 67, 255, 1979.
15. A. E. Oouglas and W. E. Jones, Can. J. Phys., 44, 2551, 1966.
16. G. Herzberg, Spectra of Oiatomic Molecules, p. 152, Van Nostrand Reinhold Comp. 1950
17. P. H. Tennyson, A. Fontijn and M. A. A. Clyne, Chem. Phys., 62, 171, 1981.

18. K. A. Mohamed, B. N. Khanna and K. M. Lal, Ind. J. Pure App. Phys., 12, 243, 1974.

19. G. Herzberg, Spectra of Diatomic Molecules, p. 200, Van Nostrand, Reinhold Co., 1950.

20. Ian W. M. Smith, Kinetics and Dynamics of Elementary Gas Reactions, Butterworth and Co., Ltd., London, 1980.

CHAPTER 4 KINETIC STUDIES OF $NF(b^1\Sigma^+)$

The Radiative Lifetime τ and Wall Quenching Rate Constant k_w

The lifetime of $NF(b^1\Sigma^+)$ and the quenching by the pyrex glass wall were evaluated by measuring the first order [NF(b)] decay versus Ar pressure for constant NF_2 with no added quenching reagent. For each Ar concentration, the decay constant, $k' = \tau^{-1} + \frac{k_w}{[Ar]} + k_{Ar}[Ar] + k_{NF_2}[NF_2]$, was determined by moving the PMT along tube. Fig. 4.1 shows typical plots of NF(b) decay vs. Δt; Δt and pumping speed were obtained by eq. 3.25 and 3.26 in the previous chapter with plug flow assumption. The linear dependence of resulting decay constants vs. $\frac{1}{[Ar]}$ is shown in fig. 4.2. Plot e was the first experiment and the liq. N_2 level in the dewar for the molecular sieve traps for Ar line was not kept constant throughout the experiment; therefore the pressure in the flow tube was not constant and the calculated Ar flow rate, hence Δt, were effected. Thus, τ and k_w value resulting from this plot are used only as referential purpose and were dropped out in the final results. The remaining plots were from four separate experiments; they suggest an average intercept of ~ 49 sec^{-1}, which is the value of $\tau^{-1} + k_{Ar}[Ar] + k_{NF_2}[NF_2]$. The value of k_{Ar} is known to be < 10^{-17} $cm^3 molec^{-1} sec^{-1}$ and k_{NF_2} was determined to be 5.37 x 1^{-15} $cm^3 molec^{-1} sec^{-1}$ in this work. In the experiment, [Ar] was less than 5 torr and NF_2 was ~ 5 x 10^{13} molec/cm^3. Therefore, $k_{NF_2}[NF_2]$ and $k_{Ar}[Ar]$ are 0.4 and < 1.6 sec^{-1}, respectively; both are smaller than the intercepts in fig. 4.2

Fig. 4.1 Plots of [NF(b)] vs. Δt for various [Ar]

The $[NF_2]$ was held constant and the decay rate constant, $k' = \tau^{-1} + \frac{k_w}{[Ar]} + k_{Ar}[Ar] + k_{NF_2}[NF_2]$, was determined by the slope of the plots. The resulted values of the slopes are listed as following and give plot a in fig. 3.10.

P(torr)	slope (sec^{-1})
0.2	96.5
0.25	84.4
0.4	73.0
0.5	70.3
0.6	66.8
0.8	59.9
0.9	60.5
1.4	56.7
1.8	55.8
2.2	57.4

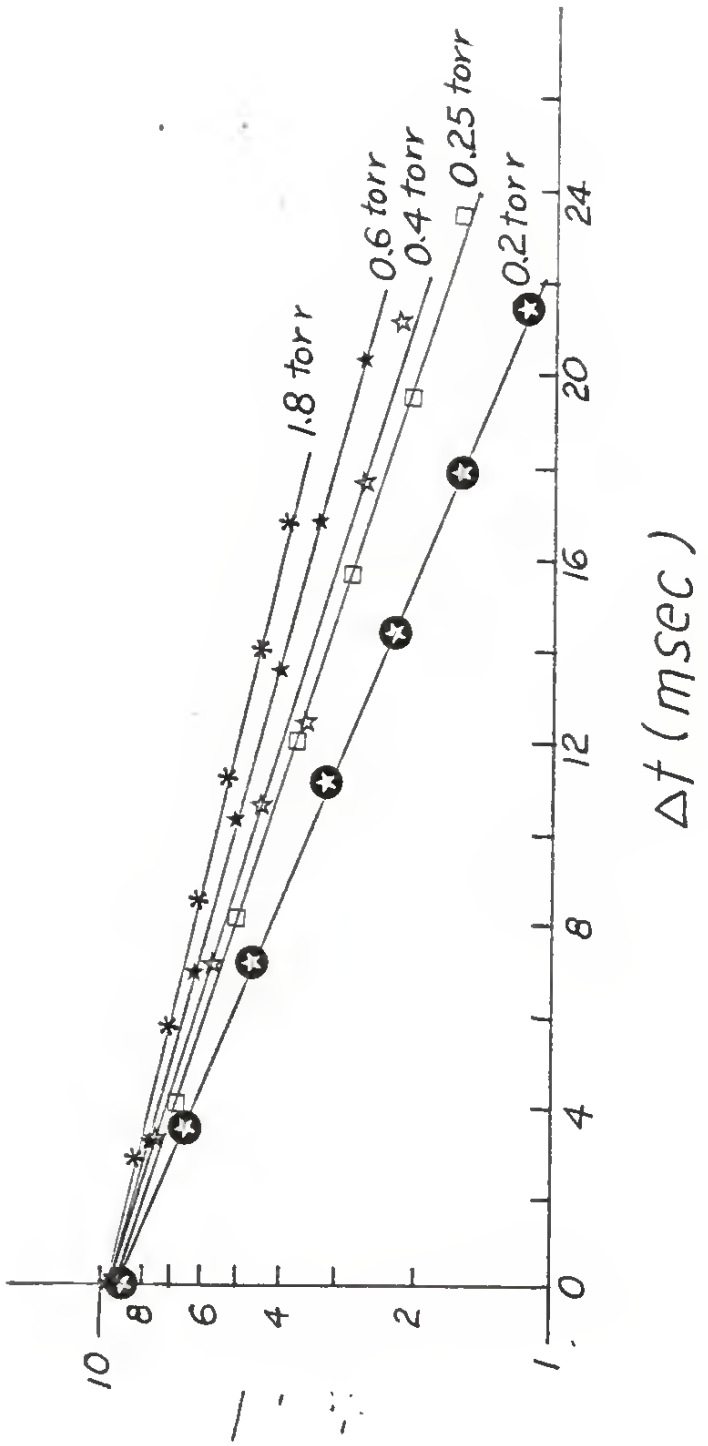
1.8 torr
0.6 torr
0.4 torr
0.25 torr
0.2 torr
10
8
6
4
2
0
4
8
12
16
20
24
Δt (msec)

Fig. 4.2 The Linear Relation Between NF(b) Decay Rate k' and $\frac{1}{[Ar]}$. The equation $k' = \tau^{-1} + \frac{k_w}{[Ar]}$ was used to give τ^{-1} = (20.2 ± 0.5) msec and kw = (8.97 ± 0.23) sec^{-1} torr.

a ●	$\tau^{-1} = 51.22\ sec^{-1}$	$k_w = 8.78\ sec^{-1}\ torr^{-1}$
b ◎	$\tau^{-1} = 49.75\ sec^{-1}$	$k_w = 9.09\ sec^{-1}\ torr^{-1}$
c ☆	$\tau^{-1} = 49.32\ sec^{-1}$	$k_w = 8.99\ sec^{-1}\ torr^{-1}$
d ✱	$\tau^{-1} = 48.21\ sec^{-1}$	$k_w = 9.27\ sec^{-1}\ torr^{-1}$
e ★	$\tau^{-1} = 43.3\ sec^{-1}$	$k_w = 8.71\ sec^{-1}\ torr^{-1}$

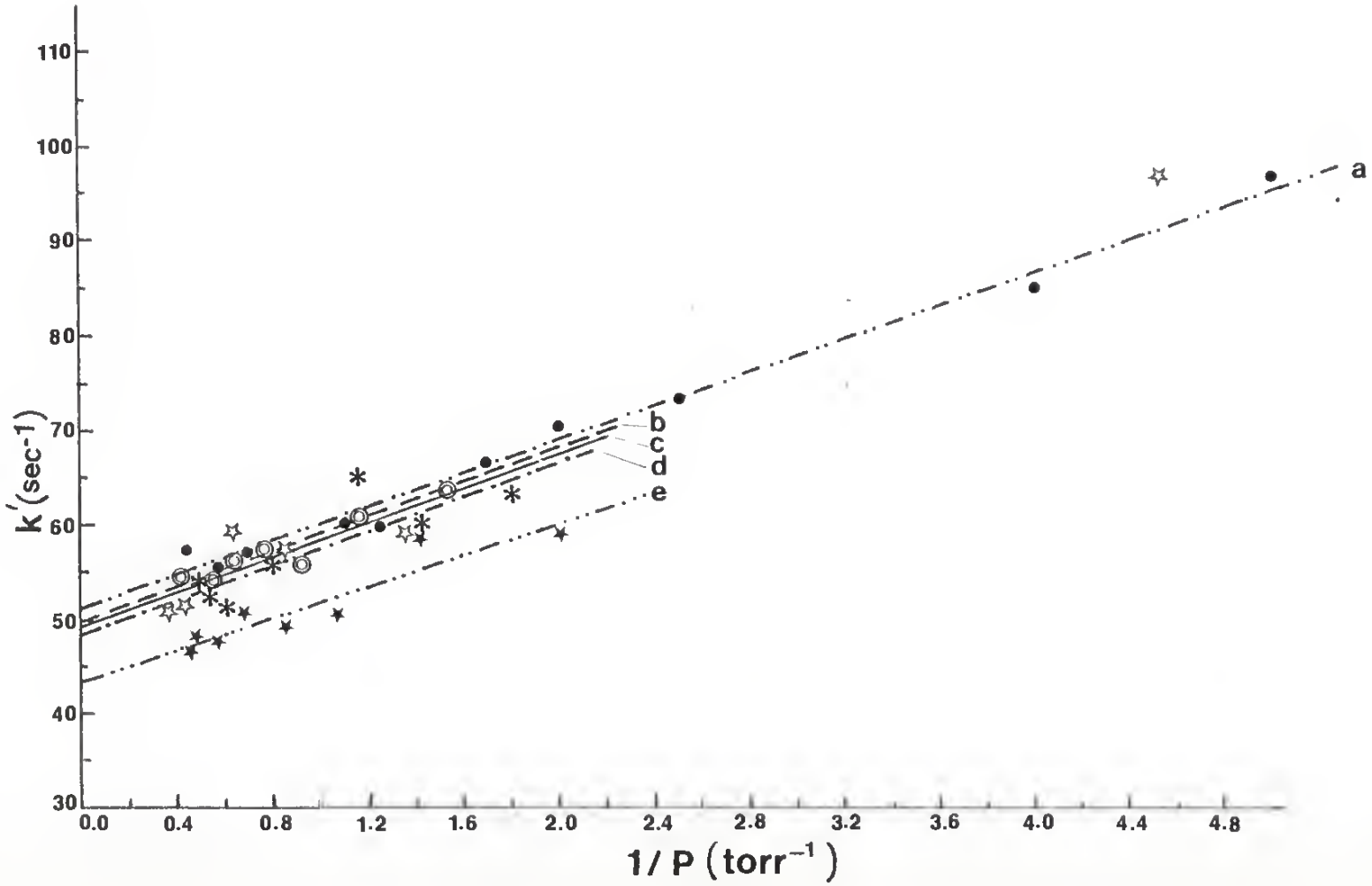
110
100
90
80
70
60
50
40
30
k′(sec⁻¹)
0.0
0.4
0.8
1.2
1.6
2.0
2.4
2.8
3.2
3.6
4.0
4.4
4.8
1/ P (torr⁻¹)
a
b
c
d
e

and are neglected. The lifetime of NF(b), 20.2 ± 0.5 msec, was obtained by taking the reciprocals of the mean intercept from a, b, c, and d in fig. 4.2.

Slopes of the straight lines in fig. 4.2 are fairly consistent and give a k_w value of 8.96 ± 0.23 sec^{-1} torr. For 1.5 torr Ar concentration, the typical [Ar] in experiments, $\frac{k_w}{[Ar]}$ is 6.0 sec^{-1}, which is relatively small but observable. This is a desirable result in that NF(b) is not readily quenched by prex glass and can be easily generated and studied in a glass apparatus. However, the surface quenching properties may change dramatically if the wall is activated by adsorption of reagents; the possible resulting change should be kept in mind for studies with added reagents.

Quenching Rate Constants of $NF(b^1\Sigma^+)$ for Well Behaved Reagents

Quenching rate constants of NF(b) were measured for 24 reagents and the results are listed in Tab. 4.1. Most measurements were done by the fixed point method. As shown in fig.4.3, the expected pseudo first order kinetics are confirmed by the linearity of the log I versus [Q] plots. To test the uncertainty of the plug flow assumption and the fixed point method, k_{CH_3Cl} was measured by the fixed point method at various PMT positions (fig. 4.4). Also k_{Br_2} was determined by the moveable detector technique. Fig. 4.4 shows the [NF(b)] decay vs. $[CH_3Cl]$ for various detecting positions on two separate days. The

Fig. 4.3 Plots for log I vs. [Q]

The quenching rate constants are obatined by the equation

$$k_Q = \frac{2.303 \text{ slope}}{\Delta t}$$

Δt value are somewhat different for each compound and the obtained k_Q required correction by the viscosity constant of the quenching reagent relative to Ar to give the number listed in Tab. 3.4, 3.5

Δt for each compound is listed as following. The P_{Ar} was ~1.5 torr for these measurements.

CH_3Cl = 23.8 msec, CH_4 = 21.6 msec, CF_3Br = 23.5 msec, CO = 21.6 msec, HCl = 26.6 msec, CH_3Br = 27.0 msec, O_2 = 21.7 msec, CO_2 = 23.1 msec, N_2F_4 = 22.4 msec, CF_3NO = 22.8 msec.

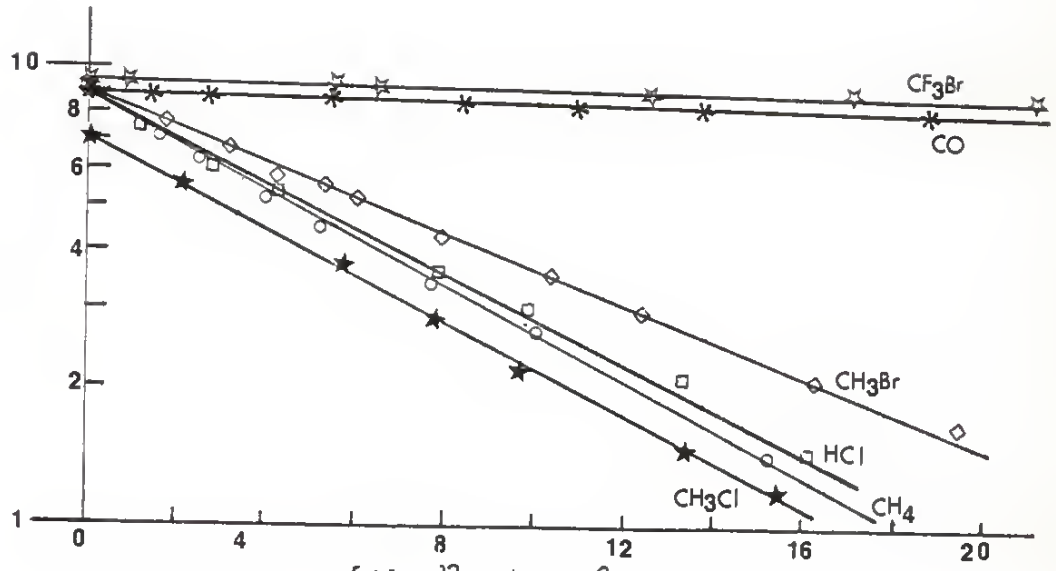

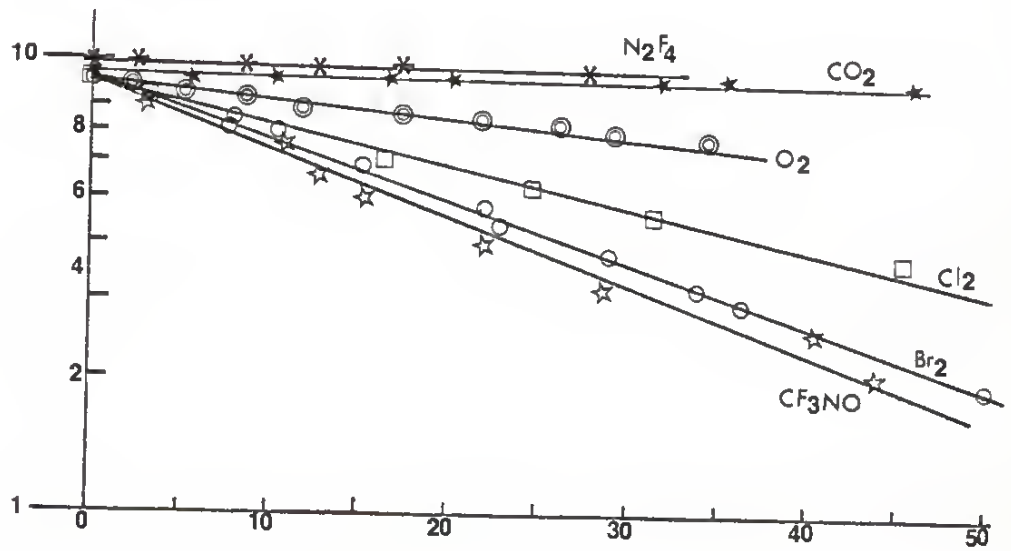

N_2F_4, CO_2, O_2, CF_3NO (10^{13} molec / cm^3)

Cl_2, Br_2 (10^{10} molec / cm^3)

Fig. 4.4 Plots of log I vs. $[CH_3Cl]$

The experiments were done by the fixed point method at various positions along the flow tube. The values of Δt and k_{CH_3} are given as follows.

	Δx(cm)	Δt(msec)	$k_{CH_3Cl}(10^{-13}cm^3molec^{-1}sec^{-1})$	
a	10.5	7.06	2.02	
b	19	12.79	2.43	ave. 2.41 ± 0.28
c	27.1	18.24	2.69	
d	35.5	23.89	2.51	
a'	23.7	15.65	2.34	
b'	27.1	17.83	2.12	ave. 2.28 ± 0.14
c'	35.5	23.42	2.38	

The $[CH_3Cl]$ in the plot was not corrected by viscosity constant however the k value listed above were corrected. Trials a, b, c, d and a', b', and c' were done on two separate days.

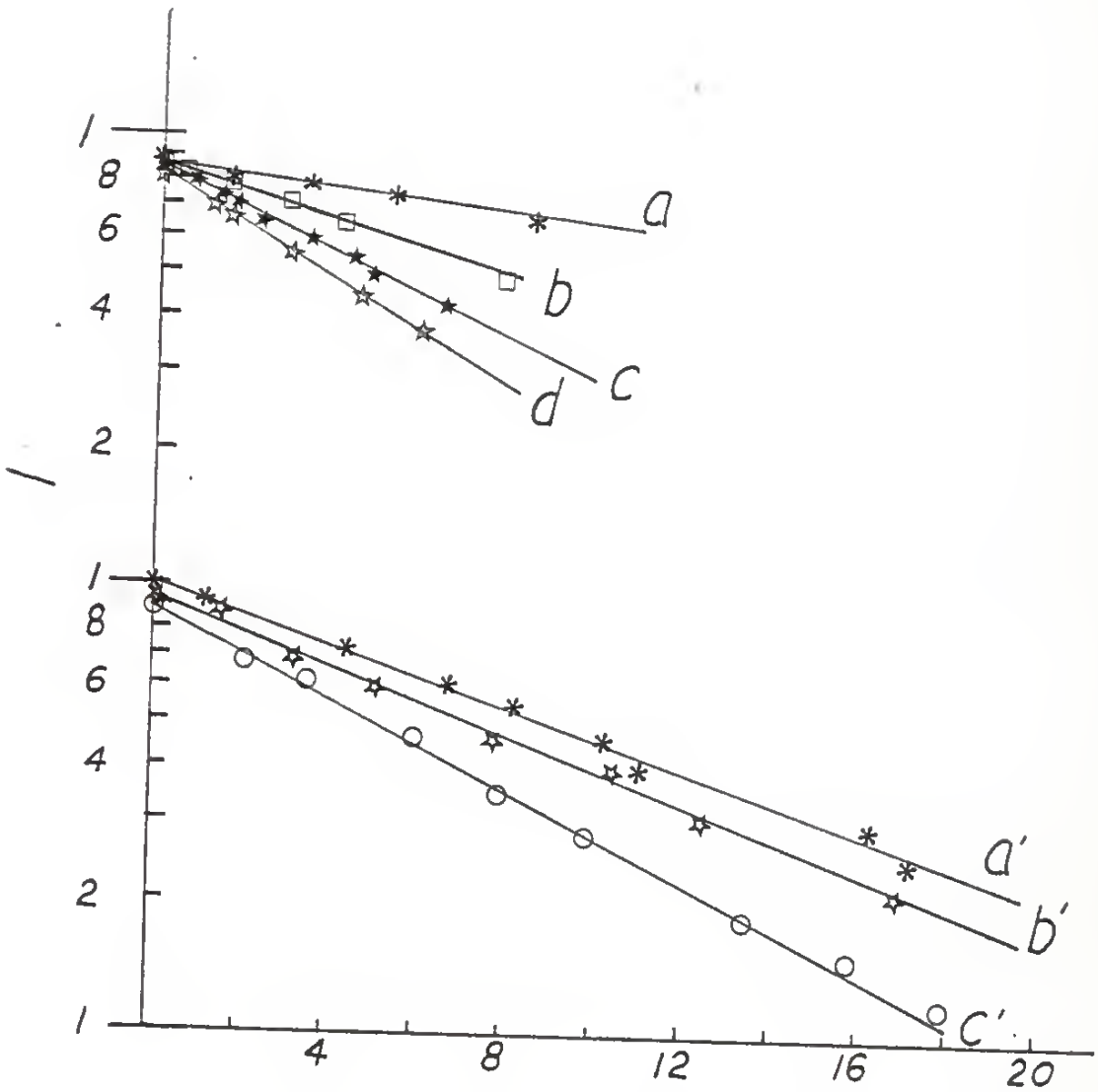
1
8
6
4
2
1
a
b
c
d
1
8
6
4
2
1
a'
b'
c'
4
8
12
16
20
CH3Cl (10^13 molec/cm^3)

deviation of the obtained k_{CH_3Cl} values are within 10%, and we conclude that the kinetics are well behaved and that plug flow is adequate for converting Δx to Δt.

Fig. 4.5 is the plots of log I vs. Δt for 6 constant Br_2 concentrations using the moveable detector technique. The resulting slopes of fig. 4.5 gave a k_{Br_2} value of 1.54×10^{-10} $cm^3 molec^{-1} sec^{-1}$ from the slope of plot (a) in 4.6. Comparing this with the fixed point value, $1.12 \times 10^{-10} cm^3 molec^{-1}$ shows ± 30% difference. This is an indicator of the uncertainty of k_Q values measured by these two methods.

Also shown in fig. 4.6 are the plots of k' vs. $[NF_2]$ (plot b.c) obtained by moving detector technique. The Ar concentration was held constant and the decay of [NF(b)] was monitored along tube for several NF_2 concentrations. The Ar pressure was ~1.7 torr without any throttling for the experiments and the log I vs. Δt plots for each $[NF_2]$ are similar to that of 1.8 torr Ar in fig. 4.1. As in fig. 4.6, the k' values were almost constant for the experimental $[NF_2]$ range, a small quenching rate constant, $\leq 5.4 \times 10^{-15} cm^3 molec^{-1} sec^{-1}$ is estimated. The quenching rate constant of NF(b) by N_2F_4 is of the same order of magnitude, 4×10^{-15} $cm^3 molec^{-1} sec^{-1}$, as determined by fixed point method, fig. 4.3. The rate constant with NF_3 was reported as 1.8×10^{-12} $cm^3 molec^{-1} sec^{-1}$. However, this seems unusually large relative to N_2F_4 and NF_2, and the NF_3 quenching needs to be independently checked before the large value is accepted.

Most of the reagents measured have small quenching effect on NF(b) except Cl_2 and Br_2. Cl_2 and Br_2 seemed to be adsorbed by the Pyrex glass wall and tremendously reduced the NF(b-X) emission by changing the quenching properties of the tube wall. If a pure Cl_2 sample was pumped

Fig. 4.5 Plot of log I versus Δt for various $[Br_2]$

k' were obtained from the plot according to the equation

$$\ln\frac{I}{I_o} = -2.303\, k'\, \Delta t$$

$$= -2.303 \{\tau^{-1} + k_w/[Ar] + k_{Ar}[Ar] + k_{NF_2}[NF_2] + k_{Br_2}[Br_2]\}\Delta t$$

The Br_2 concentrations of each line are:

a = 0

b = 0.8×10^{11} molec/cm^3

c. 3.5×10^{11} molec/cm^3

d. 5.3×10^{11} molec/cm^3

e. 8.2×10^{11} molec/cm^3

f. 12.0×10^{11} molec/cm^3

A 1.51% Br_2/Ar mixture was used and no viscosity correction to the flow rate is required.

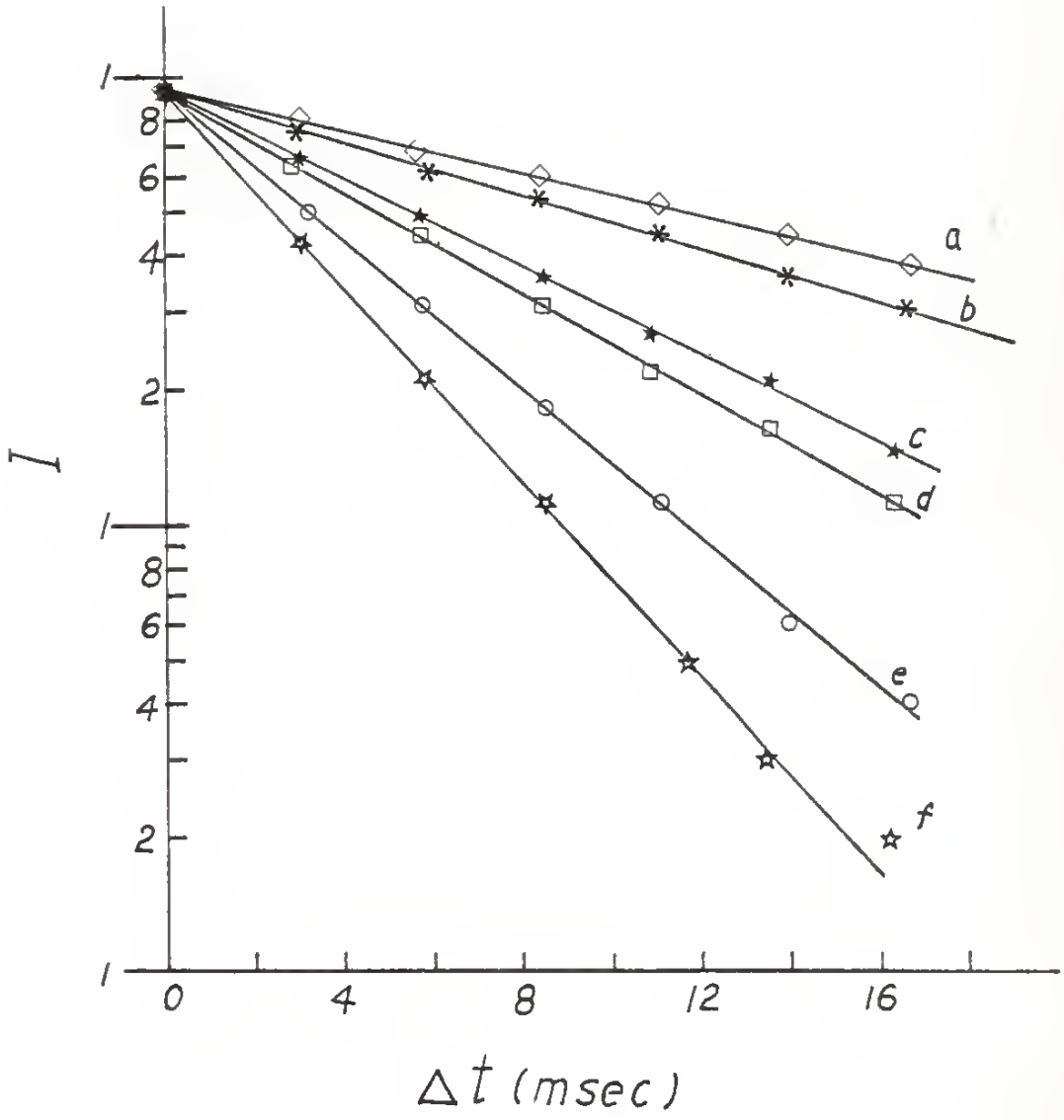
I
1
8
6
4
2
1
8
6
4
2
1
0
4
8
12
16
Δt (msec)
a
b
c
d
e
f

Fig. 4.6 Plot of k' versus $[Br_2]$ and $[NF_2]$

a = k' vs. $[Br_2]$

b,c = k' vs. $[NF_2]$, two independent experiments.

where $k' = \tau^{-1} + k_w/[Ar] + k_{Ar}[Ar] + k_{NF_2}[NF_2] + k_{Br}[Br_2]$

and $[Br_2] = 0$ for plots b, c.

The intercept is 49.7 sec^{-1} for plot a and are 52.9, 53.4 for plots b, c. The lifetimes of NF(b) from these intercepts are 20.1, 18.9, and 18.7 msec, which are in agreement with independent best balue of 2.0 ≥ ± 0.5 msec.

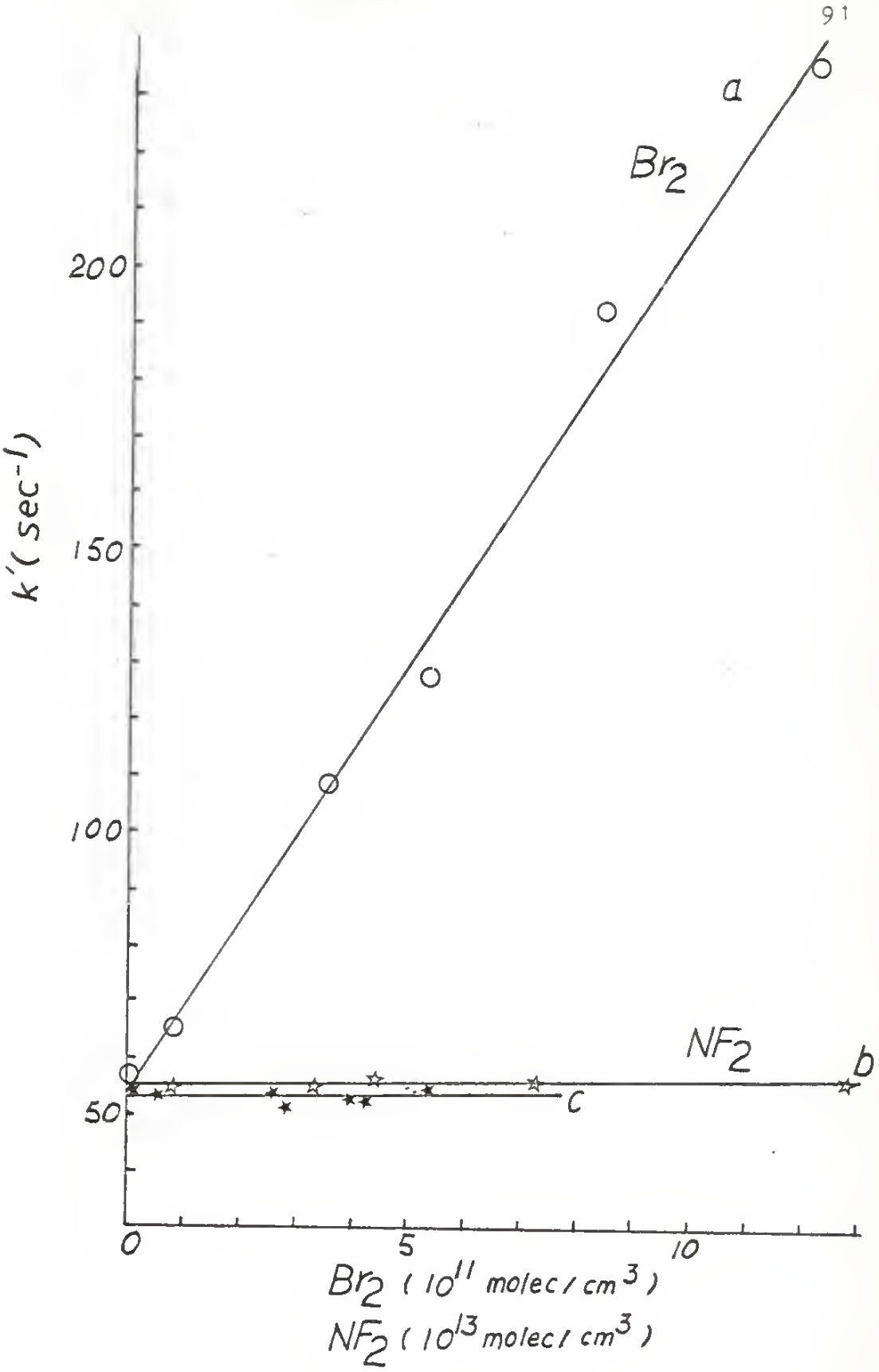
a
Br2
200
150
100
50
k'(sec-1)
NF2
b
c
0
5
10
Br2 (10^11 molec/cm^3)
NF2 (10^13 molec/cm^3)

Table 4.1 Rate Constants for Quenching of NF(b), $O_2(b)$, $O_2(a)$, $O(^1S)$, $O(^1D)$, NH(b)

The k_Q measured in this work are expressed in the form of mean value and mean value ± S.D.

The rate constants listed are of the unit: 10^{14} $cm^3 molec^{-1} sec^{-1}$

	NF(b)	$O_2(b)$	$O_2(a)$	$O(^1S)$	$O(^1D)$	NH(b)
HCl	30.2 ± 1.9[a]	4 ± 2[e] 7.3 ± 0.2[j] 6.7 ± 3.5[k]	0.013[r] 0.0025[e]		13000[v]	
HBr	fast 86.7 ± 1.3[a] slow 0.75 ± 0.5[a]	20 ± 4[e]				
HF	97 ± 15[b] 100[c]	110 ± 20[e]	0.02[e]			
CH_4	22.1 ± 1[a]	7.5[m]		4.7[n] 2.7[v]	1500[v]	18 ± 3[g]
CH_3F	20.7 ± 0.3[d]					

Table 3.4, continued

	NF(b)	O_2(b)	O_2(a)	O(^{1}S)	O(^{1}D)	NH(b)
CH_3Cl	23.6 ± 1.0[a] 21.4 ± 4.1[d]	80 ± 40[e]				
CH_3Br	17.9 ± 1.0[a] 21.5 ± 0.8[d]					
CH_3I	35.9 ± 4.2[d]		0.0004[e]			
CH_2Br_2	25.9[d]					
$CHCl_3$	6.4 ± 1.7[d]					
CHF_3	63.5[d]				5400[v]	
CF_3NO	11.6 ± 1.2[a] 23[b]		200[e]			
CF_3Br	1.20 ± 0.18		<0.00005[e] 0.000037[t]			

Table 3.4, continued

	NF(b)	O_2(b)	O_2(a)	$O(^1S)$	$O(^1D)$	NH(b)
NH_3	8.91 ± 0.18[d]	200[m] 130 ± 10[e]	0.00089[r]	50000[n]	27000[v]	41 ± 7[n]
H_2	fast 259.7 ± 17.6[a][p] slow 5.8 ± 1.0[a][p] fast 66.7 ± 7.7[a][q] slow 11.0 ± 0.2[a][q]	45 ± 20[e] 92 ± 43[k] 40[m] 82.4 ± 10.3[l]		0.028[n]	12500[v]	86 ± 15[o]
D_2	fast 377.0 ± 27.2[a][p] slow 15.99 ± 3.67[a][p] fast 97 ± 5[a][q] slow 7.71 ± 3.4[a][q]	2[m] 1.8[o]				1.7 ± 0.1[g]
CO_2	0.53 ± 0.41[a]	30 ± 10[e]	0.000037[t] <0.00005[e]	36[v]	10000[v]	

Table 3.4, continued

	NF(b)	O_2(b)	O_2(a)	O(^{1}S)	O(^{1}D)	NH(b)
NO	fast 12.6 ± 2.5[a]	2.8[r]	0.0035[v]	55000[v]	4000[v]	
	slow 1.3 ± 0.4[a]		0.0025[s] 0.0050[e]			
O_2	3.8 ± 0.2[a]	0.01[u]		32[u]	3700[v]	
	1.8 ± 0.3[b]			28[v]		
CO	1.50 ± 1.23[a]	0.33[u]		9.4[u]	3600[v]	
Cl_2	7020 ± 1130[a]		0.0003[e]		18000[v]	
	8716 ± 705[c]					
Br_2	11830 ± 839[a]					
NF_2	0.5 ± 0.4[a]					
N_2F_4	0.4 ± 0.1[a]					
NF_3	180 ± 70[i]					

Table 3.4, continued

	NF(b)	O_2(b)	O_2(a)	O(^{1}S)	O(^{1}O)	NH(b)
Ar	<0.001[i]			0.00048[v]	30[v]	
H	300[c]					

(i) The numbers from this work are listed together with standard deviation.

(ii) The reagent concentration for the measurements are Cl_2 = 1.64%, Br_2 = 1.51%, H_2 = 15.31%, O_2 = 14.01%. The other reagents were done with pure concentration.

(iii) a = this work; b = ref. 1; c = ref. 2; d = ref. 3; e = ref. 4; f = ref. 17; g = ref. 11; h = ref. 12; i = ref. 18; j = ref. 5; k = ref. 6; l = ref. 7; m = ref. 8; n = ref. 9; o = ref. 10; p = NF(b) was generated by NF_2 + Ar*; q = NF(b) was generated by N_2F_4 + Ar*; r = ref. 13, s = ref. 14; t = ref. 15; u = ref. 16.

through the flow tube containing NF(b) radicals and the Cl_2 flow was then shut off, more than one hour was required for the NF(b-X) signal to return to the base line position before Cl_2 was added. Even for ~10% Cl_2/Ar or Br_2/Ar mixtures, this surface adsorption problem was still observed and the measurements were difficult. Yet the unusually fast quenching rates of Cl_2 and Br_2 made the k_{Br_2} and k_{Cl_2} determination possible by very dilute Cl_2/Ar (1.64%) and Br_2/Ar (1.51%) mixtures.

Quenching by Reagents with Complicated Kinetics

Abnormal kinetics were observed in the experiments using H_2, D_2, NO, and HBr as quenching reagents. Some plots illustrating the problem are shown in fig. 4.7. The non-linear relationship between log I and [Q] shows that the simple pseudo first order assumption for NF(b) quenching is not being followed. The kinetics for these molecules do not seem to have been caused by a changing k_w since immediate return of I_{NF} to I_0 was observed when the quenching reagent flow was turned off. The kinetics appear to be describable by the sum of two first order plots, and the two rate constants listed in Tab. 4.1 for these reagents were obtained by taking the slopes at both ends of the curves.

The kinetics of H_2 also were investigated by the moveable detector technique; the data are shown in fig. 4.8.a. The plots in fact show first order decay for all [H_2] and pseudo first order rate constants are obtained. However the plot of k' vs. [H_2] (fig. 4.8.b) is non-linear; the rate of quenching slows down with increasing [H_2]; this is to be

compared with the measurement of k_{Br_2} (fig. 4.6) by movable detector technique for the abnormal behavior. Thus, the two methods gave the same result. A large rate constant for $[H_2] \leq 10^{13}$ molec/cm^3 and a small k for $[H_2] \geq 1.5 \times 10^{13}$ molec/cm^3.

Fig. 4.7 Abnormal quenching phenomenon of H_2, HBr, NO and D_2 on NF(b) decay.

The solid lines in Fig. b indicate that NF_2 + Ar* was used as NF(b) source while the broken lines show that N_2F_4 + Ar* was applied as NF(b) source.

(a)

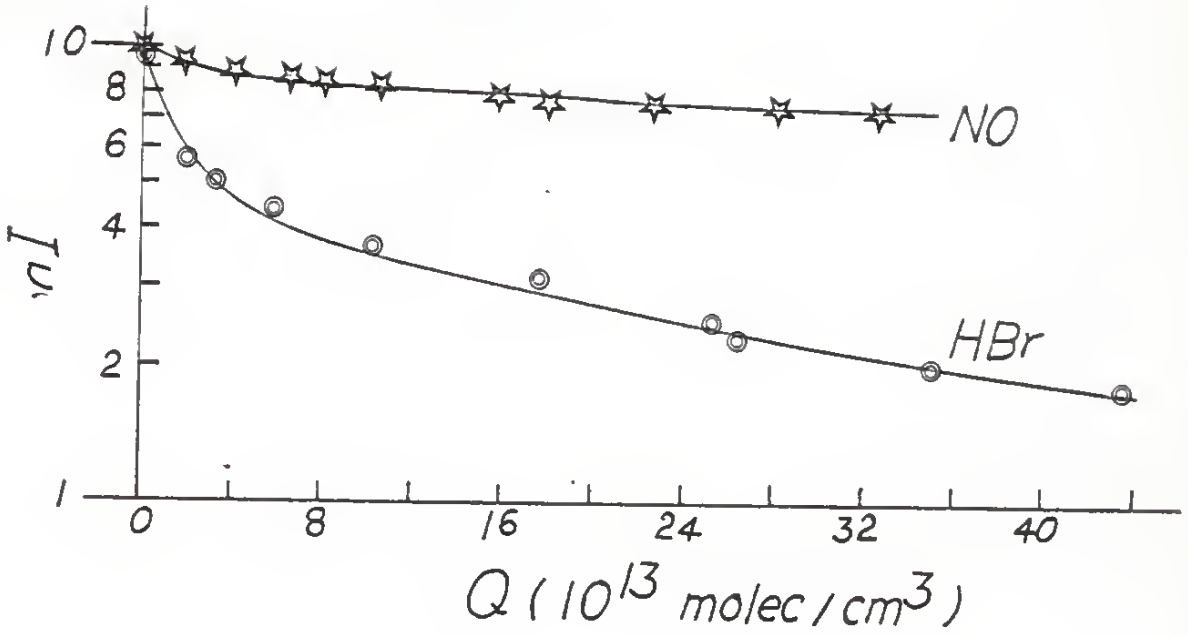
10
8
6
4
2
1
τ1
NO
HBr
0
8
16
24
32
40
Q (10^13 molec / cm^3)

(b)

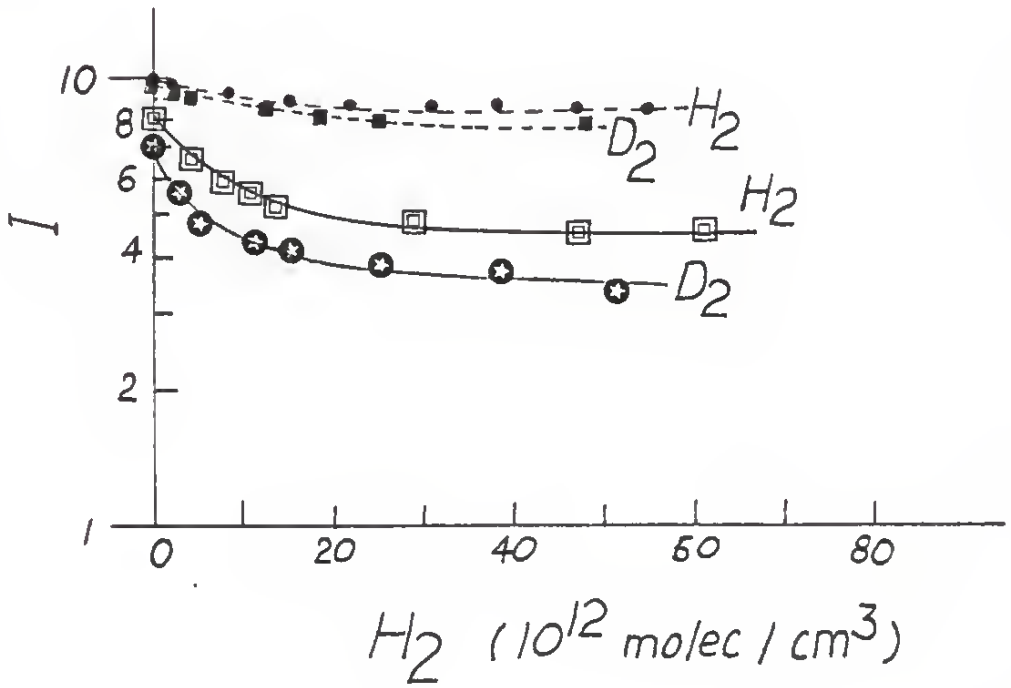
10
8
6
4
2
1
I
H2
D2
H2
D2
0
20
40
60
80
H2 (10^12 molec / cm^3)

Fig. 4.8

(a) Plot of log I vs. Δt of Various $[H_2]$ Using Moveable Detector Technique.

The linear dependence of log I on Δt suggests that pseudo first kinetics was obeyed for a given $[H_2]$.

a = $[H_2]$ = 0 molec/cm^3

b = $[H_2]$ = 2.02 x 10^{12} molec/cm^3

c = $[H_2]$ = 2.90 x 10^{12} molec/cm^3

d = $[H_2]$ = 3.37 x 10^{12} molec/cm^3

e = $[H_2]$ = 17.41 x 10^{12} molec/cm^3

(b) Plot of k' obtained from fig. 4.8.a versus $[H_2]$. The curve shows abnormal kinetics.

a.

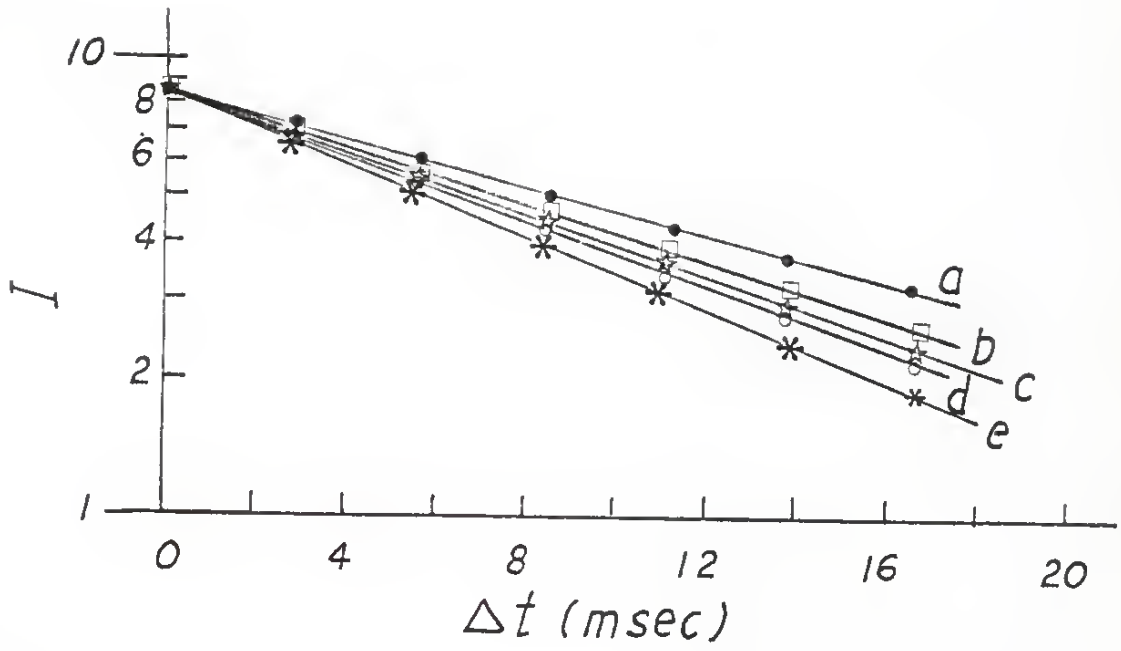
10
8
6
4
2
1
I
0
4
8
12
16
20
Δt (msec)
a
b
c
d
e

b.

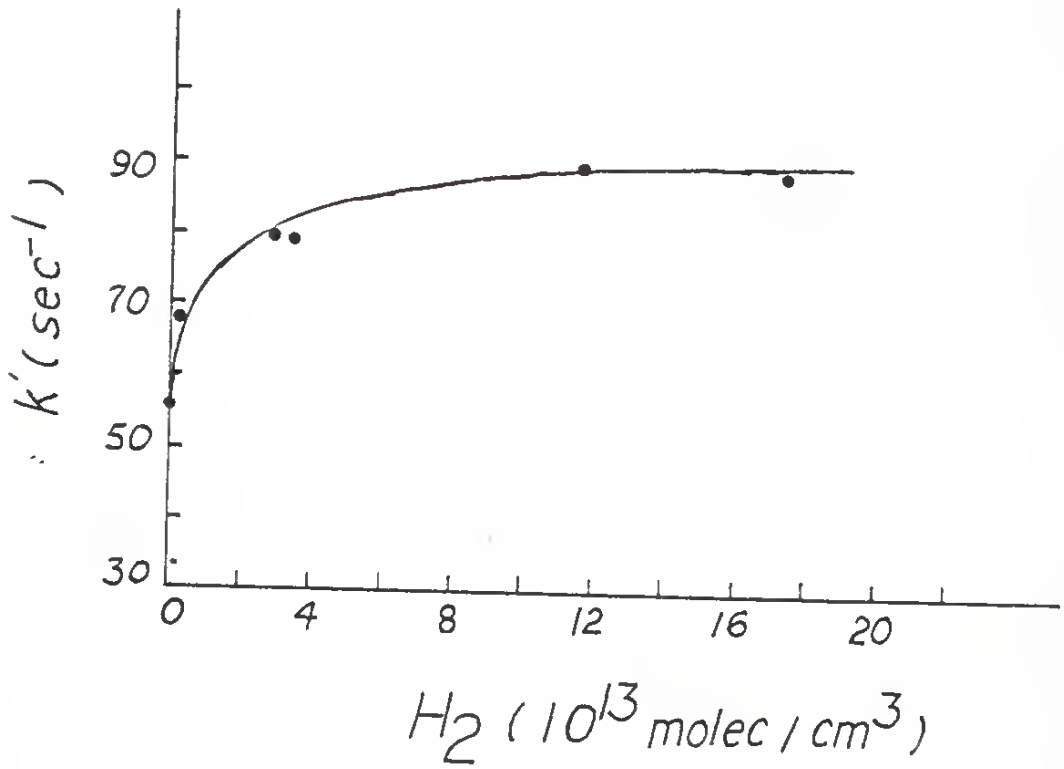
90
70
50
30
k' (sec⁻¹)
0
4
8
12
16
20
H2 (10^13 molec / cm^3)

References:

1. J. P. Singh and D. W. Setser, unpublished work.
2. M. A. Kwok, J. M. Herbelin and N. Cohew, Electronic Transition Lasers, p. 8, 2nd Ed., 1975. The MIT Press, Ed. by Steinfield.
3. P. Green and D. W. Setser, unpublished work.
4. J. P. Singh and D. W. Setser, J. Phys. Chem., to be published.
5. R. G. O. Thomas, and B. A. Thrush, Proc. Roy. Soc. A, 287, 350, 1977.
6. M. J. E. Gunthjer, and D. R. Snelling, J. Photochem., 4, 27, 1975.
7. D. F. Mullar and P. L. Houston, J. Phys. Chem., 85, 3568, 1981.
8. A. Leiss, V. Schurath, K. H. Becker, and E. H. Fink, J. Photochem., 8, 211, 1978.
9. V. Filseth, F. Stuhl and K. H. Welge, J. Chem. Phys., 52, 239, 1970.
10. C. Zetzsch and F. Stuhl, Ber. Bunsenges, Phys. Chem., 79, 1156, 1975.
11. C. Zetzsch and F. Stuhl, J. Chem. Phys., 66, 3107, 1977.
12. C. Zetzsch and F. Stuhl, Chem. Phys. Lett., 33, 375, 1975.
13. R. B. Boodaghians, P. M. Borrell and P. Borrell, Chem. Phys. Lett., 97, 193, 1983.
14. M. Yaron, A. von Engel and P. H. Vidand, Chem. Phys. Lette., 37, 159, 1976.
15. I. A. McLaren, N. W. Morris and R. P. Wayne, J. Photochem., 16, 311, 1981.
16. F. Stuhl and K. H. Welge, Can. J. Chem., 47, 1870, 1969.
17. K. Schofield, J. Photochem., 9, 55, 1978.

18. P. H. Tennyson, A. Fontijn and M. A. A. Clyne, Chem. Phys., 62, 171. 1981.

CHAPTER 5. DISCUSSION AND CONCLUSIONS

The NF(b) source using NF_2 + Ar*

The NF_2 + Ar* reaction in a flowing afterglow system was found to be a preferred NF(b) source for kinetic and spectroscopic studies on the NF(b) state. The vibrational levels of NF(b) are formed to v ≈ 9, but most of the population is in the v'=0 level. The concentration of NF(b) generated by the method is ~ 10^9 molec/cm^3. Wall quenching and the quenching by parent molecule, NF_2, are slow for NF(b) state. Therefore the kinetic studies utilizing this source are desirable if there is no interferent reaction of the added reagent with other active species in the system. The main interfering species are NF_2 and F atoms from the Ar* + NF_2 reaction.

A possible source of $NF(B^3\Sigma^-)$ or $NF(A^3\Sigma^+)$ states: He* + N_2F_4

Although the electronic states of O_2 lying above X, a, b states have been known since 1935, such as $O_2(B^3\Sigma_u^-)$ state by Schuman-Runge bands[1],[2] and $O_2(A^3\Sigma_u^+)$ by Herzberg bands;[1] the only electronic states found for NF are $X(^3\Sigma^-)$, $a(^1\Delta)$, and $b(\Sigma^+)$ states. The existence of $NF(B^3\Sigma^-)$ and $NF(A^3\Sigma^+)$ are expected if the analogy between O_2 and NF is true as predicted by MO theory. The $NF(B^3\Sigma^-)$ state is of especial interest since the fully allowed $B^3\Sigma^- - X^3\Sigma^-$ transition can be studied by LIF technique if ν(B-X) is known and a source of NF(X) is available. The unidentified bands in the range of 3000 ~ 3750A from reaction of

N_2F_4 + He* are suspected to be the NF(B-X) or NF(A-X) emission, based on a theoretical calculation of the NF electronic states.[3] Ellis and Bandyard reported the spectroscopic constants for NF(A) and NF(B) states as in table 5.1 using Dunham analysis. The calculated constants of A and B states may be $\gtrsim$ 10% in error, since a 10% deviation was found between the calculated and experimental results of X, a, and b states. Fig. 5.1 shows the theoretical potential curves of NF radical, and the curves of O_2[1] are also shown as a comparison. The relative positions of A and B states are different for O_2 and NF; A state is below B state in the case of NF while it lies above B state for O_2 molecule. The displacement of r_e values of A, B states from that of X state results in a red shift of the most favored ν(B-X) and ν(A-X) transitions from the ν_{00} values. The wavelength of the favored transitions are roughly estimated from fig. 5.1 to be ~ 3300A which is near the unidentified bands from N_2F_4 + He* experiments. However, this assignment remains to be confirmed by more careful investigation.

Reproducibility and Reliability of the Kinetic Measurements

The lifetime of NF(b) was concluded to be 20.2 ± 0.5 msec from the intercepts of the plots of I vs. $1/P_{Ar}$. This value is in close agreement with that reported by Herbelin et al.[4] and Clyne[5] et al. as 16 and 22 msec, respectively. The statistic standard deviation of 4 separate runs was ~ ± 0.5 msec. The number measured by Clyne and White[6] in 1970 as 160 msec seems to be of larger error.

Table 5.1 Theoretical Values of Spectroscopic Constants (cm^{-1}) for NF(A) and NF(B) States

	$T_e(cm^{-1})$	$r_e(A)$	ω_e	$\omega_e x_e$	$\beta_e(cm^{-1})$	$\alpha_e x10^{-2}$	$\nu_{00}(cm^{-1})$
$NF(A^3\Sigma^+)$	62425	1.81	432	35.8	0.637	3.155	45495 (2200A)
$NF(B^3\Sigma^-)$	44092	1.85	480	35.0	0.609	2.345	43719 (2300A)

Fig. 5.1 Potential Curves of NF by Theoretical Calculation

The broken line in (a) represents the position of four curves shown in (b)[3]; (c) shows the corresponding X, a, b, A, B states of O_2.[1] The Roman numbers appear in fig. a and b are used to distinguish states of same term symbol.

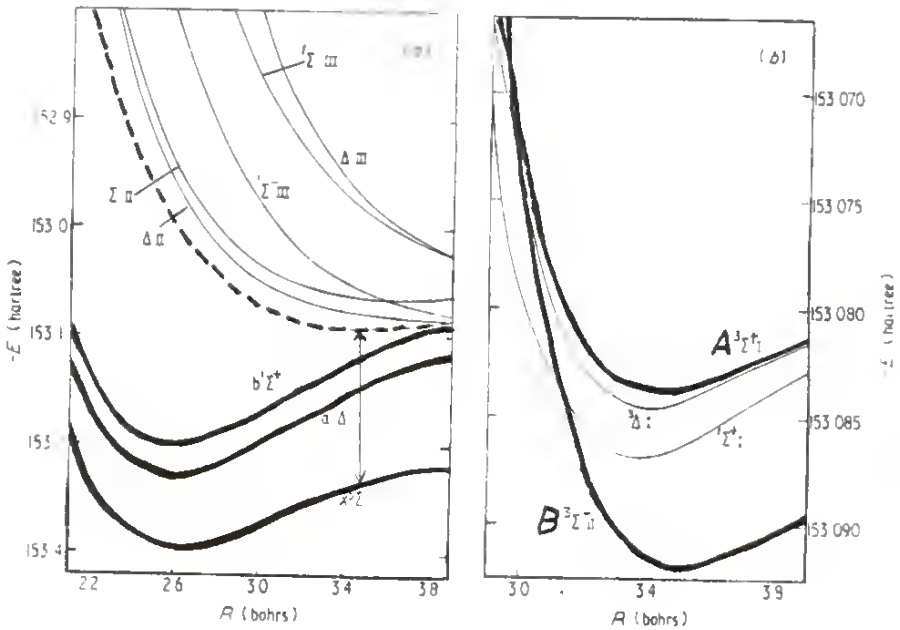
(b)
153 070
153 075
153 080
153 085
153 090
$A^3\Sigma_u^+$
$^3\Delta$:
$^1\Sigma_u^+$:
$B^3\Sigma_u^-$
30
34
38
R (bohrs)

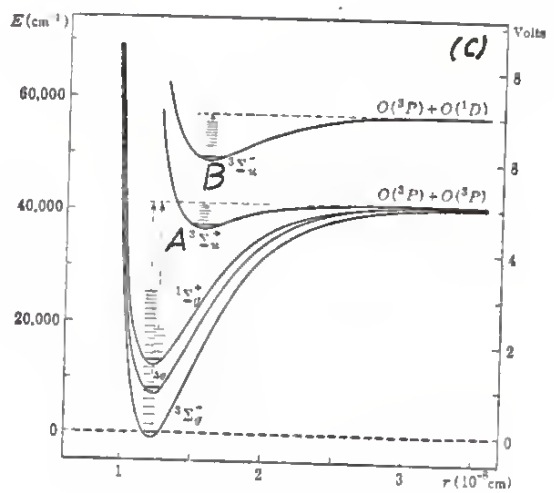
(c)
Volts
60,000
40,000
20,000
0
$O(^3P)+O(^1D)$
$O(^3P)+O(^3P)$
$B^3\Sigma_u^-$
$A^3\Sigma_u^+$
$^1\Sigma_g^+$
$^3\Sigma_g^-$
1
2
3
r(10^{-8} cm)

The reproducibility of the k_Q measurements is represented as a standard deviation following each k_Q listed in tab. 3.4. The day-by-day reproducibility was tested by using CH_3Cl as quenching reagent. Separate measurements showed agreement within 90% (fig. 3.12) for various runs which were three days apart. The k_{Br_2} values determined by fixed point and movable detector shows ~ 30% uncertainty between the two methods.

The measurements are estimated to have ~ 35% absolute uncertainty. The major uncertainty was from evaluation of Δt which was calculated by eq. 3.25 with plug flow assumption. As discussed in a previous review by Kolts and Setser[7], however, a correction is required for Δt calcuation if a parabolic flow or a flow in a transition between parabolic flow and plug flow were occurring at the observing point (eq. 5.2).

$$\Delta t' = \Delta t/C \qquad \text{(eq. 5.2)}$$

In eq. 5.2, $\Delta t'$ is the value to be applied to equations in chapter 3 for k_Q calculation and Δt is the value obtained by plug flow assumption (Eq. 3.25). The constant C in the equation is 1.6 for a fully developed parabolic flow for a species that is quenched at the wall, and between 1 ~ 1.6 if the flow is in a transition of parabolic and plug flow. For the particular flow system used in this work, the flow tube i.d. was 4.1 cm, and the typical pressure and pumping speed are 1.6 torr and 1600 cm/sec, respectively. The length required for Ar parabolic flow to fully develope in the tube is ~ 47.5 cm, which was calculated using the following equations[7]:

$$Le = 0.114\ \ell\ Re \qquad \text{(eq. 5.3)}$$

$$Re = \frac{\ell \rho V}{\eta} \qquad \text{(eq. 5.4)}$$

where Le: length required to fully develope parabolic flow, cm

ℓ: the diameter of flow tube, cm

Re: Reynolds number

ρ: Ar density, g/cm^3

V: the velocity of the carrier gas, cm/sec

η: viscosity of the carrier gas, poise-

The observing point was mostly at 35.5 cm and the flow was in a transition between parabolic and plug flow. Therefore, the plug flow assumption in the calcuation may cause some error. This possibly was checked by measuring k_{CH_3Cl} by the fixed point method at various observing positions from 10.5 to 35.5 cm (fig. 4.4). The k_{CH_3Cl} values obtained at different positions would have some differences if the effective fow speed was changing along the tube. However the resulted k_{CH_3Cl}'s are of ~ 10% variation, and $\lesssim$ 15% uncertainty from plug flow assumption seems to be the case. The uncertainty of Ar flow should be <5% since two separate calibrations (fig. 2.2) show 1% deviation for the Ar flow rate used in kinetic measurement.

Other factors such as Δx determination and gas handling also caused error. Because of the inhomogeneous mixture of Q/NF(b) near the reagent inlet, and the 4 mm wide slit set in front of the detecting units, the measurement of effective Δx contained certain uncertainty. About 10% of error was raised from these factors. A 15% of error was possible from

the gas impurity and gas handling, including reading the manometers and flowmeters, calibration of flowmeters, and correction of reagent flow rate from Ar flow rate by the viscosity constant.

System with Complicated Kinetics

The quenching of NF(b) by H_2, D_2, HBr, CF_3I, and NO showed complex kinetics; the quenching behavior of these reagents appears to be describable by a sum of two reactions, one slow and one fast. A possible explanation for the phenomena is the interaction of the added reagents with reactive species other than NF(b). The F atom can react with H_2, D_2, and HBr while the abnormal kinetics of NO perhaps can be explained by a trace amount of N atom in the system. The possibilities will be examined as below.

Although the monochromator scanning showed no N_2(B-A) emission from the recombination of N atom; the reaction of NF_2 + Ar* may still generate trace amounts of N atom N_2(B-A) being observed. The reaction of N atom with NO generated a O atom (rxn 5.5) which in turn reacts with another NO to generate an excited NO_2 molecule (rxn. 5.6). The excited NO_2 emitts with a broad spectrum which includes the transmissible

$$N + NO \rightarrow N_2 + O \qquad \Delta H = -103.98 \text{ kcal/mole}^{(1)} \qquad \text{(rxn 5.5)}$$

$$O + NO \rightarrow NO_2^* \qquad \text{(rxn 5.6)}$$

wavelength range of the interference filter used to monitor NF(b). The band width of the filter was 10 nm and fairly large amounts of photon

from the NO_2 emission was collected by PMT simultaneously. Thus, after NF(b) was quenched to certain extent, the NO_2* emission could dominate the signals reaching the PMT and no further decrease of $I_{NF(b)}$ would be measured. As a consequence, slow decay of log I vs. [NO] could be observed. This suggestion needs to be confirmed by obervation of NF(b) with a monochromator. The interaction of F atoms are discussed as below; however, the low F concentration is to be kept in mind in deciding the possibility of interference from F atoms.

The F atoms react with H_2 exothermically to give HF and H (rxn. 5.7), and the resulting H atom reacts rapidly with NF_2, one of the major species in the system, to produce another HF and NF(a) (rxn. 5.8).

$$F + H_2 \rightarrow HF + H \qquad \Delta H = -31.3 \text{ kcal/mole}^{(9)} \qquad \text{(rxn. 5.7)}$$

$$k_{298} = 2.9 \times 10^{-11} \text{ cm}^3\text{molec}^{-1}\text{sec}^{-1}$$

$$H + NF_2 \rightarrow HF + NF(x,a,b) \qquad \text{(rxn 5.8)}$$

$$k_{298} = (1.5 \pm 0.2) \times 10^{-11} \text{ cm}^3\text{molec}^{-1}\text{ sec}^{-1} \ ^{(10)}$$

Therefore, the added H_2 converts F to HF and NF. The value of k_{H_2} is presumably small and the quenching of NF(b) was dominated by k_{HF} at this moment. After more H_2 was added, F atoms were completely consumed; increasing $[H_2]$ had no effect on [HF] and k_{slow} value observed became k_{H_2}.

HBr might react with F atom in two ways (rxn 5.9 and rxn 5.10).

$$F + HBr \rightarrow HF + Br \qquad \Delta H = -47.7 \text{ kcal/mole}^{(9)} \qquad \text{(rxn 5.9)}$$

$$k_{298} = 4.7 \times 10^{-11}\ cm^3 molec^{-1} sec^{-1} \quad (11)$$

$$F + HBr \rightarrow BrF + H \qquad \Delta H \approx +31.8\ kcal/mole^{(9)} \qquad (rxn\ 5.10)$$

However, rxn 5.8 is excluded since it is endothermic. Therefore the added HBr reacts with F atom through rxn 5.9 and the kinetics was dominated by HF at low [HBr].

Although HCl and CH_4 react with F atom in a similar way as HBr and H_2 (rxn 5.11, rxn 5.12), pseudo first order kinetics were obserbved for these two reagents even the reaction rate of CH_4 with F is faster than

$$F + HCl \rightarrow HF + Cl \qquad \Delta H \approx -32.18\ kcal/mole^{(9)} \qquad (rxn.\ 5.11)$$

$$k_{298} = 0.9 \times 10^{-11}\ cm^3 molec^{-1} sec^{-1}\ )10)$$

$$F + CH_4 \rightarrow HF + CH_3 \qquad \Delta H \approx -40.3\ kcal/mole \qquad (rxn\ 5.12)$$

$$k_{298} = 7.2 \times 10^{-11}\ cm^3 molec^{-1} sec^{-1} \quad (11)$$

H_2 and HBr. A reason for this is that the differences between k_{HCl}, k_{CH_4}, and k_{HF} might not be large enough to show the nonlinear behavior on log I vs. [HCl], [CH_4] plots.

The mentioned mechanisms using the reaction of F atoms with H_2, D_2, and HBr are still in question. The problem is the small concentration of F atoms ($\lesssim 10^{10}$ molec/cm^3) in the system even if it exists. Therefore, reactions of the added reagents with active species of higher concentration are other possibilities to give the unusual kinetics. As shown in tab. 3.4, the k_{fast} values of H_2 and D_2 showed large difference for NF(b) generated by NF_2 + Ar* and N_2F_4 + Ar* (fig. 4.7, Tab. 4.1). Since the chemical properties of NF_2 and N_2F_4 are not well known, product identification seems to be important to conclude the kinetics.

Comparisons for k_Q of NF(b), $O_2(b)$, $O_2(a)$, NH(b), $O(^1D)$, $)(^1S)$

Together with k_Q of NF(b), listed in Tab. 3.4 are also k_Q of $O_2(b)$, $O_2(a)$, NH(b), $O(^1D)$, and $O(^1S)$ from various references. The $O(^1D)$ atom usually are quenched through chemical reaction and the rate constants are large compared with other excited species in tab. 3.4. The quenching of $O(^1S)$ differs from that of $O(^1D)$; the quenching rate constants of $O(^1S)$ varies from 10^{-10} to 10^{-18} $cm^3molec^{-1}sec^{-1}$. Although the k_Q values of NF(b) also shows large variation from 10^{-10} to 10^{-17} $cm^3molec^{-1}sec^{-1}$, no obvious correlation between k_Q of NF(b) and $O(^1S)$ was observed. Both $O_2(a)$ and $O_2(b)$ are quenched by an E-V mechanism. $O_2(a)$ is quenched to the ground state and the quenching rates are very slow whilst $O_2(b)$ is quenched to the $O_2(a)$ state and the rate constants generally are about three orders of magnitude larger than that of $O_2(a)$. The quenching rate constants of NH(b) are more or less similar to $O_2(b)$ in terms of reactivity, and this analogy was favored by Zetzsch and Stuhl[8] in 1977. A similar correlation is found here for the analogy of NF(b) and $O_2(b)$ states, the quenching rate constants of NF(b) are within ~ 2 orders of magnitude of those for $O_2(b)$ and the patterns of the rate constants are similar. It seems that NF(b) is quenched by E-V mechanism with the product state being NF(a). Nevertheless, further kinetic studies with identification of products are necessary to prove the generation of NF(a) state in the quenching of NF(b) to support the above conclusion.

For X_2 and perhaps other molecules with low energy electronic states, E-E transfer is possible and this explains the large rate constants for Cl_2 and Br_2. Qualitative (visual) as well as preliminary

spectroscopic studies indicate that the quenching does not give Cl_2 or Br_2 emission so the quenching gives either metastable halogen states or dissociative states.

References

(1) G. Herzberg, F. R. S., Spectra of Diatomic Molecules, 2nd Ed. Van Nostrand Reinhold Company, New York, 1950.

(2) H. P. Knauss and H. S. Ballard, Phys. Rev., 48, 796, 1935.

(3) D. J. Ellis and K. E. Banyard, J. Phys. B: Atom. Molec. Phys., 7, 2021 1974.

(4) M. A. Kwok, J. M. Herbelin and N. Cohen, Electronic Transition Lasers, 2nd Ed., p. 8, the MIT Press, 1975.

(5) P. H. Tennyson, A. Fontijn and M. A. A. Clyne, Chem. Phys. Lett., 62, 171, 1981.

(6) M. A. A. Clyne and I. F. White, Chem. Phys. Lett., 6, 465, 1970.

(7) J. H. Kolts and D. W. Setser, Reactive Intermediates in the Gas Phase, Ch. 3, Academic Press, Inc., New York, 1979.

(8) C. Zetzsch and F. Stuhl, J. Chem. Phys., 66, 3107, 1977.

(9) Bond Dissociation Energies in Simple Molecules, NSRDS, 1970.

(10) C. T. Cheah, M. A. A. Clyne, P. D. Whitefield, J. C. S. Faraday II, 76, 711, 1980.

(11) K. Tamagake, D. W. Setser and J. P. Sung, J. Chem. Phys., 73, 2203, 1980.

(12) CRC Hand Book of Chemistry and Physics, Ed. by R. C. Weast, Chem. Rubber Publishing Company, 1979.

APPENDIX A Table of the Viscosity Coefficients of the Quenching Reagents

The unit of the viscosity coefficients is: 10^{-6} poise

reagent	Ar	HCl	HBr	CH_4	CH_3F	CH_3Cl	CH_3Br	CH_3I
η	221[1]	156[1]	182[1]	109[1]	108[3]	106[1]	104[1]	232[2]

reagent	CH_2Br_2	$CHCl_3$	CHF_3	CF_3NO	CF_3Br	NH_3	H_2	D_2
η	139*	101*	131[3]	152*	216*	92[1]	88[2]	122*

reagent	CO_2	NO	O_2	CO	Cl_2
η	148[1]	178[1]	206[1]	166[1]	147[1]

*The viscosity coefficient was calcualted by the following equation[4]:

$$\eta \times 10^7 = \frac{266.93\ MT}{\sigma^2 \Omega^{(2,2)}(T^*)}$$

where η = viscosity in poise (g/cm·sec)

T = temperature in K

T^* = reduced temperature $\frac{T}{(\varepsilon/k)}$

M = molecular weight

σ = collision diameter in A

ε/k = potential parameter, K

$\Omega^{(2,2)*}(T^*)$ = Ω integrals from Tab. I-M of the mentioned reference for calculating the transport coefficients.

In this calculation, the temperature used is 293K and the values of σ and εk are from appendix Tab. I-A of the reference:

(i) $CHCl_3$ — ε/k = 327K, σ = 5.430Å

(ii) D_2 — ε/k = 39.3K, σ = 2.948Å

(iii) CH_2Br_2 — ε/k and σ value of CH_2Cl_2 were used as an approximation

ε/k = 406K, σ = 4.759Å

(iv) CF_3NO, CF_3Br — ε/k and σ values of CH_3Cl were used as approximation

ε/k = 855K, σ = 3.375Å

References:

1. Methon Gas Data Book, 1966.

2. C.R.C. Handbook of Chemistry and Physics, 62nd Ed., 1981-1982.

3. V. F. Kochubei, F. B. Moin, Zh. Fizkim., 15-17, 52(1), 1978.

4. J. O. Hirschfelder, C. F. Curtiss and R. B. Bird, Molecular Theory of Gases and Liquids, p. 529, John Wiley & Sons, Inc., 1964.

APPENDIX B The Uncertainty of Measuring Gas Flows by Capillary Flowmeter Calibrated for Ar

The capillary flowmeter used to measure the reagent flow rate was calibrated for Ar. Therefore, eq. 2.8 is applied to convert the flow rates from the calibration curve to the real flow rate of the gas reagent.

$$F_{reagent} = F_{argon} \times \frac{\eta_{argon}}{\eta_{reagent}} \qquad \text{eq. 2.8}$$

The uncertainty of the conversion was determined to be ~10%.

A quite check on the uncertainty of eq. 2.8 was done using CH_4 and H_2. The gas was stored in a reservoir of known volume. The pressure drops, ΔP_2's, in the reservoir were measured after being pumped for a certain time interval, Δt's. The flow rates were calculatged by:

$$F = \frac{\Delta n}{\Delta t} = \frac{\Delta P_2 V}{RT\Delta t}$$

$P_{2,0}$, $P_{2,t}$ = the reservoir pressures at time zero and t

In the meanwhile, the gas flows were also read from the calibration curve (fig. 2.4) and corrected by eq 2.8. The $\bar{P}\Delta P$ values were given by average P_2 and ΔP values of a specific Δt.

$$P_{2,ave} = \frac{P_{2,t} + O_{2,0}}{2}$$

$$\Delta P_{ave} = \frac{\Delta P_t + \Delta P_0}{2}$$

ΔP_t, ΔP_0 = the pressure differences at two ends of the capillary tube at time t and zero

The resulted data are shown in Tab. B.1 and Tab. B.2, and a 10% of uncertainty is concluded.

Tab. B.1. The Comparison of CH_4 Flow Rates Obtained by Using Ar Calibration Curve and Oirect Measurement.

T = 300K, η_{Ar}(20°C) = 221 μp, η_{CH_4}(20°C) = 106 μp

$F_{CH_4,corr.}$ = the flow rates corrected by eq. 2.8.

$F_{CH_4,exp}$ = CH_4 flow rates obtained by direct measurement

$\bar{P}_{ave}\Delta P_{ave}$ (cmHg·mmHg)	F_{Ar} 10^{-4}mole/min	$F_{CH_4,corr.}$ 10^{-4}mole/min	$F_{CH_4,exp}$ 10^{-4}mole/min	$\frac{F_{CH_4,corr.}-F_{CH_4,exp}}{F_{CH_4,exp}}$ (%)
108.65	3.72	7.76	8.01	-3.1
62.24	2.14	4.46	4.31	3.5
42.44	1.50	3.13	3.07	2.0
35.77	1.23	2.56	2.79	-8.2
23.87	0.80	1.67	1.75	-4.6
11.44	0.37	0.77	0.82	-6.1

Tab. B.2. The Comparison of H_2 Flow Rates Obtained by Using Ar Calibration Curve and Direct Measurement

T = 300K, η_{H_2}(20°C) = 88 μp

$\bar{P}_{ave}\Delta P_{ave}$ (cmHg·mmHg)	F_{Ar} 10^{-4}mole/min	$F_{CH_4,corr.}$ 10^{-4}mole/min	$F_{CH_4,exp}$ 10^{-4}mole/min	$\frac{F_{CH_4,corr.}-F_{CH_4,exp}}{F_{CH_4,exp}}$ (%)
231.72	8.00	20.18	20.37	-0.9
149.18	5.13	12.94	13.52	-4.3
98.72	3.41	8.60	9.20	-6.5
71.84	2.46	6.21	6.39	-2.8
50.64	1.23	3.10	3.61	-14.0
32.67	1.13	2.85	2.83	0.7
15.52	0.50	1.26	1.34	-6.0
8.47	0.26	0.66	0.59	11.9

Acknowledgements

I would like to express my gratitude and appreciation to my advisor, Dr. D. W. Setser, for his scientific guidance and patience.

The help of Dr. Y. C. Yu to get me started on research and some data of quenching rate constant provided by Dr. J. P. Singh and Mr. P. Green and are gratefully acknowledged.

My work could not have been done without the help of Mr.'s Al Weyerts, Ohno and Richard Bachamp in maintaining the research facilities. I thank Ms. Linda Heinz for her patience in typing this thesis. I wish to thank the Chemistry Department for financial support in the form of teaching and assistantships. The U. S. Air Force and Petroleum Research Fund provided funds for research and for research assistantships.

The warm friendship and stimulating discussion of all members in the Chemistry Department made my research and living in Manhattan a pleasant experience.

Finally, many thanks are due to my parents for their encouragement and moral support.

A FLOWING AFTERGLOW SOURCE OF $NF(b^1\Sigma^+)$: QUENCHING RATE CONSTANT MEASUREMENTS

by

DAIMAY LIN

B.S., National Taiwan University, 1980

AN ABSTRACT OF A MASTER'S THESIS

submitted in partial fulfillment of the

requirements for the degree

MASTER OF SCIENCE

Department of Chemistry

KANSAS STATE UNIVERSITY
Manhattan, Kansas

1984

Abstract

Possible NF(b) sources were investigated using N_2F_4/NF_2 + Ar*, Xe* and He* reactions in a flowing afterglow system. Analysis using the known thermodynamic and kinetic data showed that N_2F_4 and NF_2 are parent molecules of NF(b) at room temperature and 500K, respectively. NF_2 + Ar* was the preferred NF(b) source and was used for the kinetic and spectroscopic studies.

The lifetime of NF(b) was measured to be 20.2 ± 0.5 msec and k_w was small, (8.97 ± 0.23) sec^{-1} torr. Quenching rate constants of 27 reagents were studied at room temperature. Analogy between $O_2(b)$ and NF(b) is concluded by comparing the k_Q values. Complex kinetics were found in the quenching of NF(b) by H_2, D_2, HBr, and NO.

The quenching rate constants at 300K of the well behaved reagents are listed as following: (10^{-14} cm^3 $molec^{-1}$ sec^{-1})

HCl: 30.2 ± 1.9, CH_4 = 22.1 ± 2, CH_3Cl = 23.6 ± 2.3, CH_3Br = 17.9 ± 1.0, CF_3NO = 16.9 ± 1.7, CF_3Br = 1.23 ± 0.18, CO_2 = 0.53 ± 0.41, O_2 = 3.8 ± 0.1, CO = 1.50 ± 1.23, Cl_2 = 7020 ± 1130, Br_2 = 11830 ± 839, NF_2 = 0.5 ± 0.4, N_2F_4 = 0.4 ± 0.1.